November 2015

# Soil-Structure Modeling and Design Considerations for Offshore Wind Turbine Monopile Foundations

Wystan Carswell
*University of Massachusetts Amherst*

# SOIL-STRUCTURE MODELING AND DESIGN CONSIDERATIONS FOR OFFSHORE WIND TURBINE MONOPILE FOUNDATIONS

A Dissertation Presented

by

WYSTAN CARSWELL

Submitted to the Graduate School of the

University of Massachusetts Amherst in partial fulfillment

of the requirements for the

DOCTOR OF PHILOSOPHY IN CIVIL ENGINEERING

September 2015

Civil and Environmental Engineering

**SOIL-STRUCTURE MODELING AND DESIGN CONSIDERATIONS FOR OFFSHORE WIND TURBINE MONOPILE FOUNDATIONS**

A Dissertation Presented

by

WYSTAN CARSWELL

Approved as to style and content by:

Sanjay R. Arwade, Co-Chairperson

Don J. DeGroot, Co-Chairperson

Matthew A. Lackner, Member

Andrew T. Myers, Member

Jörgen Johansson, Member

Richard N. Palmer, Department Head

Civil and Environmental Engineering Department

# ACKNOWLEDGEMENTS

This research was supported through the NSF-sponsored IGERT: Offshore Wind Energy Engineering, Environmental Science, and Policy (Grant Number 1068864) as well as grants CMMI-1234560 and CMMI-1234656 and the Massachusetts Clean Energy Center.

Beyond a source of funding, the IGERT was instrumental to my development as a doctoral candidate. With the IGERT cohort I had the opportunity to travel abroad, present my research, and learn extensively not only about the engineering of offshore but also the political and environmental aspects as well. The IGERT supported me for five months as a visiting researcher at the Norwegian Geotechnical Institute (NGI), which was a transformative experience – I am extremely grateful to Don DeGroot for his role in arranging my stay in Oslo so that I could participate in high-caliber research with renowned scholars in the field. In addition to Jörgen Johansson, special thanks to Finn Løvholt and Christian Madshus at NGI for their collaboration and guidance on the topic of soil damping.

I am also very grateful to Sanjay Arwade for not only ensuring the financial support of my doctorate, but also for his honest and prompt feedback of my work and clear direction throughout the course of my graduate career.

Thank you to my family for their continued support, but especially to Joe (for all the things).

# ABSTRACT

SOIL-STRUCTURE MODELING AND DESIGN CONSIDERATIONS FOR OFFSHORE WIND TURBINE MONOPILE FOUNDATIONS

SEPTEMBER 2015

WYSTAN CARSWELL, B.S. LAFAYETTE COLLEGE

M.S.C.E., UNIVERSITY OF MASSACHUSETTS AMHERST

Ph.D., UNIVERSITY OF MASSACHUSETTS AMHERST

Directed by: Sanjay R. Arwade and Don J. DeGroot

Offshore wind turbine (OWT) support structures account for 20-25% of the capital cost for offshore wind installations, making it essential to optimize the design of the tower, substructure, and foundation to the extent possible. This dissertation focuses on monopile foundations, as the vast majority (approximately 75%) of currently installed OWTs are supported by monopile structures. The objective of this dissertation is to provide information on the behavior of monopile support structures to better substantiate design and planning decisions and to provide a basis for reducing the structural material costs. In pursuit of these objectives, research is presented on the topics of hysteretic soil-structure damping (referred to as foundation damping), cyclic degradation of soil properties, and the impact of marine growth on OWT monopile support structures.

OWTs are lightly damped structures that must withstand highly uncertain offshore wind and wave loads. In addition to stochastic load amplitudes, the dynamic behavior of OWTs must be designed with consideration of stochastic load frequency from waves and mechanical load frequencies associated with the spinning rotor during power production. The close proximity of the OWT natural frequency to excitation frequencies combined with light

damping necessitates a thorough analysis of various sources of damping within the OWT system; of these sources of damping, least is known about the contributions of damping from soil-structure interaction (foundation damping), though researchers have back-calculated foundation damping from "rotor-stop" tests after estimating aerodynamic, hydrodynamic, and structural damping with numerical models. Because design guidelines do not currently recommend methods for determining foundation damping, it is typically neglected. The significance of foundation damping on monopile-supported OWTs subjected to extreme storm loading was investigated using a linear elastic two-dimensional finite element model. A simplified foundation model based on the soil-pile mudline stiffness matrix was used to represent the monopile, and hysteretic energy loss in the foundation was converted into a viscous, rotational dashpot at the mudline to represent foundation damping. The percent critical damping contributed to the OWT structural system by foundation damping was quantified using the logarithmic decrement method on a finite element free vibration time history, and stochastic time history analysis of extreme storm conditions indicated that mudline OWT foundation damping can significantly decrease the maximum and standard deviation of mudline moment.

Further investigation of foundation damping on cyclic load demand for monopile-supported OWTs was performed considering the design situations of power production, emergency shutdown, and parked conditions. The NREL 5MW Reference Turbine was modeled using the aero-hydro-elastic software FAST and included linear mudline stiffness and damping matrices to take into account soil-structure interaction. Foundation damping was modeled using viscous rotational mudline dashpots which were calculated as a function of hysteretic energy loss, cyclic mudline rotation amplitude, and OWT natural frequency.

Lateral monopile capacity can be significantly affected by cyclic loading, causing failure at cyclic load amplitudes lower than the failure load under monotonic loading. For monopiles

in clay, undrained clay behavior under short-term cyclic soil-pile loading (e.g. extreme storm conditions) typically includes plastic soil deformation resulting from reductions in soil modulus and undrained shear strength which occur as a function of pore pressure build-up. These impacts affect the assessment of the ultimate and serviceability limit states of OWTs via natural frequency degradation and accumulated permanent rotation at the mudline, respectively. Novel combinations of existing *p-y* curve design methods were used to compare the impact of short-term cyclic loading on monopiles in soft, medium, and stiff clay.

Marine growth increases mass and surface roughness for offshore structures, which can reduce natural frequency and increase hydrodynamic loads, and can also interfere with corrosion protection and fatigue inspections. Design standards and guidelines do not have a unified long-term approach for marine growth on OWTs, though taking into account added mass and increased drag is recommended. Some standards recommend inspection and cleaning of marine growth, but this would negate the artificial reef benefits which have been touted as a potential boon to the local marine habitat. The effects of marine growth on monopile-supported OWTs in terms of natural frequency and hydrodynamic loading are examined, and preliminary recommendations are given from the engineering perspective on the role of marine growth in OWT support structure design.

# TABLE OF CONTENTS

Page

# LIST OF TABLES

# LIST OF FIGURES

# CHAPTER 1

# INTRODUCTION AND MOTIVATION

Fossil fuels (e.g. oil, coal, natural gas) form over the course of thousands of years and are consumed at a rate that vastly exceeds the rate which they can be created. While it is somewhat controversial as to when the production of these fossil fuels will peak and decline, it is generally accepted that this peak event will indeed occur – and in all likelihood within this century. With this new chapter of energy production looming in the future, the importance of researching, improving, and implementing renewable sources of energy becomes more critical. Innovations in biofuels, solar, and wind energy have increased efficiency and power production, but as of yet no renewables are truly competitive in energy markets without policy support.

Offshore wind energy has a promising but challenging future contingent on the advancement of research and state-of-the-art design. This dissertation focuses on furthering the progress of research in the areas of offshore wind turbine structural and geotechnical modeling and design – approximately 20 to 25% of the capital cost of an offshore wind project can be attributed to the support structure and foundation [1], and consequently at least 20% of the economics of offshore wind power lies in the hands of civil engineers for improvement.

This work is motivated by the need for more renewable energy generation in the U.S. A discussion of U.S. energy demands and electricity generation is presented in Section 1.1; subsequently, an overview of the issues surrounding offshore wind turbine support structures is given in Section 1.2; last, the specific objectives and format of this dissertation are detailed in Section 1.3.

## 1.1 Energy Demand and Electricity Generation in the United States

Fossil fuels provide more than 80% of the United States' energy use, with the majority of current energy demands met by petroleum and other liquid fuels (e.g. crude oil, petroleum liquids, and

liquids derived from nonpetroleum sources) and less than 10% by renewable energy sources (Figure 1.1, [2]).

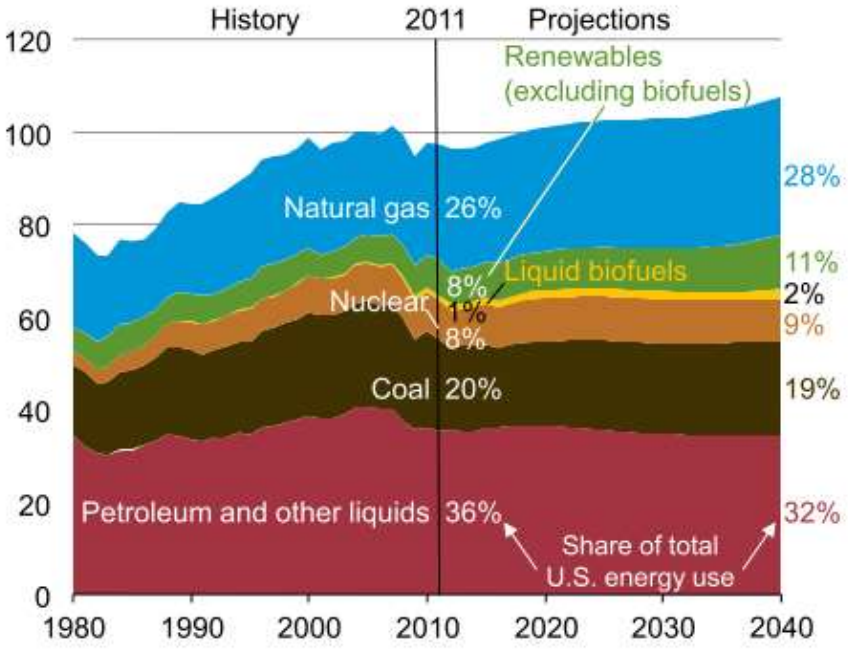


**Figure 1.1. Primary energy use by fuel in the United States in quadrillion BTU** [2]

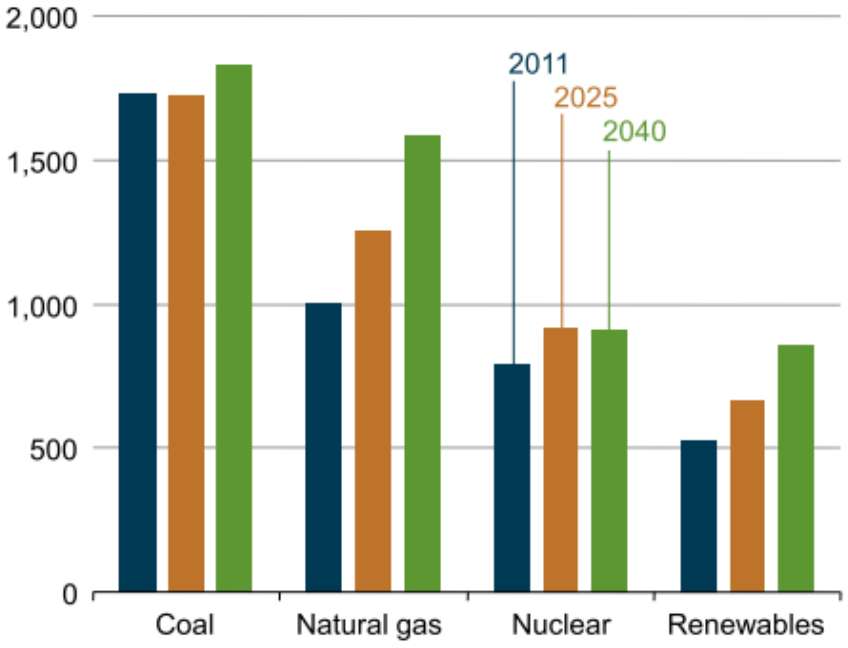


**Figure 1.2 Electricity generation by fuel, 2011, 2025, and 2040 in billion kilowatthours** [2]

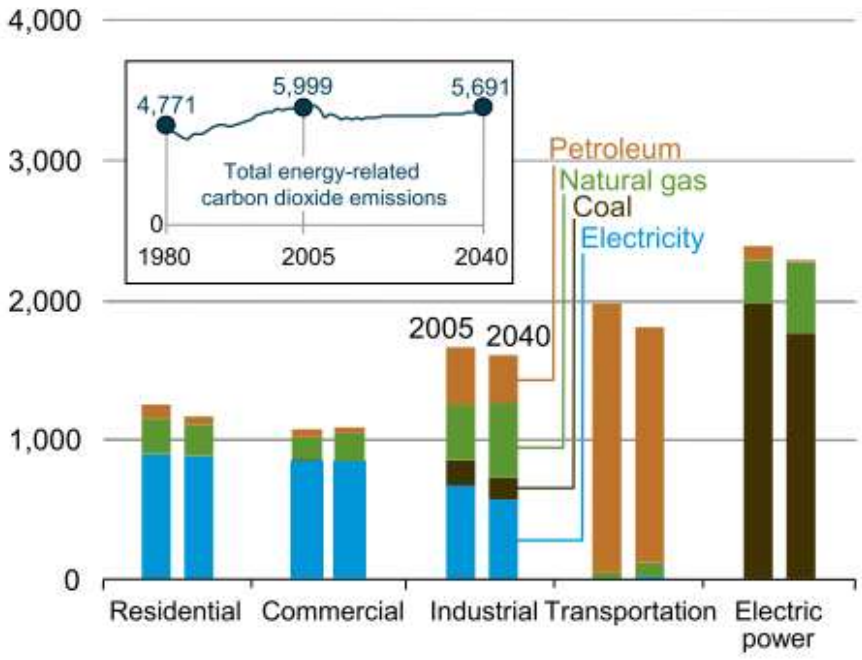


**Figure 1.3 Energy-related carbon dioxide emissions by sector and fuel, 2005 and 2040** [2]

Coal is the largest source of electricity ([2], Figure 1.2) and is abundantly available in the U.S; however, burning coal emits carbon dioxide, which is a greenhouse gas associated with global climate change. In 2005, coal accounted for 36% of total U.S. emissions of carbon dioxide (second only to petroleum, at 44%) with a projected reduction in emissions of only 2% by 2040 [2]. The dominance of coal in electricity generation (Figure 1.3) and the high percentage of U.S. emissions attributed to coal provides a compelling argument to focus research and political efforts on zero-emission energy generation.

Hydropower is the dominant source of renewable energy for the U.S., followed by wind power (Figure 1.4, [2]). Wind energy has benefited from significant policy support in the form of renewable energy tax credits and renewable energy portfolio standards; without this support, much of the wind energy which is currently installed would not be economically viable.

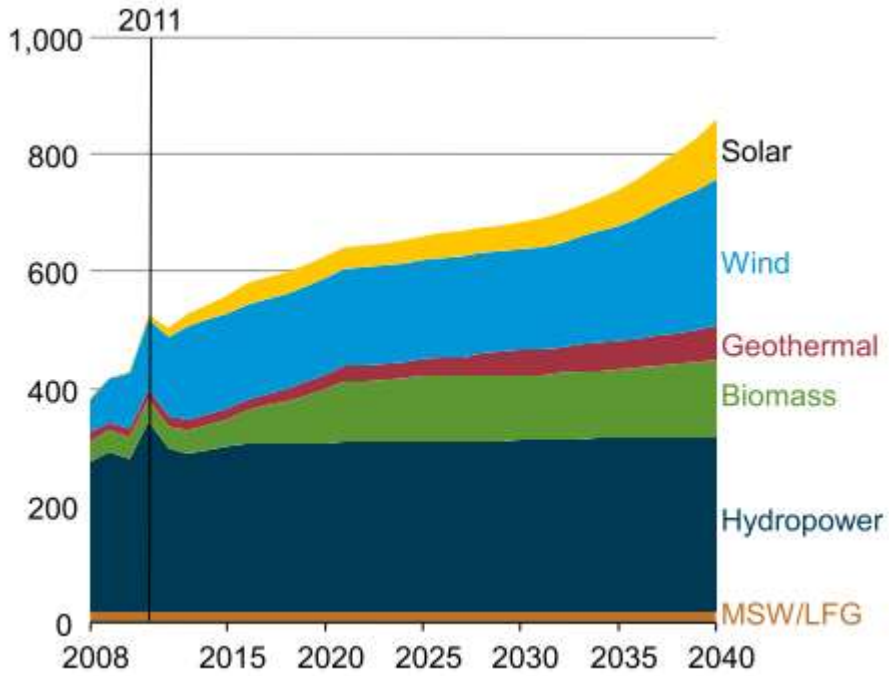


**Figure 1.4. U.S. Renewable Electricity Generation in billion kW Per Year** [2]

Even so, the U.S. wind energy is exclusively from onshore turbines; there are currently no commercial offshore wind turbines installed in U.S. waters. Offshore winds are stronger and more consistent than onshore winds and are consequently more conducive to electricity production; however, barriers to offshore installment in the U.S. have included high costs, technical challenges with installation, grid-interconnection, uncertain permitting processes, and resistance from local communities [1,3–6]. A development scenario in 2008 proposed that wind energy could supply 20% of U.S. electric energy generation by the year 2030, with offshore wind energy contributing 18% of the total wind energy [7]. This contribution (54 GW of the total 305 GW of wind proposed [7]) represents only a portion of the potential offshore wind energy available off the coast of the U.S.: It has been estimated that there is over 4000 GW of offshore wind considering the Atlantic, Great Lakes, and Gulf of Mexico (Figure 1.5), with over 1000 GW in water depths suitable for monopile foundations [3].

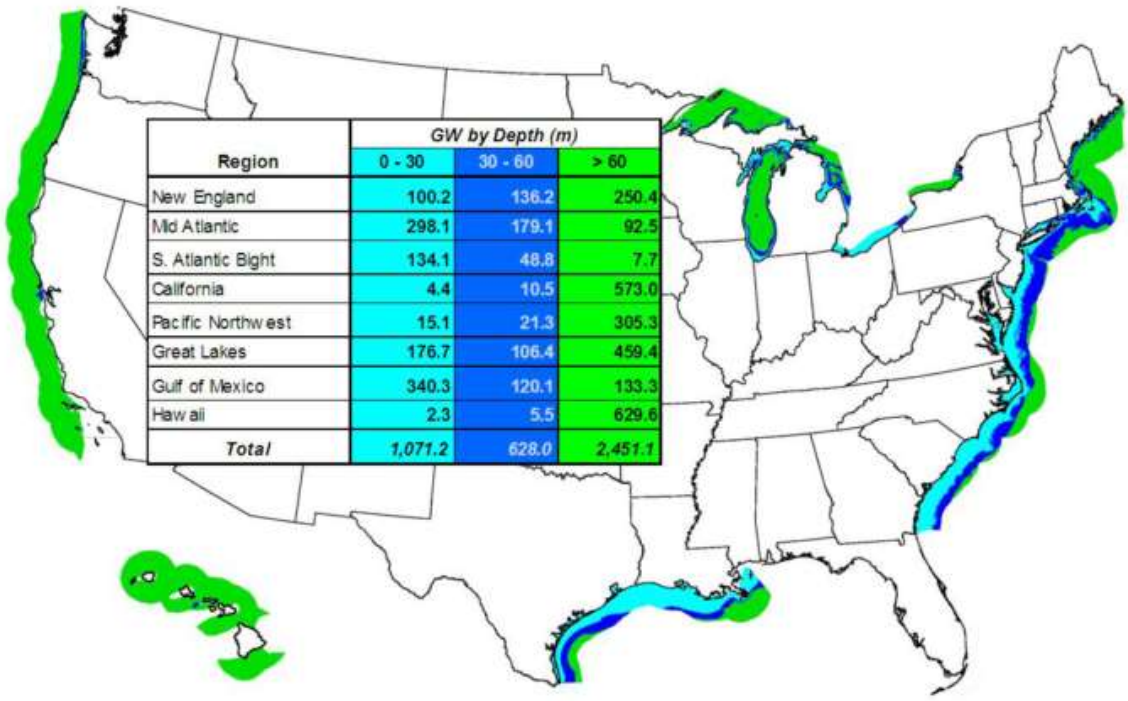


**Figure 1.5. U.S. offshore wind potential by region and depth for annual average wind speed sites higher than 7.0 m/s** [3]

## 1.2 Offshore Wind Turbine Support Structures

Offshore wind turbine (OWT) support structures present a unique design problem, as they are subjected to stochastic loading from wind, waves, and mechanical vibrations from spinning turbine blades and are situated in variable soil conditions. OWT support structure designs are consequently model and site-dependent and sometimes require unique designs even within the scope of a single offshore wind farm. As may be expected, this type of specific attention per OWT increases support structure foundation cost, not to mention the added costs associated with offshore installation and limited access for maintenance during the design life of the OWT.

Nearly 75% of OWT installations are supported by monopile foundations [1], primarily due to the fact that they are the least expensive for shallow water depths (less than approximately 30 m) – monopiles are axisymmetric (which is useful in an omnidirectional loading environment) and relatively simple to model. The commonly analyzed OWT is the NREL 5MW Reference Turbine

("NREL 5MW") [8] supported by a 6 m diameter monopile. The NREL 5MW is an artificial wind turbine model designed as a compilation of several realistic large-scale offshore wind turbines – because the design information is open source, the NREL 5MW provides a common ground for researchers to compare results. Lack of site-specific data or limited access to proprietary design information is a major hurdle for offshore wind research, and an issue that will be addressed in more depth in the conclusions of this dissertation.

While structural and geotechnical design for OWTs is similar to offshore oil & gas (O&G), there are several key differences – (1) wind loading plays a much more significant role for OWTs than for offshore platforms due to wind exposure at higher elevations (particularly during operational conditions) and the large moment arm posed by the tower; (2) the diameter of monopile-supported OWTs is much larger than the foundations used for O&G installations, and consequently design methods based on behavior of smaller diameter, flexible piles (e.g. the *p-y* method for lateral soil-pile interaction) no longer yield accurate results; (3) the majority of foundation loads for O&G platforms are vertical due to coupled action of lattice-type jacket structures under moment loading, whereas monopile-supported OWTs are non-redundant and must withstand large lateral loads and moments; (4) O&G platforms are unique designs which must include life safety precautions, whereas OWTs are installed in the context of several (if not dozens) of similar structures in an array; and (5) OWT project economics necessitate tighter margins on support structure design, leading to more frugal usage of structural material and consequently larger fundamental periods for OWTs than O&G platforms. As a result of these differences, only some of the robust body of research which serves O&G is applicable for the design of OWT support structures.

The non-redundancy and lateral load capacity required by monopile-supported OWTs cause soil-structure interaction to play a major role in OWT support structure design and behavior. Even under best in situ testing and soil sampling practice, there is uncertainty in the characterization of

offshore soil properties. Soil sampling is a challenging and costly pursuit (especially if performed at each proposed OWT location), and therefore the amount of soil information at a given site is often extremely limited. The longer embedment depths of monopiles (often in the range of 20-40 m) provide some design independence from soil property variation with depth, i.e., shallower foundations such as gravity base systems and suction caissons are much more reliant on the soil properties near the surface. It should be noted however that the hammering of monopiles into the seabed during installation is a major environmental concern, not to mention the impacts of decommissioning monopile-supported OWTs on the marine habitat due to artificial reefs which may form during operation.

## 1.3 Dissertation Objectives and Format

This dissertation is subdivided into four primary chapters which stand alone as papers, and consequently the term "paper" and "chapter" are interchangeable within this document. The first paper-chapter has been published in a peer-reviewed journal [9], the second has been submitted and is currently under review, and the third and fourth in preparation for submission.

It is important to note that OWT structural and geotechnical design is often decoupled (meaning that the OWT structure and foundation are designed separately), and it is unclear how much communication there is between the structural and geotechnical design communities during the design process despite the critical contribution of both the foundation to structural behavior and structural dynamics to foundation design. This dissertation fuses structural and geotechnical design by combining programs and models which fit an individual purpose (e.g., cyclic pile foundation behavior, or the structural dynamics of an OWT under operational conditions) via lumped parameter (i.e., reduced-order) modeling in order to best capture the fully-integrated behavior of a monopile-supported OWT.

The objective of this dissertation is first and foremost to reduce structural material costs by introducing a methodology for taking into account foundation damping in OWT design; secondly, this dissertation seeks to better substantiate design and planning decisions by improving understanding of monopile support structure behavior; thirdly, this dissertation provides methodology and narrative for the importance of coupling structural and geotechnical design of OWT support structures. In pursuit of these objectives, the following topics are addressed in the following paper-chapters:

**Foundation damping.** OWTs are lightly damped structures whose natural frequencies are in close proximity to mechanical and wave load frequencies. Of all the sources of OWT damping (structural, hydrodynamic, aerodynamic, foundation, and sometimes tuned mass dampers), the least is known about foundation damping (i.e., the damping associated with soil-structure hysteresis) and no methodology is currently recommended in design guidelines for calculating the contributions of foundation damping to the OWT support structure. Chapter 2 proposes a methodology for calculating viscous mudline dashpot coefficients as a function of hysteretic energy loss, cyclic rotation amplitude, and natural frequency. This methodology allows designers to forego complicated hysteretic analysis by instead including a linear rotational dashpot at the mudline. Including foundation damping into the analysis of monopile-supported OWTs reduces ultimate limit state design loads, thereby providing an opportunity to reduce structural material costs.

**Influence of foundation damping on design.** Because foundation damping is not typically included in OWT design and analysis, the influence of foundation damping on cyclic demand is more broadly assessed in Chapter 3 for the design situations of power production, emergency shutdown, and parked conditions. By quantifying the impact of foundation damping in the analysis of these different design situations, the overall importance of incorporating foundation damping in the design of OWT monopile support structure design is better defined.

**Cyclic degradation of soil properties.** Cyclic loading is of particular concern for foundations in clay, where foundation failure can occur at cyclic amplitudes lower than the monotonic foundation capacity. The serviceability limit state for monopile foundations requires the designer to ensure that the monopile does not exceed a certain rotation limit (typically on the order of 0.25°) as a result of a cyclic loading during the design life of the OWT. The most commonly used lateral pile-soil resistance model is the *p-y* method, wherein lateral soil-pile resistance *p* is represented by a series of nonlinear elastic springs along the length of the pile whose deflection is denoted as *y*. Despite the stringent requirements of the serviceability limit state and the prevalence of the *p-y* method, design guidelines do not recommend the use of the *p-y* method to assess the serviceability limit state because of the impact of initial slope assumptions for the *p-y* curves [10]. Assumedly, a conservative design ensures that the peak amplitude of rotation does not exceed the serviceability limit state; Chapter 3 proposes a novel, elastic-perfectly-plastic hybrid *p-y* method for taking into account the degradation of soil resistance as a function of load cycle and amplitude for clays, as well as a method for estimating permanent mudline rotation. This model is then used to assess the serviceability limit state for extreme storm conditions, as well as the impact of soil property degradation on the natural frequency of the OWT.

**Marine growth.** Marine growth adds mass and thickness to the OWT structure which can lead to decreases in natural frequency, increased surface roughness and effective diameter, and larger hydrodynamic loads. Moreover, marine growth can interfere with corrosion protection systems and fatigue inspections. Some design guidelines recommend an inspection and cleaning schedule for marine growth [10,11], but cleaning off marine growth would negate the potential environmental benefits from artificial reef effect. Chapter 5 discusses marine growth on OWTs from an engineering perspective by quantifying the reduction in natural frequency which may be associated with added mass and the increases in hydrodynamic loading as a function of increased effective diameter and drag. Defining the impact of marine growth from an engineering

perspective facilitates decision-making with regard to the allowable environmental impact posed by monopile-supported OWTs in marine habitats (i.e., whether the benefits of artificial growth outweigh the higher risks of invasive species colonization).

The conclusions and recommendations section (Chapter 6) reprises the results of the studies in the paper-chapters and discusses opportunities for future work in the field of monopile-supported OWTs.

## References


[1] Hamilton, B., Battenberg, L., Bielecki, M., Bloch, C., Decker, T., Frantzis, L., Paidipati, J., Wickless, A., and Zhao, F., 2013, Offshore Wind Market and Economic Analysis: Annual Market Assessment, Navigant Consulting, Inc., Burlington, MA.

[2] Conti, J. J., Holtberg, P. D., Beamon, J. A., Napolitano, S. A., Schaal, A. M., and Turnure, J. T., 2013, Annual Energy Outlook 2013 with Projections to 2040, Washington, D.C.

[3] Musial, W., and Ram, B., 2010, Large-Scale Offshore Wind Power in the United States: Assessment of Opportunitites and Barriers, Golden, CO.

[4] Beaudry-Losique, J., Boling, T., Brown-Saracino, J., Gilman, P., Hahn, M., Hart, C., Johnson, J., McCluer, M., Morton, L., Naughton, B., Norton, G., Ram, B., Redding, T., and Wallace, W., 2011, A National Offshore Wind Strategy: Creating an Offshore Wind Energy Industry in the United States.

[5] Van der Horst, D., 2007, "NIMBY or not? Exploring the relevance of location and the politics of voiced opinions in renewable energy siting controversies," Energy Policy, **35**(5), pp. 2705–2714.

[6] Snyder, B., and Kaiser, M. J., 2009, "Ecological and economic cost-benefit analysis of offshore wind energy," Renew. Energy, **34**(6), pp. 1567–1578.

[7] U.S. Department of Energy, 2008, 20% Wind Energy by 2030: Increasing Wind Energy's Contribution to U.S. Electricity Supply.

[8] Jonkman, J., Butterfield, S., Musial, W., and Scott, G., 2009, Definition of a 5-MW Reference Wind Turbine for Offshore System Development.

[9] Carswell, W., Johansson, J., Løvholt, F., Arwade, S. R., Madshus, C., DeGroot, D. J., and Myers, A. T., 2015, "Foundation damping and the dynamics of offshore wind turbine monopiles," Renew. Energy, **80**, pp. 724–736.

[10] DNV, 2013, DNV-OS-J101 Design of Offshore Wind Turbine Structures, Det Norske Veritas AS.

[11] ABS, 2010, "Offshore Wind Turbine Installations," US Pat. App. 13/318,316, (December).

# CHAPTER 2

# FOUNDATION DAMPING AND THE DYNAMICS OF OFFSHORE WIND TURBINE MONOPILES

## Authors

Carswell, W., Johansson, J., Løvholt, F., Arwade, S. R., Madshus, C., DeGroot, D. J., and Myers, A. T., 2015, "Foundation damping and the dynamics of offshore wind turbine monopiles," *Renew. Energy*, **80**, pp. 724–736.

## Abstract

The contribution of foundation damping to offshore wind turbines (OWTs) is not well known, though researchers have back-calculated foundation damping from "rotor-stop" tests after estimating aerodynamic, hydrodynamic, and structural damping with numerical models. Because design guidelines do not currently recommend methods for determining foundation damping, it is typically neglected. This paper investigates the significance of foundation damping on monopile-supported OWTs subjected to extreme storm loading using a linear elastic two-dimensional finite element model. The effect of foundation damping primarily on the first natural frequency of the OWT was considered as OWT behavior is dominated by the first mode under storm loading. A simplified foundation model based on the soil-pile mudline stiffness matrix was used to represent the monopile, hydrodynamic effects were modeled via added hydrodynamic mass, and 1.00% Rayleigh structural damping was assumed. Hysteretic energy loss in the foundation was converted into a viscous, rotational dashpot at the mudline to represent foundation damping. Using the logarithmic decrement method on a finite element free vibration time history, 0.17% of critical damping was attributed to foundation damping. Stochastic time history analysis of extreme storm conditions indicated that mudline OWT foundation damping decreases the maximum and standard deviation of mudline moment by 8-9%.

## Keywords

Offshore wind turbine; monopile; soil-structure interaction; damping

## Nomenclature

| | |
|---|---|
| $A$ | Amplitude |
| $c_{\theta\theta}$ | Rotational damping constant |
| $C_m$ | Inertia coefficient |
| $C_D$ | Drag coefficient |
| D | Damping factor |
| $E_h$ | Hysteretic energy loss |
| $f$ | Frequency |
| $G$ | Shear modulus |
| $H_x$ | Horizontal mudline shear |
| $k$ | Mudline spring stiffness |
| $k'$ | Decoupled spring stiffness |
| $k_{mud}$ | Mudline stiffness matrix |
| $L_{eq}$ | Rigid decoupling length |
| $M_\phi$ | Mudline moment |
| $n$ | Number of amplitudes |
| $s_u$ | Undrained shear strength |
| $u$ | Mudline displacement |
| $u_{top}$ | Tower top displacement |
| $x$ | Horizontal translation degree of freedom |
| $\alpha$ | Rayleigh mass coefficient |
| $\beta$ | Rayleigh stiffness coefficient |
| $\delta$ | Log decrement |
| $\eta$ | Loss factor |
| $\phi$ | Rotational degree of freedom |
| $\theta$ | Mudline Rotation |
| $\mu$ | Mean |
| $\nu$ | Poisson's ratio |
| $\sigma$ | Standard Deviation |
| $\xi$ | Critical damping ratio |
| $\omega_n$ | Frequency (rad/s) |
| $\Delta$ | Perturbation |
| IEC | International Electrotechnical Commission |
| MSL | Mean sea level |
| NGI | Norwegian Geotechnical Institute |
| NREL | National Renewable Energy Laboratory |
| OWT | Offshore wind turbine |
| LPM | Lumped parameter model |

## 2.1 Introduction

Economics are a major impediment for utility-scale offshore wind installations. Offshore wind farms require large capital investments and can have approximately two to three times the operation and management costs as compared to onshore wind [1]; however, due to higher, more consistent wind speeds, offshore wind farms can offer more renewable energy than their onshore counterparts and it is expected that monopile foundations will continue to have a large market share despite some increase in deployment of larger turbines at greater water depths [2]. For monopiles in deeper water, the dynamic effect of wave loads becomes a design driver for OWT support structures, leading to an increased sensitivity to soil stiffness and damping [2]. Higher damping in the support structure can lead to lower design load estimates, which in turn can correspond to reduced amounts of material required to resist loading. Because support structures contribute approximately 20-25% of the capital cost for OWTs [1, 3], it is imperative therefore to identify and assess sources of damping in the effort to improve the economics of offshore wind energy.

Sources of damping for OWTs include aerodynamic, hydrodynamic, structural, and soil damping. In addition, for some turbines, tuned mass dampers are also installed in the nacelle. Aerodynamic damping occurs when the OWT blades respond to increases and decreases in aerodynamic force due to the relative wind speed from tower top motion [4, 5]. During power production, aerodynamic damping is a dominant source of damping in the fore-aft direction; however, aerodynamic damping is far less significant in the fore-aft direction for parked and feathered rotors or in the side-to-side direction for design situations including wind-wave misalignment [5–7]. During design situations such as these, other sources of damping play a much larger role in the dynamics of the structure. According to an engineering note issued by Germanischer Lloyd [8], soil damping is the contributor to OWT damping that is most uncertain. The International

Electrotechnical Commission states that "Compared with the other components of the total damping discussed, the characterization and modelling of soil damping is the most complex parameter and has a high damping contribution. Soil damping is a diffuse subject and the contribution to energy dissipation here from is not intuitive in all forms [9]." Det Norske Veritas [10] requires that realistic assumptions with regard to stiffness and damping be made in the consideration of OWT soil-structure interaction but does not recommend a method to estimate soil damping.

Soil damping comes in two main forms: radiation damping (geometric dissipation of waves from spreading) or hysteretic material (also known as intrinsic) damping. Geometric dissipation is negligible for frequencies less than 1 Hz [6, 8, 11], and the majority of wind and wave load have frequencies below 1 Hz (e.g. [12, 13]). While the first and second fore-aft and side-to-side natural frequencies of the National Renewable Energy Laboratory 5MW Reference Turbine (NREL 5MW) [15] used in this paper are from 0.3 Hz and 3 Hz, the NREL 5MW under extreme storm loading is dominated by first mode behavior. Because this first mode is at approximately 0.3 Hz, this paper neglects geometric dissipation and focuses solely on hysteretic material damping from soil. This type of soil damping should be more specifically labeled OWT monopile foundation damping (or generally referred to in this paper as "OWT foundation damping") due to the specific formulation and mechanism of hysteretic material soil damping within the OWT soil-structure foundation system.

Some researchers [3, 6, 11, 14] have examined the signals from instrumented OWTs during emergency shutdown (sometimes referred to as a "rotor-stop test"), ambient excitation, and overspeed stops [7] to estimate OWT natural frequency and damping. Subsequently, OWT foundation damping values from 0.25-1.5% have been estimated from the residual damping after aerodynamic, hydrodynamic, structural, and nacelle tuned mass damping have been accounted for in numerical modeling. Previous analytical methods have estimated OWT foundation damping

using Rayleigh damping as a function of soil strain [6] or from a hysteresis loop created by loading and unloading *p-y* curves [11].

A two-dimensional finite element model of NREL 5MW is used in this paper, taking into account added hydrodynamic mass for the substructure, Rayleigh structural damping, and foundation damping. Hydrodynamic and aerodynamic damping are not included in the scope of this paper, as the focus is specifically on the contributions of foundation damping. Because total damping for the OWT is typically estimated as a linear combination of independently modeled damping sources (e.g. [6, 7, 14]), neglecting aerodynamic and hydrodynamic damping is assumed to not influence estimations of foundation damping. Any added mass due to the mobilization of the soil during pile motion is also neglected.

The primary objective of this study is to determine the influence of OWT foundation damping on dynamic response. Section 2.2 describes the methodology, Section 2.3 describes how the foundation stiffness and damping were established, and Section 2.4 describes the combined model of the OWT structure and foundation. In Section 2.5, the percent of critical damping for the NREL 5MW OWT model which can be attributed to foundation damping is quantified via logarithmic decrement method of a free vibration time history and compared to the experimental and numerical results available in literature. Subsequently, in Section 6 stochastic time history analysis corresponding to an extreme sea state and extreme wind conditions is used to determine the significance of OWT foundation damping.

## 2.2 Methodology

The methodology introduced in this paper uses four types of models: a structural model of the OWT superstructure (the part of the OWT that extends above the mudline); a lumped parameter model (LPM) that approximates the soil-pile system with a rigid bar supported by springs at its tip below the mudline and a mudline damper; an aero-hydro-elastic model constructed in the

software package FAST; a continuum finite element model of the soil-pile system. Each of these models provides a different degree of fidelity with respect to different aspects of OWT loading and response and coupling these models in the manner described here allows the determination of wind and wave loads, soil-pile interaction, and structural dynamics in a way that is not possible within any one of the models or attendant software packages.

The flow chart in Figure 2.1 demonstrates the methodology used for determining the linear properties of the lumped parameter model (LPM) which was used to idealize distributed stiffness and damping from the OWT monopile as concentrated stiffness and damping, specifically, a coupled rotational and translational spring and a rotational dashpot. Because soil-pile stiffness and damping are load level-dependent, it was important to ensure that the load level for which the linearized LPM properties were determined was comparable to the load level which the monopile would experience during time history analysis. Several different programs were used in this study and are described in further detail later; the purpose of this section is to demonstrate the interplay of the programs and how they were used to model the OWT support structure.

The primary model of the OWT structure and foundation used for free vibration and stochastic time history analyses was created in the finite element modeling package ADINA [16]. The linearized LPM values, which define the stiffness and damping magnitudes at the mudline of the ADINA model, were iteratively determined as a function of ADINA mudline pile loads using an in-house finite element program created by the Norwegian Geotechnical Institute (NGI) called INFIDEL (INFInite Domain ELement), which models pile-soil interaction without the OWT superstructure [17, 18]. In summary, it was necessary to iterate the linearization process until the input quasi-static loads for determining LPM properties in INFIDEL agreed with the output mudline cyclic load amplitude (horizontal mudline force $H_x$ and mudline moment $M_\phi$) from the time history analysis in ADINA within 5%. Iteration was required because changes in mudline stiffness conditions for the OWT caused changes in the mudline design loads, which supports the

conclusions of other researchers regarding the influence of foundation modeling on mudline loads [19, 20].

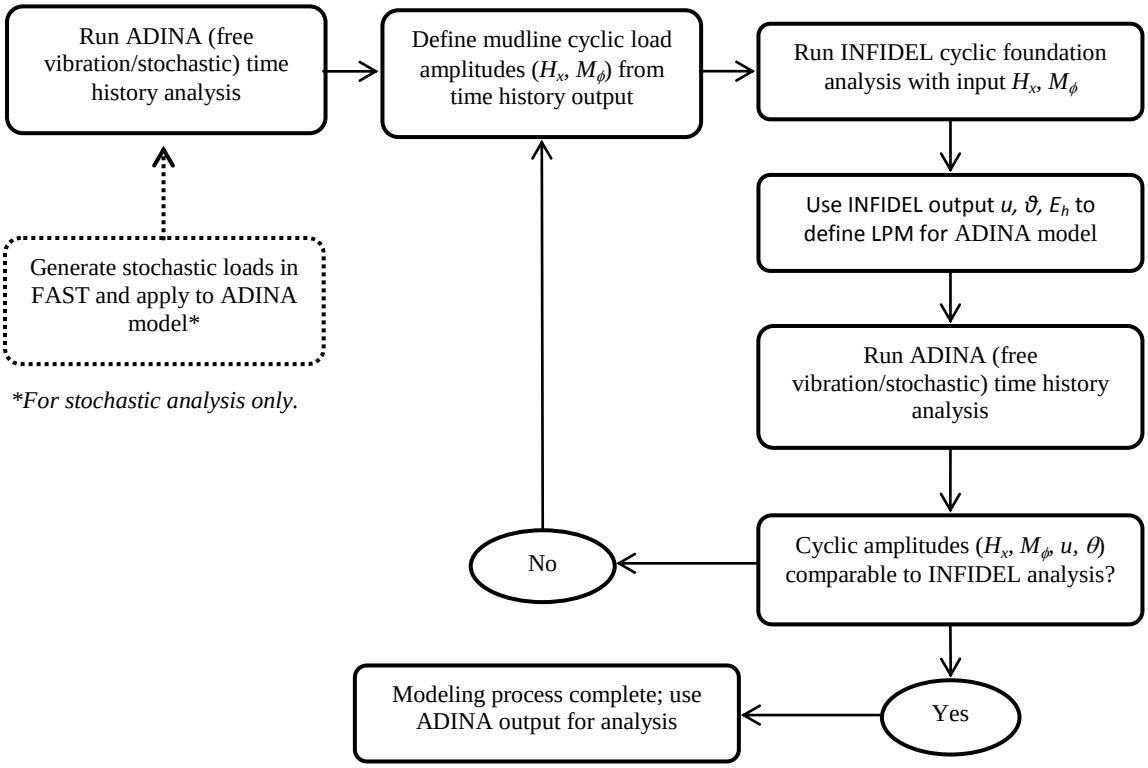


**Figure 2.1 Flow chart illustrating the iterative methodology for modeling an OWT and foundation including a LPM representing the stiffness and damping of the foundation.**

This methodology (Figure 2.1) remains consistent for both the free vibration and stochastic time history analyses, with the exception of load type: for the stochastic time history analyses, the load histories due to wind and wave were generated using NREL's aeroelastic wind turbine simulation program FAST [21] and applied to the ADINA model, whereas free vibration was induced by a tower top displacement directly in ADINA.

The stochastic load time histories generated by FAST were based on a similar structural model as the ADINA model but with a perfectly fixed boundary at the mudline (i.e., no rotation or displacement or damping due to the foundation) and a rigid tower structure. In this way, the loads applied to the ADINA model consist only of external forces and moments induced by wind and

waves on the structure. For design purposes, a second iteration would be required where the mudline stiffness and damping conditions are updated in FAST and new loads would be generated until the loads from FAST, ADINA and INFIDEL converge; however, iteration of the load input was neglected in this study.

## 2.3 Foundation Stiffness and Damping Procedures

First we give a basic background for different relevant damping formulations. Then the INFIDEL software is described followed by the procedures for defining springs and dashpots representing the foundation stiffness and damping.

### 2.3.1 Damping Formulations

As background for the following parts of the paper this section gives a description of three different damping formulations, (1) hysteretic loss, which is used in the foundation (INFIDEL) model, (2) viscous damping, which is used in the LPM representation of foundation damping in the structural model (ADINA) model and (3) Rayleigh viscous damping which is used in the structural (ADINA and FAST) models.

Damping mechanisms for mechanical systems may exhibit different mathematical formulations. According to the dynamic correspondence principle we may interpret the loss factor as the imaginary part of a complex modulus, as here exemplified for the shear modulus *G'* i.e.

$$G' = G(1 + i\eta) \tag{1}$$

Here, *G* is the secant shear modulus of the soil. Formally, the loss factor is proportional to the ratio of the energy dissipation per cycle, $E_h$, divided by the maximum potential energy, $E_p$, in the same cycle. In the case of hysteretic damping, the loss factor $\eta$ may be related to a hysteretic damping factor *D* or quality factor *Q* through the expression

$$\eta = 2D = \frac{1}{Q} = \frac{1}{2\pi}\frac{E_h}{E_p} \quad \textbf{(2)}$$

A sketch showing the interpretation of the energy loss and potential energy in a stress-strain loop is depicted in the right panel of Figure 2.2. The energy loss $E_h$ is interpreted as the area inside the load displacement loop, whereas the potential energy $E_p$ is the area under the triangle.

For a linear single degree of freedom system with a viscous damper (Figure 2.2) subject to a harmonic load, the loss factor relates to the viscous damping constant *c* at a given angular frequency $\omega=2\pi f$ (where f is the frequency) for a spring-dashpot system according to:

$$\eta = \frac{c\omega}{G} \quad \textbf{(3)}$$

Next, we denote the undamped natural frequency $\omega_n$, the critical viscous damping constant $c_{cr}$ and the fraction of critical viscous damping $\xi$ as:

$$\omega_n = \sqrt{\frac{k}{m}}, c_{cr} = 2\sqrt{k \cdot m}, \xi = \frac{c}{c_{cr}} \quad \textbf{(4)}$$

It can be shown that the loss factor equals twice the degree of critical damping at the natural frequency, i.e.

$$\eta = 2\left(\frac{\omega}{\omega_n}\right)\xi \quad \textbf{(5)}$$

In modeling dynamic systems, damping coefficients are often idealized as constants. Hence, using a frequency independent viscous damping constant *c* implies a loss factor that increases linearly with frequency. As will be discussed later, the damping parameters ($\eta$ or *c*) generally also depend on the load. Furthermore, the concept of Rayleigh damping is frequently encountered in dynamic structural analysis, and represents yet another damping formulation where the

damping varies with frequency. For the structural damping in this paper, the fraction of structural critical damping is

$$\xi_{struc} = \frac{\alpha}{2\omega_{n,i}} + \frac{\beta\omega_{n,i}}{2} \quad \textbf{(6)}$$

where $\omega_n$ is the $i^{th}$ natural frequency in rad/s, $\alpha$ is a mass-proportional damping coefficient and $\beta$ is a stiffness-proportional coefficient [22]. All of the different damping formulations above (hysteretic loss, viscous damping, or Rayleigh damping) are present in one or more of the different models which enter the flow chart in Figure 2.1.

As the soil is assumed to have a hysteretic behavior, below we compute a hysteric foundation-energy loss with the INFIDEL model. This hysteric foundation energy loss is converted to a viscous damping constant in the LPM at the mudline of the ADINA structural model. Furthermore, the structural damping in both the ADINA and FAST structural models is formulated using Rayleigh damping. Therefore, it is important to retain the frequency dependency between the different damping formulations while linking them, particularly if the load spectrum we consider has a large bandwidth.

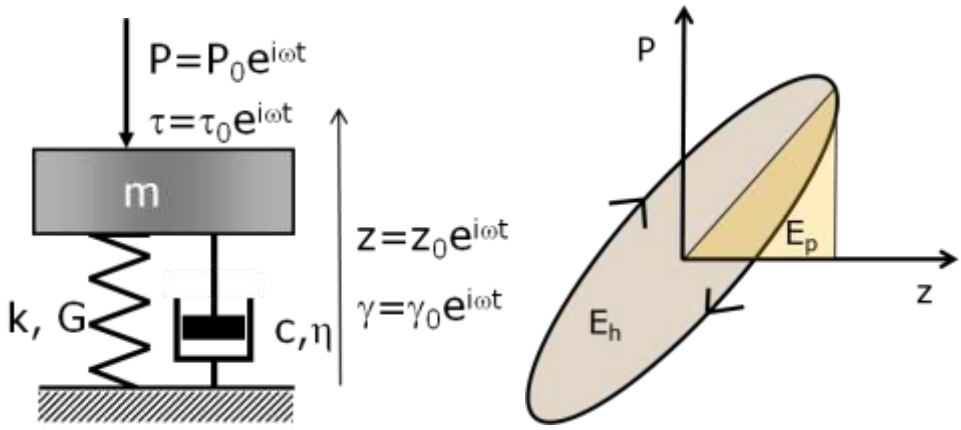


(A) (B)

**Figure 2.2 (A) Sketch of a single degree of freedom spring-dashpot system subject to periodic loading (both force and stress); (B) Sketch showing the interpretation of potential energy and energy loss in a hysteretic loop.**

### 2.3.2 Foundation Response Software

The INFIDEL software is used to compute foundation stiffness and damping which define the LPM at the mudline of the ADINA model. INFIDEL handles axisymmetric 3-dimensional quasi-static soil-structure interaction problems with infinite extent and non-linear materials. Circular or elliptic structures are described by Fourier series expansion in the tangential direction. The cyclic loads on the foundation are applied incrementally to compute cyclic displacement and rotation amplitudes of the foundation.

The monopile is modeled as linear elastic, whereas the material model used for the soil is modeled with an isotropic non-linear elastic constitutive model appropriate for undrained materials such as clay. The input parameters for the soil model are the secant shear modulus at small strains, $G_0$, undrained shear strength, $s_u$, and Poisson's ratio, ν. The shape of the soil stress strain curve is modelled with the following equation

$$\log\left(\frac{G_t}{s_u}\right) = \log\left(\frac{G_0}{s_u}\right) - C_1 \log\left(\frac{\tau_{cy}}{s_u}\right) - C_2 \log\left(\frac{\tau_{cy}}{s_u}\right)^2 - C_3 \log\left(\frac{\tau_{cy}}{s_u}\right)^3 \quad \textbf{(7)}$$

Where $G_t$ is the tangential shear modulus and $\tau_{cy}$ the cyclic shear stress. The three fitting constants, $C_1$-$C_3$, control the shape of the stress strain curve and are determined from a so-called modulus reduction curve giving the ratio of the secant shear modulus to the small strain shear modulus for different cyclic shear strain amplitudes as shown in Figure 2.3(A). For computation of foundation damping the hysteretic material damping factor, *D*, as a function of shear strain is also needed as shown in Figure 2.3(B). The shapes of the modulus reduction and damping curves are dependent on the plasticity index, and to a lesser degree on the confining pressure and over consolidation ratio (OCR). Further description of modulus reduction and damping curves and how they are determined in laboratory tests are given in e.g. [23].

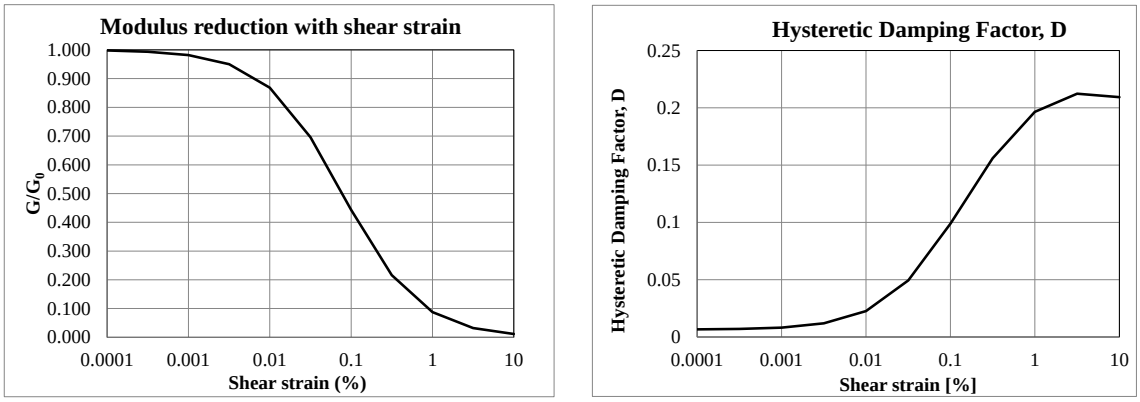


(A) (B)

**Figure 2.3. Examples of (A) the Modulus Reduction curve and (B) the Damping Curve for a representative offshore soil.**

For each load amplitude and corresponding shear strain level in the soil, the hysteretic energy density corresponding to one load cycle (area of hysteresis loop) is computed in each element as

$$E_h = 4\pi E_p D \tag{8}$$

and summed over the entire soil volume to compute a corresponding global foundation damping factor,

$$D = \frac{\Sigma E_h}{4\pi \Sigma E_p} \tag{9}$$

where $E_h$, is the total hysteretic energy for all elements, $E_p$ is the total elastic strain energy for all elements.

### 2.3.3 Foundation Spring Stiffness

Because time history analysis can be computationally demanding, it was desirous to use a reduced-order lumped parameter model (LPM) to represent the OWT monopile foundation stiffness and damping. In an aeroelastic program such as FAST, it is typical to model foundation stiffness as a linear 6×6 stiffness matrix at the mudline; however, it is not often possible to define a stiffness matrix at a point in a finite element program such as ADINA. For this paper, out-of-plane (i.e. side-to-side), vertical, and torsional motions of the OWT were not considered, reducing the mudline stiffness matrix to a 2×2 mudline stiffness matrix

$$k_{mud} = \begin{bmatrix} k_{xx} & k_{x\phi} \\ k_{\phi x} & k_{\phi\phi} \end{bmatrix} \tag{10}$$

in which the subscript $x$ refers to horizontal in-plane translation degree of freedom and the $\phi$ refers to the in-plane rotational degree of freedom. In order to simplify the model by decoupling the stiffness matrix, the off-diagonal coupled stiffness coefficients ($k_{x\phi}$ and $k_{\phi x}$) were kinematically condensed into decoupled horizontal translation ($k_{xx}$') and rotation ($k_{\phi\phi}$') springs located at the end of a rigid bar of length $L_{eq}$ (Figure 2.5). The LPM properties $k_{xx}$', $k_{\phi\phi}$', and $L_{eq}$ were determined using NGI's in-house finite element program INFIDEL.

For a linear elastic stiffness matrix the rigid bar length is

$$L_{eq} = \frac{k_{x\phi}}{k_{xx}}. \tag{11}$$

For a nonlinear foundation behavior, the length $L_{eq}$ can be found with help of two INFIDEL analyses using the same horizontal load but slightly different moments. For a small difference in moment the difference in translation at the mudline will be due to a rotation around a point at distance, $L_{eq}$, below the mudline. Using the perturbation in the moment, $\Delta M_\phi$, $L_{eq}$ is determined by

$$L_{eq} = -\frac{u(H_x, M_\phi) - u(H_x, M_\phi + \Delta M_\phi)}{\theta(H_x, M_\phi) - \theta(H_x, M_\phi + \Delta M_\phi)}. \quad \textbf{(12)}$$

Subsequently, the decoupled spring stiffnesses $k_{xx}'$ and $k_{\phi\phi}'$ can then be calculated as

$$k_{xx}' = k_{xx} = \frac{H_x}{u + L_{eq}\theta} \quad \textbf{(13)}$$

and

$$k_{\phi\phi}' = \frac{M_\phi - L_{eq}H_x}{\theta} \quad \textbf{(14)}$$

### 2.3.4 Foundation Viscous Dashpot

Because the LPM condenses soil-pile interaction, a viscous rotational dashpot was introduced at the mudline to represent concentrated hysteretic damping from cyclic pile-soil interaction. Research has shown that pile head rotation controls mudline serviceability limit states for OWT monopiles [24] and moment typically dominates mudline loading for OWT monopiles, thus the authors believe that a rotational dashpot may more appropriately represent foundation damping than a traditional horizontal translation dashpot. While using both a rotational and translational dashpot is possible, it is not clear that one could decompose the hysteretic energy dissipation in the INFIDEL analysis into parts corresponding to translation and rotation degrees of freedom. Therefore, since a unique solution would not be possible for the parameters of the translational and rotational dashpots, computation of those parameters would depend on some *ad hoc* assumption regarding the partitioning of damping to the rotation and translation degrees of

freedom. Consequently, all foundation damping here has been assigned to the rotational degree of freedom.

The computed hysteretic energy loss ($E_h$) dissipated from a single load cycle in INFIDEL can be converted into a viscous rotation damper. For a harmonic rotation at the mudline to have the same energy loss in the dashpot in one cycle as hysteretic energy loss in the foundation, the dashpot viscous damping constant is computed as

$$c_{\phi\phi} = \frac{E_h}{2\theta_0^2 \pi^2 f} \quad \textbf{(15)}$$

Where $\theta_0$ is the rotation amplitude in radians, and $f$ is the loading frequency, which can be estimated from the Fourier spectrum of the loads. The resulting foundation dashpot coefficient is therefore dependent on 1) the load level (since hysteretic energy, $E_h$, varies with load level), 2) the cyclic rotation amplitude and 3) the vibration frequency. A few iterations between the structural dynamic analysis and foundation analysis may be needed to determine an appropriate dashpot value for a specific load level, rotation amplitude and loading frequency; Figure 2.1 outlines the iterative methodology.

Because the mudline load conditions during free vibration differ from the stochastic time history analysis presented below, different LPMs were developed to more appropriately match the mudline conditions for each type of analysis.

## 2.4 Combined OWT and Foundation Model

The NREL 5MW Reference Turbine (Table 2.1) is used in this paper to quantify the significance of foundation damping for monopile-supported OWTs. A two-dimensional finite element model of the NREL 5MW was created in ADINA, supported by a LPM representing a 34 m-monopile in

clay for a site with an assumed mean sea level (MSL) of 20 m and a hub height of 90 m (Figure 2.5).

The finite element model of the NREL 5MW was defined by elastic Euler-Bernoulli beam elements with linear elastic material properties. The modulus of elasticity for the tower and substructure was assumed to be 210 GPa with a density of 8,500 kg/m$^3$ to account for the additional mass of paint, flanges, bolts, etc. [15]. The OWT model used a lumped mass matrix, with a concentrated mass of 350,000 kg assigned to the top of the finite element model to take into account the mass of the blades and rotor-nacelle assembly. The blades themselves were not modeled because it was assumed that aside from the mass added to the tower top, parked and feathered blades have minimal impact on the natural frequency and damping of the OWT.

**Table 2.1 Offshore Wind Turbine Model Properties**

| Property | NREL 5MW |
|---|---|
| Rating | 5 MW |
| Hub Height | 90 m |
| Rotor Diameter | 126 m |
| Tower Base, Tower Top Diameter | 6.0 m, 3.9 m |
| Nacelle & Rotor Mass | 350,000 kg |
| Tower Mass | 347,000 kg |
| Mean Sea Level | 20 m |
| Substructure Diameter, Wall Thickness | 6.0 m, 0.11 m |
| Pile Diameter, Wall Thickness | 6.0 m, 0.09 m |
| Pile Embedment Depth | 34 m |

The wall thickness for the OWT was increased from the values found in [15] in order to increase the stiffness of the support structure to maintain a natural frequency of approximately 0.3 Hz. Maintaining this natural frequency ensured that the dynamic loading from the FAST model (which was fully fixed at the mudline) was consistent with the dynamic behavior exhibited by the ADINA model (with flexible mudline due to the LPM). A comparison of the ADINA and FAST tower modes and frequencies was performed in order to ensure a consistent dynamic model. The

resulting height distribution of the moment of inertia of the OWT is compared with original NREL model in Figure 2.4.

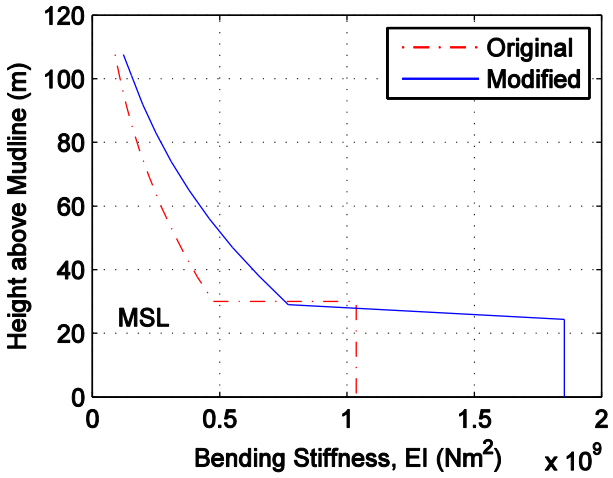


**Figure 2.4 Moment of inertia over support structure height for original vs. modified NREL 5MW reference turbine**

Added hydrodynamic mass was incorporated in the OWT substructure to represent hydrodynamic interaction effects using the simplified method for cylindrical towers proposed by [25]. Added hydrodynamic mass was calculated for each substructure element, divided by cross-sectional area, and included in the unique definition of material density per substructure element.

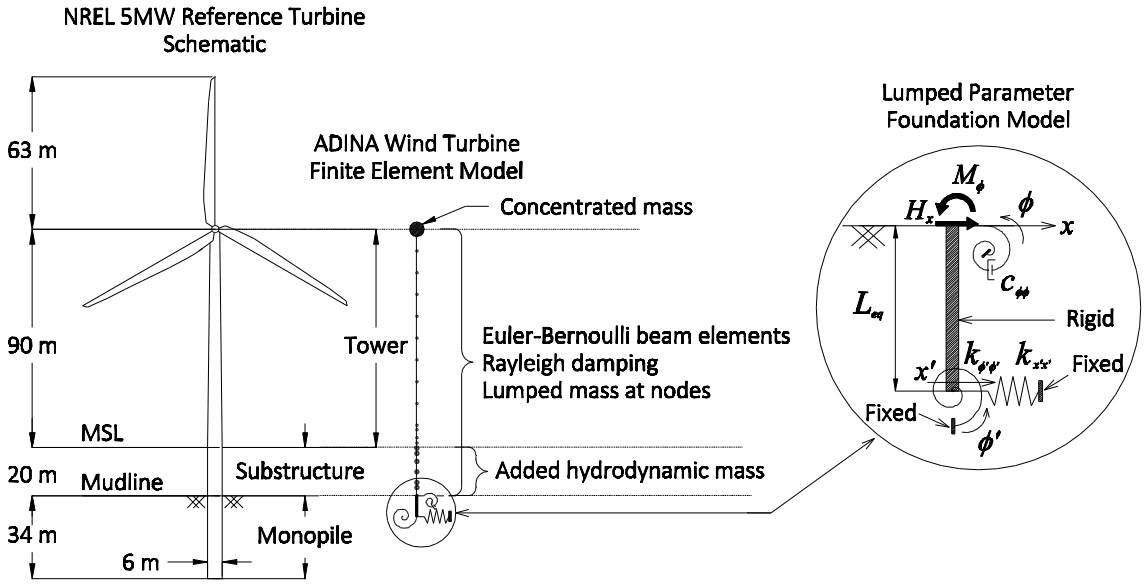


**Figure 2.5 Offshore Wind Turbine Models**

Structural Rayleigh damping of 1.00% was assumed for the NREL 5MW, which is consistent with the definition of the structure in [15]. Structural damping was applied to the tower and substructure of the ADINA finite element model using Rayleigh damping.

Assuming that source of damping can be modeled separately and superimposed (per [6–8, 14]), hydrodynamic and aerodynamic damping were neglected to more precisely focus on the significance of OWT foundation damping.

### 2.4.1 Soil and Foundation Properties

The soil profile considered in this paper was divided into three layers (soft clay, stiff clay, and hard clay) to account for changes in soil parameters with depth (Figure 2.6). Input parameters were based on a specific North Sea offshore site as shown in Figure 2.6. Based on the established soil profile and a loading frequency of 0.3 Hz, curves for shear modulus reduction and damping versus shear strain were established based on equations given in [23] assuming a density of 2000 $kg/m^3$, overconsolidation ratio of 10, and plasticity index of 20 for all layers. In principal, different modulus reduction and damping curves should be used for each layer since modulus reduction depends on confining stress and depth below the mudline. Since the effect of confinement on the modulus and confinement curves is small compared the changes in the shear modulus and shear strength themselves, the same modulus and damping reduction curves have been used for all three layers (Figure 2.3). The resulting stress strain curves for the three layers are shown in Figure 2.7.

When computing the foundation stiffness and damping with INFIDEL, the monopile was assumed to be in full contact with the soil, i.e. effects of gapping due to non-linear compression of the soil on the side of the pile and/or erosion have not been considered. Since gapping would result in a nonlinear and potentially asymmetric foundation stiffness, it could not be modelled using the current approach; however, the mudline displacements identified in this study

(approximately 0.01m) are unlikely to produce a gapping effect. Furthermore the mudline loads (i.e. the horizontal force, *H* and moment, *M*) are assumed to be in phase and were increased proportionally. Figure 2.8 gives an example of INFIDEL results showing the distribution of the ratio between cyclic shear stress and shear strength. The soil in the vicinity of the upper part of the monopile is the most strained and provides the largest contribution to the overall foundation damping.

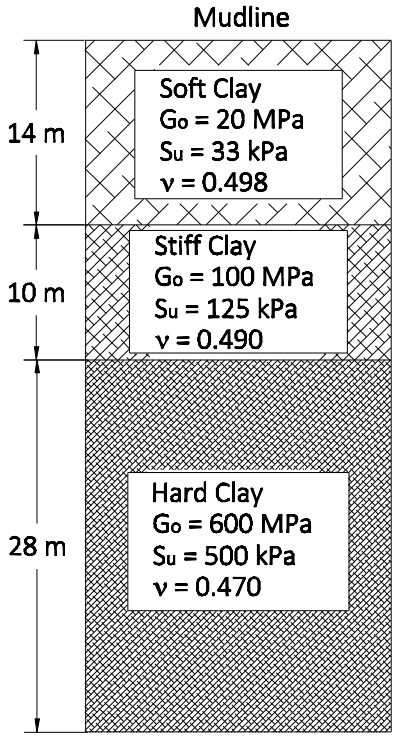


**Figure 2.6 Representative North Sea offshore soil profile used for estimating contributions of foundation damping via INFIDEL**

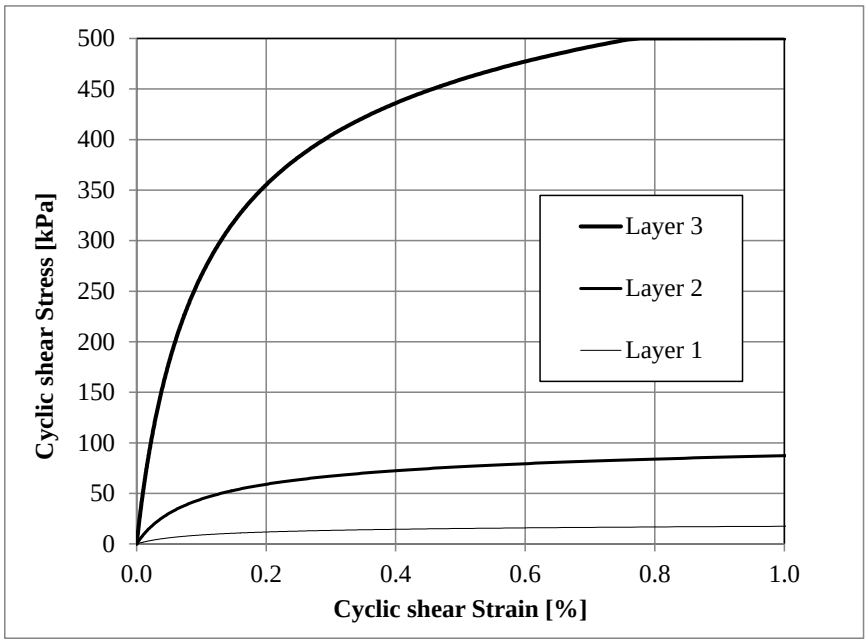


**Figure 2.7. Shear stress versus shear strain for the three different soil layers.**

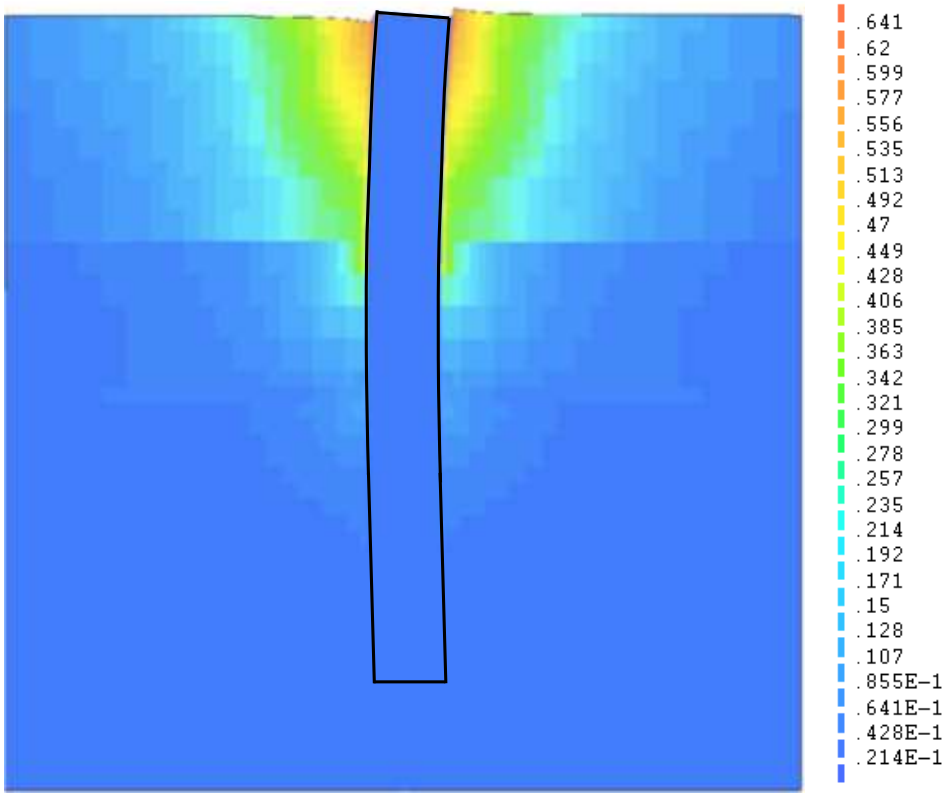


**Figure 2.8 Distribution of shear stress mobilization , i.e. ratio between maximum shear stress and shear strength.**

## 2.5 Free Vibration Analysis

A free vibration analysis was conducted on the NREL 5MW finite element model in ADINA to quantify the contribution of foundation damping to global damping. The free vibration analysis was performed by gradually displacing the tower top by 0.1 m, holding the displacement for 10 seconds to reduce any possibility of transient vibrations, and then releasing the applied displacement to allow the OWT to vibrate freely, see Figure 2.9. The 0.1m displacement was selected to fall in the middle of the range of tower top displacements found to occur during the stochastic time history analysis. Imposing a larger displacement would result in smaller foundation stiffness and larger foundation damping.

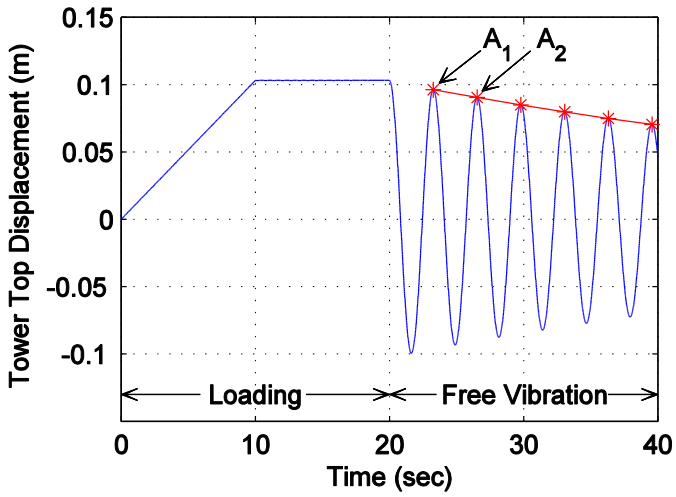


**Figure 2.9 Free Vibration Analysis Time History**

Global damping was then quantified from the free vibration time history using the logarithmic decrement method, where the logarithmic decrement

$$\delta = \frac{1}{n}\ln\left(\frac{A_1}{A_n}\right) \tag{16}$$

in which $A_1$ and $A_n$ are two successive amplitudes $n$ periods apart. A log fit of successive amplitudes was fit to the response to estimate $\delta$. The global damping ratio $\xi$ can then calculated as a function of $\delta$ by

$$\xi = \frac{1}{\sqrt{1 + (2\pi/\delta)^2}} \quad \textbf{(17)}$$

which here estimates the global damping associated with the first structural mode of the OWT.

Rayleigh structural damping was applied to the OWT superstructure and not the LPM, because the concentrated rotational dashpot was considered to account for all foundation related damping. Because Rayleigh damping is a function of natural frequency which is in turn a function of the finite element stiffness matrix, neglecting to apply Rayleigh damping to the LPM resulted in an inaccurate calculation of $\xi_{struc}$ according to Eq. (6). In order to achieve $\xi_{struc}$ = 1.00%, the Rayleigh damping mass coefficient $\alpha$ was held constant while stiffness coefficient $\beta$ was increased such that the damping obtained from the logarithmic decrement of free vibration was equal to 1.00%, with the mudline dashpot $c_{\phi\phi}$ = 0 and $\omega_{n1} = 2\pi f$ per Table 2.3 (as load frequency is equal to natural frequency in the case of free vibration). While this method of Rayleigh damping is only applicable to the first mode of vibration, it is assumed that first mode behavior is dominant for the NREL 5MW turbine.

It is arguable what the appropriate mudline load level is best for assessing linear stiffness and damping for the LPM under free vibration time history analysis (e.g. the maximum, average, or root-mean-square mudline load amplitudes could be used to assess LPM properties). While the maximum mudline load would lead to the lowest mudline stiffness due to non-linear soil-pile resistance, it would also theoretically lead to a higher levels of strain in the soil and consequently the highest amount of damping [23]. To demonstrate the importance of mudline loading on LPM properties, a free vibration case was considered by displacing the OWT tower top by 0.1 m. LPM

properties were calculated based on the static mudline loads induced by tower top displacement, $u_{top}$.

Iteration was required to achieve agreement between the mudline loads specified in the INFIDEL cyclic foundation analysis and the output static displacement load from ADINA as described the methodology section and Figure 2.1. A comparison of the INFIDEL input and ADINA output demonstrates good agreement in load amplitudes and response (see Table 2.2).

**Table 2.2 Comparison of the Peak Mudline Conditions Used in INFIDEL Cyclic Soil-Pile Analysis and ADINA Free Vibration Time History Analysis for 0.1m Tower Top Displacement**

| Parameter | INFIDEL Analysis | Free Vibration in ADINA |
|---|---|---|
| Shear, $H_x$ | 158 kN | 156 kN |
| Moment, $M_\phi$ | -16.0 MNm | -15.9 MNm |
| Displacement, $u$ | $1.19 \times 10^{-3}$ m | $1.28 \times 10^{-3}$ m |
| Rotation, $\theta$ | $-1.52 \times 10^{-4}$ rad | $-1.62 \times 10^{-4}$ rad |
| Load Frequency, $f$ | - | 0.307 Hz |
| Hysteretic Energy Loss, $E_h$ | 0.130 kJ | - |
| Foundation Damping Factor, $D$ | 0.79% | - |
| Structural Damping Ratio, $\xi_{struc}$ | - | 1.00% |
| Foundation Damping Ratio, $\xi_{fdn}$ | - | 0.17% |

The results in Table 2.2 were used as input to Eqs. 11-14 in order to obtain the LPM properties in Table 2.3.

**Table 2.3 Lumped Parameter Foundation Model Properties for ADINA Free Vibration Analysis for 0.1m Tower Top Displacement**

| Lumped Parameter Model Property | $u_{top}$ = 0.1 m |
|---|---|
| $L_{eq}$ | 7.60 m |
| $k_{xx}$' | $3.89 \times 10^{9}$ N/m |
| $k_{\phi\phi}$' | $1.14 \times 10^{11}$ Nm/rad |
| $c_{\phi\phi}$ | $9.34 \times 10^{8}$ Nm-s/rad |

An example of the 0.1 m free vibration time history from ADINA for the NREL 5MW finite element model is shown in Figure 2.10.

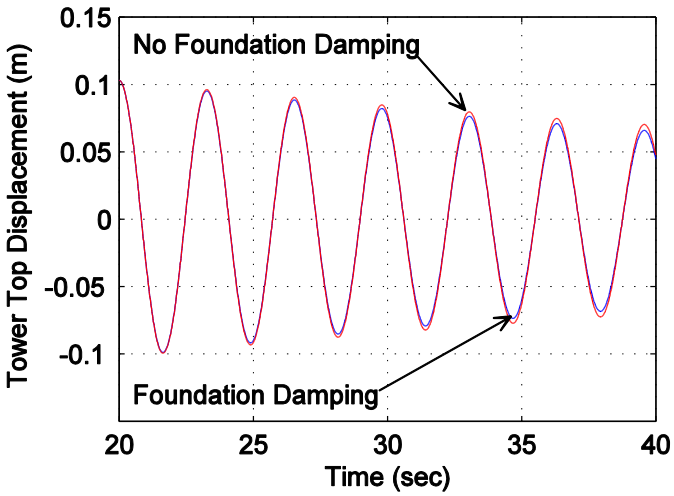


**Figure 2.10 Free Vibration of the NREL 5MW Reference Turbine, with and without Foundation Damping**

It can be visually concluded from Figure 2.10 that the inclusion of mudline foundation damping effects tower top vibration, with the damped mudline vibration amplitude decreasing slightly faster than the case considering only structural damping. From the logarithmic decrement method, the damping ratio from the $u_{top}$ = 0.1 case was $\xi_{tot}$ = 1.17% – subtracting the 1.00% Rayleigh structural damping ($\xi_{struc}$), this means that 0.17% of damping can be attributed to foundation damping ($\xi_{fdn}$). The LPM calculations and resulting $\xi_{struc}$ are sensitive to input load level; if the free vibration analysis is repeated for a tower top displacement of $u_{top}$ = 0.16 m for instance, $\xi_{struc}$ increases to 0.28%.

Table 2.4 compares the results of the free vibration study and of other foundation damping studies for OWTs. The results of the current analysis yield a relatively low amount of foundation damping compared to the damping found by other researchers, but are similar to the experimental results estimated by Shirzadeh *et al*. (2011) [7], Damgaard *et al.* (2012) [14] and to the minimum of the range defined by Tarp-Johansen *et al.* (2009) [6]. The majority of the researchers provide free vibration response of the OWT in terms of acceleration; however, in the case of [3], the loads at the bottom of the tower would indicate rough agreement with the mudline loads analyzed in this paper.

**Table 2.4 Summary of Monopile-Supported Offshore Wind Turbine Damping Results from Literature**

| | **Tarp-Johansen *et al.* (2009)** | **Versteijlen *et al.* (2011)** | **Damgaard *et al.* (2012)** | **Damgaard *et al.* (2013)** | **Shirzadeh *et al.* (2013)** | **Carswell *et al.* (2014)** |
|---|---|---|---|---|---|---|
| **Method** | Experimental | Experimental | Experimental | Experimental | Experimental | Numerical |
| **Analysis** | 3D FEM | Modified *p-y* | Hysteretic *p-y* | Hysteretic *p-y* | HAWC2, Rayleigh | 3D and 2D FEM |
| **Turbine** | 3.5 MW (Scaled NREL 5MW) | Siemens 3.6MW | - | Vestas V90-3MW | Vestas V90-3MW (Scaled NREL 5MW) | NREL 5MW |
| **Soil Profile** | Generalized sandy or clayey North Sea | - | Top layer loose sand, very stiff to very hard clay | Medium dense sand and soft clay | Dense sand with layer of stiff clay | Soft, stiff, and hard clay |
| $\xi_{fdn}$ | 0.56%-0.80% | 1.5% | 0.58% | 0.8-1.3% | 0.25% | 0.17%-0.28% |
| $\xi_{struc}$ | 0.19% | 1.5% | 0.19% | - | 0.6% | 1.00% |
| **Sum:** | 0.75-0.99% | 3.0% | 0.77% | 0.8-1.3% | 0.85% | 1.17%-1.28% |

Several different methods were used to estimate foundation damping, so it is unsurprising that a variation in results was observed. Damgaard *et al.* (2012) and (2013) [8, 11] used a hysteretic *p-y* method, wherein a hysteretic loop was defined using a traditional *p-y* spring-supported pile per [10], whereas Versteijlen *et al.* (2011) [3] used modified *p-y* curves adjusted for rigid-behavior monopiles with damping proportional to spring stiffness. Minimal description of the soil modeling was given in Shirzadeh *et al.* (2013) [7], only that a form of Rayleigh damping was used to apply damping as part of the input for the aeroelastic code HAWC2. Most similarly to the process used in this paper, Tarp-Johansen *et al.* (2009) [6] estimated foundation damping from a three dimensional solid finite element model of the soil and OWT support structure, assuming generalized linear elastic soil material properties. Soil damping was taken into account as a form of Rayleigh damping, assuming a loss factor of 10%.

Germanischer Lloyd [8] experimentally determined a foundation damping value of 0.53%, theoretically calculated foundation damping of 0.88%, but also lists estimations from 0.6%-1% depending on soil behavior assumptions. It can be concluded therefore that a certain amount of variation in OWT foundation damping should be expected, and that these results are sensitive to modeling assumptions.

## 2.6 Stochastic Time History Analysis

### 2.6.1 Load Input

The finite element model of the NREL 5MW Reference Turbine was subjected to six different 1-hr stochastic load histories corresponding to extreme wave and wind loading to determine the effects of OWT foundation damping on the OWT response.

NREL's aeroelastic code FAST [21] was used to generate stochastic time history loads due to wind and waves. FAST models wind turbines as a system of rigid and flexible bodies and computes wind turbine response to stochastic loading using lumped parameter and modal analysis [26]. The OWT loads were calculated per IEC design load case 6.1a [9] using the environmental site conditions shown in Table 2.5.

**Table 2.5 Environmental Site Conditions**

| 50-year Conditions | Value |
|---|---|
| Water Depth | 20 m |
| 10-min Average Hub Height Wind Speed | 34 m/s |
| Significant Wave Height | 8.5 m |
| Peak Spectral Wave Period | 10.3 s |

IEC dictates that for design load case 6.1a, six 1-hr simulations for different combinations of extreme wind speed and extreme sea state must be performed considering misalignment and multi-directionality. This study considers six 1-hr load time histories with co- and uni-directional wind and waves, which is conservative from a design perspective; however, it is assumed that co-

and uni-directional loading will best demonstrate the effects of OWT foundation damping in a two-dimensional, parked wind turbine context.

Wind loading was applied to the NREL 5MW finite element model in ADINA via tower top force and moment histories generated in FAST, and wind loads on the tower were neglected (Figure 2.11). Tower wind loads are not directly calculated by FAST (version 7, available during the conduct of this study), and were thus excluded from all of the modeling included here to preserve consistency with FAST. If tower wind loads were included in the analysis mudline moment and shear would increase, the stiffness of the foundation would decrease and the amount of foundation damping would increase. Wind speed is assumed to increase with height according to a power law, causing a net negative moment (according to a right-hand rule sign convention, per Figure 2.11) around the nacelle due to wind on the parked and feathered rotors due to their configuration with a single blade pointed upward.

Wave kinematics were generated in FAST at seven nodes along the OWT structure. Wave forces per unit length were calculated from the wave kinematics using Morison's equation for a cylinder multiplied by a tributary length to approximate the wave shear profile (Figure 2.11). A fluid density of 1027 kg/m$^3$ was assumed for seawater and $C_m$ and $C_D$ were taken to be 1.75 and 1.26 respectively for a substructure with intermediate surface roughness.

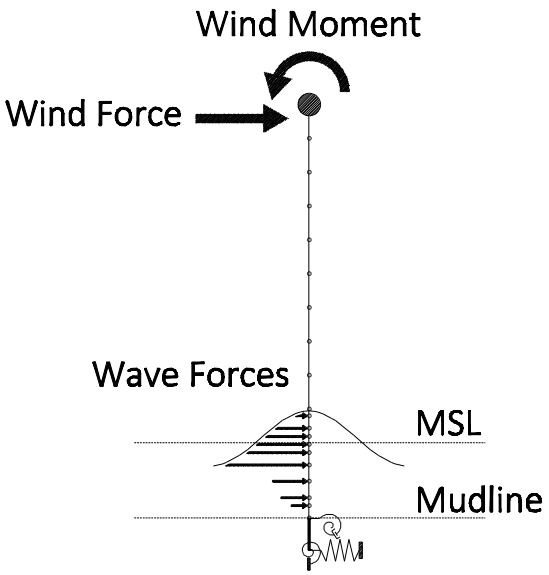


**Figure 2.11 Example Time Step of Wave Force Loading on ADINA NREL 5MW Finite Element Model**

Because the viscous mudline dashpot $c_{\phi\phi}$ was derived for a single degree of freedom system subjected to harmonic loading and because the actual loading of an OWT is stochastic, it was necessary to establish a harmonic load amplitude that was in some sense representative of the load amplitudes experienced during the stochastic loading. The load amplitude level selected was three standard deviations (3σ, Figure 2.12) from the mean of the stochastic loading history. This load amplitude appeared to best represent the amplitude of the stochastic loading – the 3σ limit is only exceeded by the most severe load cycles – and had little variation across the six 1-hr stochastic time histories. Due to the iteration required, only one of the 1-hr stochastic time history was used for determining LPM properties for the six simulations (Figure 2.12).

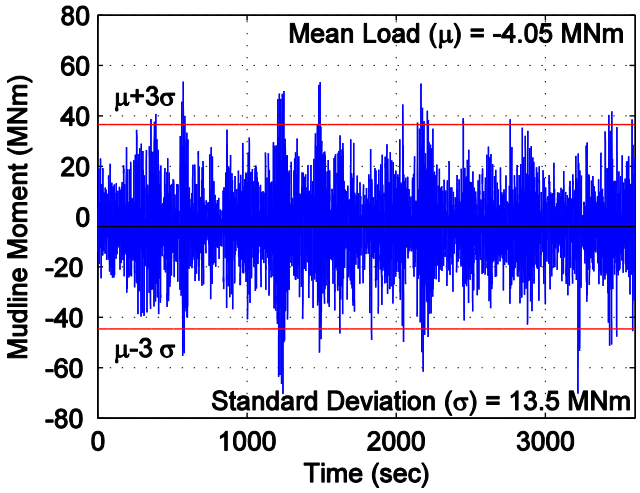


**Figure 2.12 Time History of Mudline Moment Indicating Three Standard Deviation Amplitude**

Several iterations were required to obtain mudline load and rotation amplitudes which agreed with those used in cyclic foundation analysis. Table 2.6 compares the load and response amplitudes of the single stochastic time history to those from the cyclic foundation analysis. The resulting LPM properties are given in Table 2.7.

**Table 2.6 INFIDEL Foundation Analysis and ADINA Stochastic Time History Analysis Results**

| Mudline Condition | INFIDEL Foundation Analysis | Damped Mudline Stochastic Time History (3σ) |
|---|---|---|
| Shear, $H_x$ | 2610 kN | 2606 kN |
| Moment, $M_\phi$ | -41.2 MNm | -40.5 MNm |
| Displacement, $u$ | $6.45 \times 10^{-3}$ m | $6.73 \times 10^{-3}$ m |
| Rotation, $\theta$ | $-6.23 \times 10^{-4}$ rad | $-6.55 \times 10^{-4}$ rad |
| Dominant Load Frequency, $f$ | - | 0.302 Hz |
| Hysteretic Energy Loss, $E_h$ | 7.61 kJ | - |
| Foundation Damping Factor, $D$ | 2.88% | - |
| Structural Damping Ratio, $\xi_{struc}$ | - | 1.00% |
| Foundation Damping Ratio, $\xi_{fdn}$ | - | 0.72% |

**Table 2.7 Lumped Parameter Foundation Model Properties for Stochastic Time History Analysis**

| Lumped Parameter Model Property | Value |
|---|---|
| $\boldsymbol{L_{eq}}$ | 9.12 m |
| $\boldsymbol{k_{xx}'}$ | $3.38 \times 10^{9}$ N/m |
| $\boldsymbol{k_{\phi\phi}'}$ | $1.04 \times 10^{11}$ Nm/rad |
| $\boldsymbol{c_{\phi\phi}}$ | $3.29 \times 10^{9}$ Nm/s |

Logarithmic decrement of the OWT model supported by the LPM properties in Table 2.7 yielded $\xi_{fdn}$ of 0.72%, which is significantly larger than the results from the 0.1 m free vibration analysis (0.17%). The higher damping is due primarily to the increase in $E_h$ associated with the higher load levels (-41.2 MNm for the 3σ stochastic results vs. -16.0 MNm for the 0.1 m free vibration analysis).

### 2.6.2 Stochastic Time History Results

Six different 1-hr stochastic load histories were analyzed for the NREL 5MW for two cases: (1) Rayleigh structural damping alone ("No Foundation Damping") and (2) Rayleigh structural damping in addition to mudline OWT foundation damping ("Foundation Damping") for a total of 12 stochastic time histories. The reduction in mudline moment amplitude attributed to foundation damping can be seen in the example time history shown in Figure 2.13.

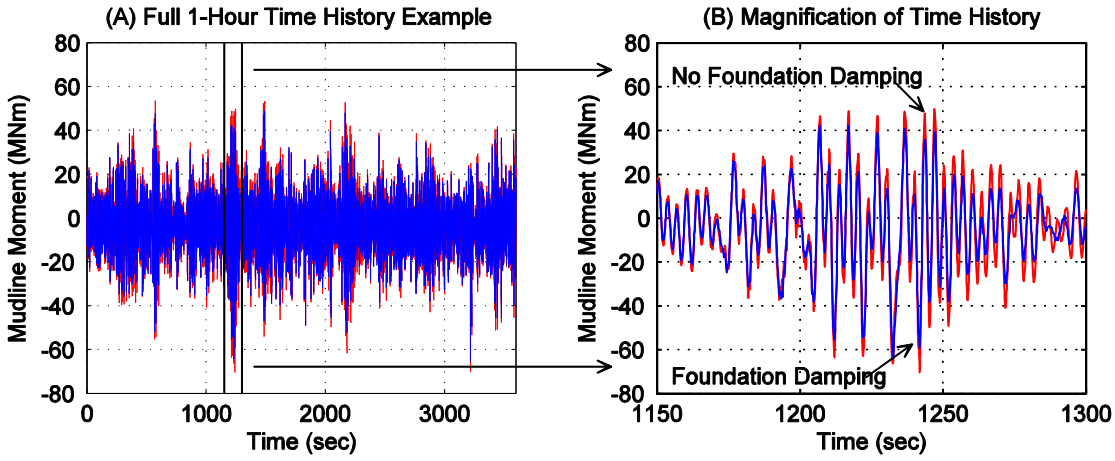


**Figure 2.13 Example Mudline Moment Time History Results**

A summary of the maximum and standard deviation of mudline load and displacement amplitudes as well as maximum tower top amplitude $u_{top}$ from each time history can be seen in Table 2.8.

While mudline moment and shear were highly correlated (the average correlation coefficient was approximately 0.8), mudline moment was more significantly reduced by foundation damping than

mudline shear (Table 9). A decrease in wind or wave force is magnified by the length of the moment arm to the mudline; consequently, a small decrease in OWT support structure forces results in a non-proportional decrease at the mudline. Notably, both maximum mudline moments as well as the 3σ estimation of cyclic moment amplitude decreased by an average of 7-9% due to foundation damping; additionally, it can be noted from Table 2.8 that the standard deviation of mudline moment decreased by nearly 10% with the inclusion of foundation damping.

**Table 2.8 Maximum and Standard Deviation of Mudline Reactions**

| | | Time History | | | | | | Statistics | |
|---|---|---|---|---|---|---|---|---|---|
| **Case** | **Reaction** | **1** | **2** | **3** | **4** | **5** | **6** | **Average** | **% change** |
| **No Foundation Damping** | $H_x$ (kN) | 4229 | 3963 | 4388 | 3881 | 4025 | 4110 | 4099 | - |
| | $\sigma$(kN) | 864 | 880 | 861 | 850 | 894 | 896 | 874 | - |
| | $M_\phi$(MNm) | -70.5 | -60.5 | -74.0 | -60.4 | -71.5 | -77.2 | -69.0 | - |
| | $\sigma$(MNm) | 13.5 | 13.2 | 12.9 | 13.5 | 13.9 | 14.1 | 13.5 | - |
| | $u$ ($10^{-3}$ m) | 11.9 | 9.9 | 12.5 | 10.1 | 11 | 12.4 | 11.3 | - |
| | $\sigma$ ($10^{-3}$ m) | 2.24 | 2.25 | 2.21 | 2.23 | 2.33 | 2.34 | 2.27 | - |
| | $\theta$ ($10^{-4}$ rad) | -11.6 | -9.71 | -12.2 | -9.87 | -10.9 | -12.2 | -11.1 | - |
| | $\sigma$ ($10^{-4}$ rad) | 2.18 | 2.18 | 2.14 | 2.17 | 2.26 | 2.27 | 2.20 | - |
| | $u_{top}$ (m) | 0.322 | 0.272 | 0.261 | 0.321 | 0.309 | 0.322 | 0.301 | - |
| | $\sigma$(m) | 6.49 | 6.15 | 5.97 | 6.50 | 6.60 | 6.72 | 6.41 | - |
| **Foundation Damping** | $H_x$ (kN) | 4232 | 3863 | 4213 | 3769 | 3962 | 4009 | 4008 | -2.2 |
| | $\sigma$(kN) | 864 | 880 | 861 | 850 | 894 | 896 | 874 | 0 |
| | $M_\phi$(MNm) | -65.5 | -56.5 | -70.8 | -55.6 | -61.7 | -70.0 | -63.3 | -8.2 |
| | $\sigma$(MNm) | 12.1 | 12.1 | 12.0 | 12.2 | 12.8 | 12.8 | 12.3 | -8.8 |
| | $u$ ($10^{-3}$ m) | 11.4 | 9.52 | 11.9 | 9.23 | 10.9 | 11.8 | 10.8 | -4.4 |
| | $\sigma$ ($10^{-3}$ m) | 2.15 | 2.18 | 2.15 | 2.14 | 2.25 | 2.27 | 2.19 | -3.5 |
| | $\theta$ ($10^{-4}$ rad) | -11.0 | -9.13 | -11.7 | -8.97 | -10.6 | -11.5 | -10.5 | -5.4 |
| | $\sigma$ ($10^{-4}$ rad) | 2.08 | 2.10 | 2.07 | 2.07 | 2.17 | 2.20 | 2.11 | -4.1 |
| | $u_{top}$ (m) | 0.258 | 0.249 | 0.257 | 0.291 | 0.274 | 0.287 | 0.269 | -10 |
| | $\sigma$($10^{-2}$ m) | 5.48 | 5.34 | 5.32 | 5.51 | 5.73 | 5.78 | 5.53 | -14 |

Mudline displacement and rotation amplitudes decreased similarly with foundation damping, with an average reduction of 3-4% in the 3σ estimation of cyclic amplitude and 5-6% in the average maximum from the six time histories.

**Table 2.9 Summary of Average and Maximum Reduction in Mudline Response from Foundation Damping, Considering Time History Maxima and Three Standard Deviation Estimation of Cyclic Amplitude**

| | Cyclic Amplitude, 3σ | | Maximum Response | |
|---|---|---|---|---|
| **Mudline Response** | **Average Reduction** | **Maximum Reduction** | **Average Reduction** | **Maximum Reduction** |
| $H_x$ (kN) | 0.48% | 0.52% | 2.2% | 4.0% |
| $M_\phi$ (MNm) | 8.9% | 10% | 7.2% | 9.3% |
| $u$ ($10^{-3}$ m) | 3.4% | 4.0% | 4.5% | 8.6% |
| $\theta$ ($10^{-4}$ rad) | 3.9% | 4.7% | 5.5% | 9.1% |

A rainflow count of mudline moment from all six stochastic analyses was performed to further quantify the effect of foundation damping on load cycle amplitudes (Figure 2.14). The rainflow counts indicate reductions (note that the vertical axis is a log scale) in cycle counts across the range of cycle amplitudes. This indicates that foundation damping may serve to reduce fatigue damage. This effect requires substantial further study, however, since the 50-year storm conditions investigated here do not occur frequently and do not contribute significantly to lifetime fatigue damage. Fatigue damage estimates, therefore, would require simulation of response over a range of operational and non-operation wind speeds amounting to at least many tens of sets of simulations. Such work is the subject of ongoing research on the part of the authors.

For loading frequencies closer to the natural frequency, the juxtaposition of load frequency and natural frequency content would produce a more pronounced reduction in higher amplitude cycles. Figure 2.15 depicts the relationship between the Kaimal and JONSWAP power density spectra for wind and waves (respectively) and the ratio of dynamic amplification factors for the cases with ($R_{d,tot}$) and without foundation damping ($R_{d,struc}$) included, where

$$R_d = \frac{1}{\sqrt{\left(1-\omega^2/\omega_n^2\right)^2 + \left(2\xi\omega/\omega_n\right)^2}} \quad \textbf{(8)}$$

in which ω is the loading frequency and $\omega_n$ is the natural frequency in rad/s. A free vibration analysis of the NREL 5MW supported by the LPM defined by Table 2.7 yielded $\xi_{fdn}$ = 0.72%, which broadly agreed with the results presented earlier given the amplitudes of $u_{top}$, $u$, and $\theta$.

Despite the difference in damping ratio for the two cases considered (1.72% and 1.00% for the cases with and without foundation damping, respectively), the ratio of dynamic amplification factors considering a 0.1 Hz wave load frequency is effectively 1. Given Figure 2.15a, it is apparent that the tails of the wind and wave spectra coincide with the dynamically amplified region, and that increased frequency content from higher wave frequency (i.e., lower peak spectral period) would have a significant effect on mudline loading. An examination of Fast Fourier Transforms (Figure 2.15b) of the mudline moment for the stochastic time histories with and without foundation damping demonstrated a 40% reduction in the magnitude of the spectral response at the first natural frequency (for which the foundation was calculated). Similarly, estimation of OWT natural frequency in a design context is inherently uncertain and dependent on available data and modeling techniques; in turn, the sensitivity of the load amplification is reliant on the accurate estimation of both OWT natural frequency and load frequency spectra.

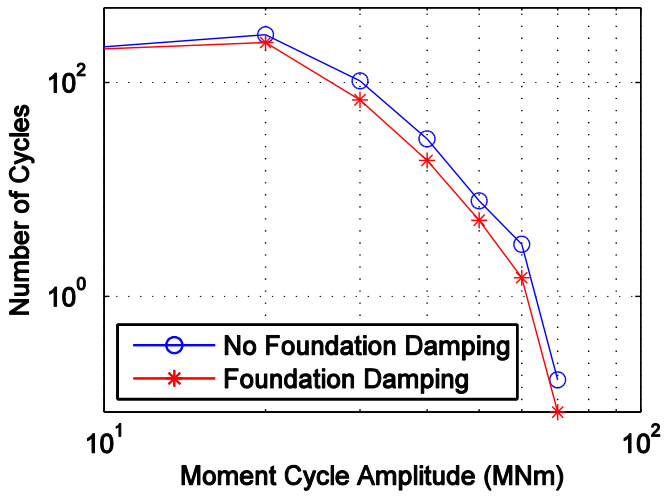


**Figure 2.14 Average Rainflow Count Results of Mudline Moment from Six Stochastic Time History Simulations**

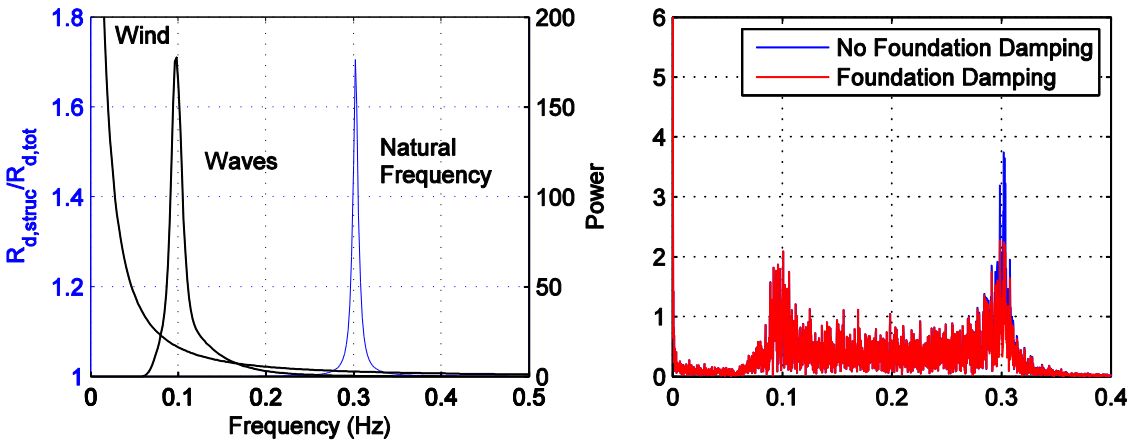


**Figure 2.15 (a) Ratio of Dynamic Amplification Factors for Cases With and Without Foundation Damping Compared to Load Spectra and (b) spectral response with and without foundation damping.**

## 2.7 Conclusion

The proximity of wind and wave load frequencies to offshore wind turbine (OWT) natural frequency necessitates a thorough examination of different sources of damping – aerodynamic, hydrodynamic, structural, and soil damping – in order to reduce design loads and improve offshore wind energy economics. Of all the sources of damping, soil damping has been the least studied and presents the largest discrepancy between measured and theoretical results [8]. Because the effect of soil damping on OWT dynamics is innately a function of soil-pile interaction, a more appropriate term for this dynamic quantity is "foundation damping." In an effort to better quantify foundation damping, this paper presents a method for converting hysteretic energy loss into a viscous, rotational mudline dashpot to represent OWT foundation damping for a lumped parameter model (LPM).

A two-dimensional finite element model of the NREL 5MW Reference Turbine [15] was examined in free vibration and stochastic time history in order to ascertain the significance of OWT foundation damping. Using logarithmic decrement, mudline OWT foundation damping was estimated to contribute 0.17% of critical damping to total OWT damping. While these results are

at the lower end of the range of results from other researchers [6, 7, 11, 14], they are broadly in agreement with previous estimates of foundation damping, taking into account differences in soil type, monopile foundation, wind turbine, and mudline load conditions.

The mudline response from six 1-hr stochastic time histories was used to assess the significance of OWT foundation damping during extreme loading due to wind and waves. Three standard deviations ($3\sigma$) were used as a measure of cyclic amplitude for mudline response (i.e., shear, moment, displacement, and rotation) and to determine the properties of the LPM. Logarithmic decrement of the $3\sigma$ LPM (Table 2.7) yielded 0.72% critical damping from the monopile foundation, which was significantly larger than the free vibration results primarily due to the increase in hysteretic energy. Including OWT foundation damping reduced maximum mudline moment by 9%, but had a much less significant effect on mudline shear (approximately 2% reduction). Foundation damping caused an average reduction of approximately 3-5% in both the maximum and $3\sigma$ amplitudes of mudline displacement and rotation. The results shown here emphasize the importance of modeling assumptions in foundation damping estimation, with particular attention to the mudline loads used in this paper to determine the properties of the LPM.

Significant reductions in high amplitude cycle counts were observed considering the average rainflow count of mudline moment from the six stochastic time histories. These results are contingent upon the estimation of OWT natural frequency and environmental load conditions, and the effects of foundation damping are expected to be more pronounced in conditions with peak wave frequencies closer to the natural frequency.

Further research is required to determine the impact of foundation damping on OWTs during other design conditions (operation or emergency shutdown, e.g.) as well as the significance of foundation damping in a fatigue limit state.

Further investigation is necessary to understand the influence of the many aspects of soil behavior on the foundation stiffness and damping, e.g. dilative materials, such as dense sand, partially drained materials, scour and gapping that can cause loss of contact between foundation and soil, and combined static and cyclic loading.

## Acknowledgements

This research was supported through the NSF-sponsored IGERT: Offshore Wind Energy Engineering, Environmental Science, and Policy (Grant Number 1068864) as well as grants CMMI-1234560 and CMMI-1234656 and the Norwegian Geotechnical Institute.

## References

[1] W. Musial and B. Ram, "Large-Scale Offshore Wind Power in the United States: Assessment of Opportunitites and Barriers," Golden, CO, 2010.

[2] M. Seidel, "Substructures for offshore wind turbines Current trends and developments," 2014.

[3] W. Versteijlen, A. Metrikine, J. Hoving, E. Smid, and W. de Vries, "Estimation of the vibration decrement of an offshore wind turbine support structure caused by its interaction with soil," in *EWEA Offshore Conference*, 2011.

[4] D. J. Salzmann and J. van der Tempel, "Aerodynamic Damping in the Design of Support Structures for Offshore Wind Turbines," in *Paper of the Copenhagen Offshore Conference*, 2005.

[5] V. Valamanesh and A. Myers, "Aerodynamic Damping and Seismic Response of Horizontal Axis Wind Turbine Towers," *J. Struct. Eng.*, 2014.

[6] N. J. Tarp-Johansen, L. Andersen, E. Christensen, C. Mørch, B. Kallesøe, and S. Frandsen, "Comparing Sources of Damping of Cross-Wind Motion," in *European Offshore Wind 2009: Conference & Exhibition: 14-16 September*, 2009.

[7] R. Shirzadeh, C. Devriendt, M. a. Bidakhvidi, and P. Guillaume, "Experimental and computational damping estimation of an offshore wind turbine on a monopile foundation," *J. Wind Eng. Ind. Aerodyn.*, vol. 120, pp. 96–106, Sep. 2013.

[8] GL WindEnergie, "Overall Damping for Piled Offshore Support Structures, Guideline for the Certification of Offshore Wind Turbines," Germanischer Lloyd WindEnergie, 2005.

[9] IEC 61400-3, “Design Requirements for Offshore Wind Turbines,” Brussels, 2009.

[10] DNV, “DNV-OS-J101 Design of Offshore Wind Turbine Structures,” Det Norske Veritas AS, 2013.

[11] M. Damgaard, J. Andersen, I. LB, and L. Andersen, “Time-Varying Dynamic Properties of Offshore Wind Turbines Evaluated by Modal Testing,” in *Proceedings of the 18th International Conference on Soil Mechanics and Geotechnical Engineering*, 2013, pp. 2343–2346.

[12] B. Petersen, M. Pollack, B. Connell, D. Greeley, D. Davis, C. Slavik, and B. Goldman, “Evaluate the effect of turbine period of vibrations requirements on structural design parameters,” Groton, CT, 2010.

[13] D. Lombardi, S. Bhattacharya, and D. Muir Wood, “Dynamic soil–structure interaction of monopile supported wind turbines in cohesive soil,” *Soil Dyn. Earthq. Eng.*, vol. 49, pp. 165–180, Jun. 2013.

[14] M. Damgaard, J. Andersen, L. B. Ibsen, and L. Andersen, “Natural Frequency and Damping Estimation of an Offshore Wind Turbine Structure,” in *Proceedings of the Twenty-second International Offshore and Polar Engineering Conference*, 2012, vol. 4, pp. 300–307.

[15] J. Jonkman, S. Butterfield, W. Musial, and G. Scott, “Definition of a 5-MW Reference Wind Turbine for Offshore System Development Definition of a 5-MW Reference Wind Turbine for Offshore System Development,” 2009.

[16] “ADINA.” ADINA R&D, Inc., Watertown, MA, 2014.

[17] O. E. Hansteen and K. Höeg, “Soil-Structure Interaction Analysis of Embedded Caisson Anchor Under Tension Load,” in *BOSS ’94, 7th International Conference on the Behavior of Offshore Structures*, 1994, pp. 49–62.

[18] NGI, “Description of INFIDEL - a non-linear, 3-D finite element program,” 1991.

[19] E. Bush and L. Manuel, “Foundation models for offshore wind turbines,” in *47th AIAA Aerospace Sciences Meeting Including the New Horizons Forum and Aerospace Exposition*, 2009, no. January.

[20] L. V. Andersen, M. J. Vahdatirad, M. T. Sichani, and J. D. Sørensen, “Natural frequencies of wind turbines on monopile foundations in clayey soils—A probabilistic approach,” *Comput. Geotech.*, vol. 43, pp. 1–11, Jun. 2012.

[21] J. Jonkman and M. J. Buhl, “FAST User’s Guide,” Golden, CO, 2005.

[22] A. K. Chopra, *Dynamics of Structures: Theory and Applications to Earthquake Engineering*, 3rd ed. Upper Saddle River, NJ: Pearson Prentice Hall, 2007.

[23] M. Darendeli, *Development of a new family of normalized modulus reduction and material damping curves*. Austin, TX: University of Texas at Austin, 2001.

[24] W. Carswell, S. R. Arwade, D. J. Degroot, and M. A. Lackner, "Probabilistic Analysis of Offshore Wind Turbine Soil-Structure Interaction," University of Massachusetts Amherst, 2012.

[25] A. Goyal and A. Chopra, "Simplified evaluation of added hydrodynamic mass for intake towers," *J. Eng. Mech.*, vol. 115, no. 7, pp. 1393–1412, 1989.

[26] J. F. Manwell, J. G. McGowan, and A. L. Rogers, *Wind Energy Explained*, 2nd ed. New York: John Wiley & Sons, Ltd., 2009.

# CHAPTER 3

# INFLUENCE OF FOUNDATION DAMPING ON OFFSHORE WIND TURBINE MONOPILE CYCLIC LOAD DEMANDS

## Authors

W Carswell, SR Arwade, DJ DeGroot

## Abstract

Offshore wind turbines (OWTs) are lightly damped structures that must withstand highly uncertain offshore wind and wave loads. In addition to stochastic load amplitudes, the dynamic behavior of OWTs must be designed with consideration of stochastic load frequency from waves and mechanical load frequencies associated with the spinning rotor during power production. The close proximity of the OWT natural frequency to excitation frequencies combined with light damping necessitates a thorough analysis of various sources of damping within the OWT system; of these sources of damping, least is known about the contributions of damping from soil-structure interaction (foundation damping). This paper analyzes the influence of foundation damping on cyclic load demand for monopile-supported OWTs considering the design situations of power production, emergency shutdown, and parked conditions. The NREL 5MW Reference Turbine was modeled using the aero-hydro-elastic software FAST considering the environmental conditions off the U.S. Atlantic coast near Delaware and included linear mudline stiffness and damping matrices to take into account soil-structure interaction. Foundation damping was modeled using viscous rotational mudline dashpots which were calculated as a function of hysteretic energy loss, cyclic mudline rotation amplitude, and OWT natural frequency. Comparing the results from time history analysis including and excluding foundation damping, the results indicated that foundation damping can reduce cyclic load demand during parked

conditions by as much as 30%. Average reductions in cyclic demand during emergency shutdown ranged from 2-8%, but only by 2-3% average reduction for power production situations.

## Nomenclature

| | |
|---|---|
| DE | Delaware |
| DLC | Design load case |
| DNV | Det Norske Vertitas |
| ESS | Extreme Sea State |
| ETM | Extreme Turbulence Model |
| EWH | Extreme Wave Height |
| EWM | Extreme Wind Model |
| EWS | Extreme Wind Shear |
| IEC | International Electrotechnical Commission |
| NGI | Norwegian Geotechnical Institute |
| NOAA | National Ocean and Atmospheric Administration |
| NREL | National Renewable Energy Laboratory |
| NSS | Normal Sea State |
| NTM | Normal Turbulence Model |
| OWT | Offshore wind turbine |
| RWH | Reduced Wave Height |
| RWM | Reduced Wind Model |
| SSS | Severe Sea State |
| SWH | Severe Wave Height |
| TI | Turbulence intensity |
| ULS | Ultimate limit state |
| $c_{mud}$ | Mudline damping matrix |
| $c_{\phi\phi}$ | Mudline rotational dashpot |
| $f$ | Natural frequency |
| $g$ | Acceleration due to gravity |
| $k_{mud}$ | Mudline stiffness matrix |
| $k_{xx}$, $k_{yy}$ | Horizontal translational stiffness |
| $k_{x\phi}$ | Coupled stiffness term |
| $k_{\phi\phi}$ | Rotational stiffness |
| $s_u$ | Undrained shear strength |
| $u$ | Cyclic amplitude of mudline displacement |
| $v_{in}$, $v_{rated}$, $v_{out}$ | Cut-in, rated, cut-out wind speed |
| $x$ | Horizontal degree of freedom in fore-aft direction |
| $y$ | Horizontal degree of freedom in side-to-side direction |
| $z$ | Vertical degree of freedom |
| $E$ | Modulus of elasticity |
| $E_h$ | Hysteretic energy loss |
| $E[\cdot]$ | Expected value |
| $G_0$ | Shear modulus at small strains |
| $H$ | Wave height |
| $H_s$ | Significant wave height |
| $H_{N\text{-}yr}$ | $N$-year wave height |
| $H_x$ | Cyclic amplitude of horizontal mudline force |

| | |
|---|---|
| $M_\phi$ | Cyclic amplitude of mudline moment |
| $T_p$ | Peak spectral period |
| $U_{10,hub}$ | 10-minute hub height wind speed |
| $U_{hub}$ | Hub height wind speed |
| $\phi$ | Rotational degree of freedom |
| $\theta$ | Cyclic amplitude of mudline rotation |
| $\nu$ | Poisson's ratio |
| $\rho$ | Density |
| $\sigma$ | Standard deviation |
| $\psi$ | Wave height reduction factor |

## 3.1 Introduction

Nearly one-quarter of the capital cost of offshore wind farms can be attributed to the foundation and support structure of offshore wind turbines (OWTs) [1]. OWT support structures are lightly damped and must withstand highly uncertain offshore wind and wave loads with stochastic load frequency and amplitude in addition to stochastic mechanical loads associated with the spinning rotor during power production. OWTs are typically designed in a so-called "soft-stiff" frequency design regime, wherein the first natural frequency is designed to lie between the 1P and 3P blade rotation frequency bands. Because a stiffer structure implies higher costs (due to increased structural material requirements), it is desirable for the first natural frequency to be near, but safely above the 1P frequency band (DNV suggests a clearance of ±10% of blade rotation frequency bands [2]). The close proximity to excitation frequencies combined with the low amount of damping present in the support structure necessitates a thorough analysis of various sources of damping within the OWT system (structural, hydrodynamic, aerodynamic, soil-foundation interaction, and sometimes tuned mass damper). Increased damping reduces structural demand, which consequently reduces structural material requirements and therefore reduces material costs.

Damping arising from soil-foundation interaction (referred to as foundation damping here) is typically neglected in OWT design, as there is no recommended method to determine foundation damping in design guidelines [2,3]. Foundation is the least understood of all these sources of

damping, and there is no consensus on its importance in an OWT design context with respect to the other sources of damping [3–6]. Previous work [3] indicated that for a monopile-supported OWT subjected to extreme storm loads, cyclic mudline demand (i.e., cyclic design loads for the pile foundation) can be reduced by as much as 10% when foundation damping is included in the analysis.

The purpose of this paper is to determine the impact of including foundation damping in OWT design and analysis for power production, emergency stop, and parked storm conditions, and in doing so assess the importance of including foundation damping in OWT design and analysis. Because nearly 75% of currently installed OWTs are supported by monopile foundations [1], this paper focuses exclusively on monopile foundation damping. Studies have shown that radiation damping is negligible for frequencies below 1 Hz [4,5,7], thus this paper only considers the contribution of hysteretic material damping from pile-soil interaction. The NREL 5MW Reference Turbine ("NREL 5MW") [8] was analyzed using the open-source aeroelastic simulation program FAST [9], considering the IEC 61400-3 design load cases (DLCs) [10] to dictate wind, wave, and turbine conditions. Soil-structure interaction was modeled in FAST via mudline stiffness and damping matrices which were calculated using the results from the soil-pile software INFIDEL (INFIinite Domain of Elements) [11,12] developed by the Norwegian Geotechnical Institute (NGI). The NREL 5MW was analyzed considering the layered clay site described by [3] and the environmental site conditions from the National Ocean and Atmospheric Administration (NOAA) buoy sited off the coast of Delaware in the U.S. Atlantic Ocean.

Section 3.2 illustrates the analysis process used to determine the influence of foundation damping on cyclic mudline demand, with further discussion of how mudline stiffness and damping matrices were calculated, the DLCs selected for analysis, and how each design situation (power production, emergency shutdown, and parked) was modeled in FAST (Figure 3.1). Section 3.3 describes the OWT model in which was used to determine monopile loads and the calculation of

the mudline stiffness matrix ($k_{mud}$). The paper concludes with a presentation of the results in Section 3.4 and conclusions and recommendations in Section 3.5.

## 3.2 Methodology

Several different methods are used in the analysis process of this paper (Figure 3.1) to define the impact of foundation damping on cyclic mudline demand. Each DLC was analyzed using the aeroelastic offshore wind turbine simulation code FAST [9] (further described in Section 3.3.1) assuming a perfectly fixed connection of the substructure to the mudline to estimate cyclic mudline load amplitudes (i.e. cyclic demand) for horizontal mudline force $H_x$ and moment $M_\phi$. Section 3.2.1 describes how each of the DLCs was modeled in FAST. These values were then used to find the cyclic mudline displacement $u_x$, rotation $\theta_\phi$, and hysteretic energy loss $E_h$ associated with the load level ($H_x$, $M_\phi$) acting on the soil-pile system using INFIDEL for a clay soil profile (described in Section 3.3.2). The mudline stiffness matrix $k_{mud}$ was then determined using $H_x$, $M_\phi$, $u_x$, and $\theta_\phi$, further described in Section 3.2.2. Given $k_{mud}$, new tower mode shapes and frequencies were calculated using the NREL-distributed program BModes [13], leading to new sixth-order polynomial coefficients to define tower mode shape in the tower property input file for FAST. The first fore-aft tower frequency was assumed to dominate for all time histories and was used in conjunction with the mudline rotation $\theta_\phi$ and hysteretic energy loss $E_h$ to compute a viscous mudline dashpot, $c_{\phi\phi}$ (Section 3.2.2). Two versions of the OWT model were analyzed for each DLC, one version including the mudline dashpot $c_{\phi\phi}$ ("DAMPED" in Figure 3.1) and one without ("UNDAMPED"), to determine the amplitude of cyclic mudline loads, displacements, and rotations. The impact of foundation damping was assessed by measuring the reduction in cyclic demand resulting from the undamped and damped models.

Because the analysis process (Figure 3.1) required to define the impact of foundation damping on cyclic OWT monopile design loads is relatively time-consuming, the DLCs were grouped

according to similar hysteretic energy loss $E_h$ and $k_{mud}$. One set of FAST executables with representative $k_{mud}$ (with and without mudline foundation damping) was compiled for each of these groups (Table 3.6). The mudline stiffness matrix in the FAST executable used for each group did not differ by more than 10% from the originally calculated $k_{mud}$ for the cyclic load amplitude per DLC and design condition (e.g. yaw misalignment angle or wind speed). In the event that input and output mudline cyclic load amplitude ($H_x$, $M_\phi$) differed by more than 20% from the fixed-base FAST analysis to the flexible-base FAST analysis, a second mudline stiffness matrix $k_{mud}$ was calculated and the flexible-base FAST analysis was repeated.

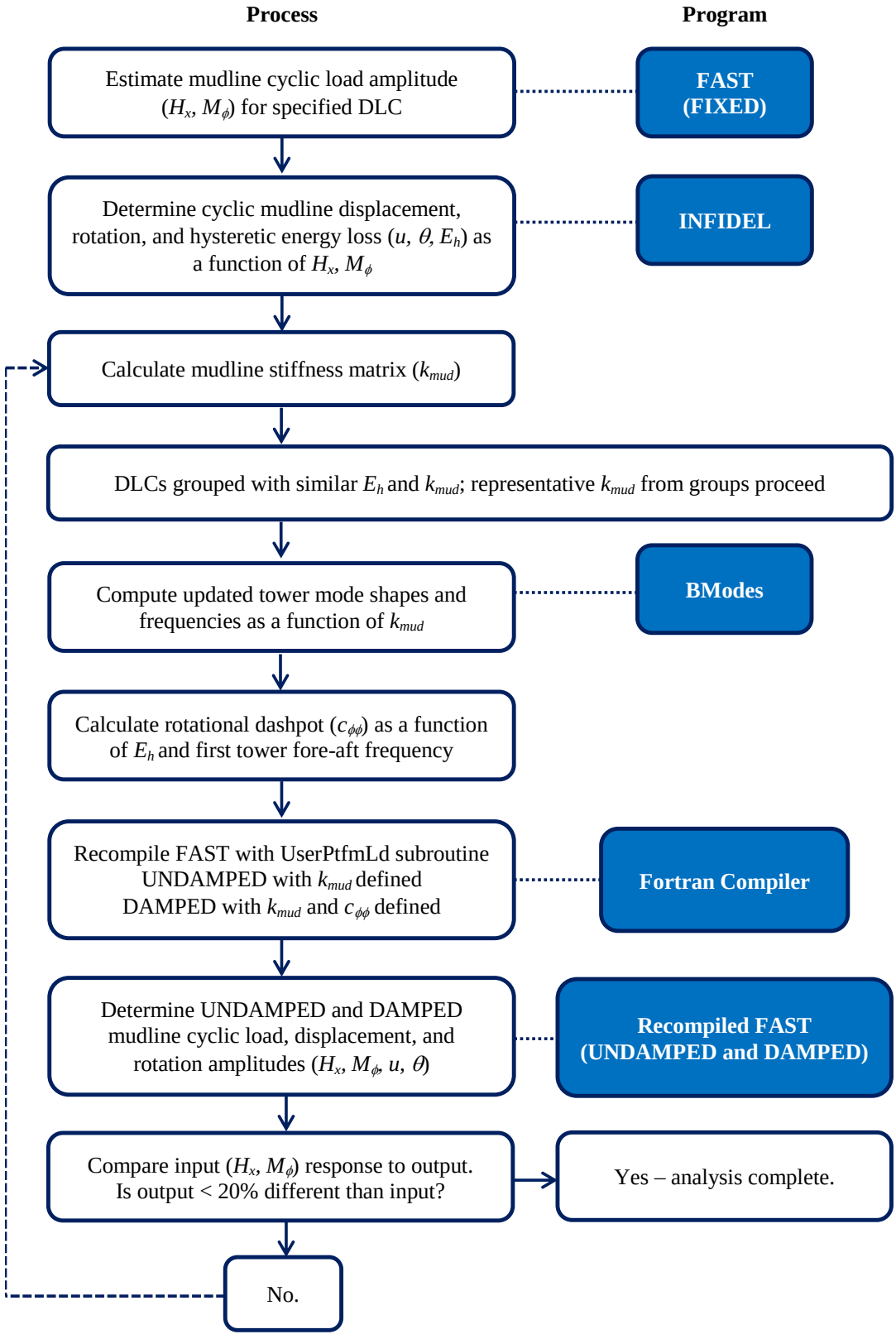


**Figure 3.1 Flowchart of foundation damping analysis process**

### 3.2.1 Offshore Wind Turbine Design Load Cases

The design load cases (DLCs) described in the OWT design standard IEC 61400-3 [10] issued by the International Electrotechnical Commission (IEC) are accepted by the OWT design community and form the basis for the vast majority of OWT designs [2,14]. These DLCs are subdivided into design situations including power production, power production plus occurrence of fault, start up, normal shutdown, emergency shutdown, parked (standing still or idling), parked and fault conditions, and transport, assembly, maintenance and repair. These DLCs are meant to inform the design of all aspects of the OWT, and consequently not all are influential in the design of the support structure and foundation.

In order to more broadly assess the significance of foundation damping in a design load context, DLCs were selected from the design situations of power production, emergency shutdown, and parked (extreme storm loading) which the authors believe broadly encompass the ultimate limit state (ULS) loads which may control structural and foundation design for monopile-supported OWTs (Table 3.1).

Fatigue limit states were considered outside the scope of this paper, as the primary objective is to define the impact of foundation damping on cyclic mudline design loads for the foundation rather than to examine the fatigue life of the structure. Wind-wave misalignment (as studied by [5]) was considered to be more significant in the assessment of OWT fatigue life and consequently wind and waves were assumed to act co-directionally in one direction for all DLCs.

**Table 3.1 IEC offshore wind turbine design load cases analyzed**

| Design Situation | Load Case | Wind Speed | Wave Height | Yaw Misalignment | Limit State |
|---|---|---|---|---|---|
| 1) Power production | 1.1 | NTM $v_{in} < U_{10,hub} < v_{out}$ TI = 11% | NSS $H_s = E[H_s\|U_{10,hub}]$ | 0˚ | ULS |
| | 1.3 | ETM $v_{in} < U_{10,hub} < v_{out}$ TI = 16% | NSS $H_s = E[H_s\|U_{10,hub}]$ | 0˚ | ULS |
| | 1.5 | EWS $v_{in} < U_{10,hub} < v_{out}$ | NSS $E[H_s\|U_{10,hub}]$ | 0˚ | ULS |
| | 1.6a | NTM $v_{in} < U_{10,hub} < v_{out}$ TI = 11% | SSS $H_s = H_{s,50\text{-}yr}\|U_{10,hub}$ | 0˚ | ULS |
| | 1.6b | NTM $v_{in} < U_{10,hub} < v_{out}$ TI = 11% | SWH $H = H_{50\text{-}yr}$ | 0˚ | ULS |
| 5) Emergency Shut Down | 5.1 | NTM $v_{rated}$, $v_{out}$ ± 2m/s TI = 11% | NSS $E[H_s\|U_{10,hub}]$ | 0˚ | ULS |
| 6) Parked Conditions | 6.1a | EWM $U_{hub} = U_{10,50\text{-}yr}$ TI = 11% | ESS $H_s = H_{s,50\text{-}yr}$ | ± 8˚ | ULS |
| | 6.1c | RWM $U_{hub} = 1.1U_{10,50\text{-}yr}$ | EWH $H = H_{50\text{-}yr}$ | ± 15˚ | ULS |
| | 6.2a | EWM $U_{hub} = U_{10,50\text{-}yr}$ TI = 11% | ESS $H_s = H_{s,50\text{-}yr}$ | ± 180˚ | ULS Abnormal |
| | 6.2b | EWM $U_{hub} = 1.4U_{10,50\text{-}yr}$ | RWH $H = \psi H_{50\text{-}yr}$ | ± 180˚ | ULS Abnormal |

**KEY**: NTM = Normal Turbulence Model; ETM = Extreme Turbulence Model; Extreme Wind Shear; RWM = Reduced Wind Model; EWM = Extreme Wind Model; NSS = Normal Sea State; SSS = Severe Sea State; SWH = Severe Wave Height; ESS = Extreme Sea State; EWH = Extreme Wave Height; RWH = Reduced Wave Height; TI = Turbulence Intensity; ULS = Ultimate Limit State; $v_{in}$ = cut-in wind speed; $v_{out}$ = cut-out wind speed; $U_{10,hub}$ = hub height wind speed (10-min average); $v_{rated}$ = rated wind speed; $U_{hub}$ = hub height wind speed; $U_{10,50\text{-}yr}$ = 50-year hub height wind speed (10-min average); $H_s$ = significant wave height; $H_{s,50\text{-}yr}$ = 50-year significant wave height; $H$ = wave height; $\psi$ = wave height reduction factor.

The details of how these DLCs were implemented in FAST are described below, as well as reasoning for the omission of any ULS or ULS Abnormal DLC within the selected design situations. The output of the FAST analyses considered in this paper are horizontal mudline force, moment, displacement, and rotation.

#### *3.2.1.1 Power Production*

Power production DLCs are relevant for wind speeds within the cut-in and cut-out wind speeds (3 m/s and 25 m/s for the NREL 5MW, respectively [8]). In controlling load cases for cyclic mudline load amplitudes, only the rated and cut-out wind speed cases were examined in this paper. The only ULS case omitted from the power production DLCs was DLC 1.4, as it was believed that the extreme direction change was primarily a test of the OWT controls and not of the integrity of the support structure.

Power production DLCs were run in FAST using the simple pitch control and variable speed control provided in the user-defined subroutines. A Thevenin generator model was assumed.

The wave heights for the power production DLCs are conditional upon wind speed and were defined per Section 3.3.1. With the exception of DLC 1.5, all power production DLCs use the Normal Turbulence Model (NTM) and thus the average cyclic load amplitude per design condition (i.e. wind speed bin) was taken from six 10-min time history simulations. It should be noted that due to computational expense, only the rated and cut-out wind speed bins were considered.

The Extreme Wind Shear (EWS) in DLC 1.5 was used with a steady (non-turbulent) wind input file in FAST, considering only vertical wind shear. Horizontal wind shear is not defined in FAST steady wind input files and was thus neglected here. Because the steady wind input file is only capable of modeling linear or power law wind shear, the power law wind shear exponent defined for EWS was taken as the average estimated power law exponent over the rotor disk for each second of the 12 second transient EWS event [2].

The first 60 seconds of every time history was discarded in order to avoid noise from analysis start-up (i.e., the effects of wind and waves interacting with a static OWT at the beginning of the analysis).

#### *3.2.1.2 Emergency Shutdown*

Emergency shutdown occurs when a safety supervisor system within the OWT shuts down the operation of the turbine to prevent damage; a robust consideration of emergency shutdown effects for OWTs can be found in [15]. For the purposes of this paper, a simplified version of the emergency shutdown procedure described in [15] was modeled as follows:

- The generator was turned off at $t$ = 200 s into the time history simulation.
- Pitch control was overridden at $t$ = 200 s and the blades were set to feather (90˚ blade pitch for the NREL 5MW) at the rated limit of 8˚/sec [8].
- The simple HSS brake was then applied 0.6 s after the blade pitch reached 90˚, which is the time it takes the NREL 5MW brake to fully engage after deployment [8].

The emergency shutdown case used the same wind field and wave trains as DLC 1.1. Similar to the power production DLCs, the first 60 seconds of the emergency shutdown time histories was ignored in analysis.

#### *3.2.1.3 Parked Conditions*

The parked DLCs were all modeled considering parked (i.e, nonrotating) blades which were feathered to 90˚, with the exception of the ULS Abnormal cases which used a blade pitch of 0˚ due to loss of electrical network connection (and assumedly therefore loss of pitch control).

The first 30 seconds of the parked DLC time histories was discarded in analysis.

### 3.2.2 Mudline Stiffness and Damping

The mudline stiffness matrix $k_{mud}$ is analyzed two-dimensionally here, assuming that the soil-pile system is radially symmetric (i.e., axisymmetric about the $z$-axis, such that the horizontal translational stiffness in the $x$-direction is the same as the $y$-direction).

Horizontal mudline force $H_x$ and moment $M_\phi$ and the associated mudline displacement $u$ and rotation $\theta$ were required to calculate $k_{mud}$. These mudline loads ($H_x$, $M_\phi$) were determined for each

DLC to be representative of the cyclic load amplitude, as cyclic soil behavior for clays is more influenced by cyclic amplitude rather than maximum response [16]. For regular wave train and steady wind DLCs, estimating cyclic load amplitude was straightforward (due to the periodic nature of the time history output, half of the difference between maximum and minimum response); for stochastic time histories (with irregular wave trains or turbulent wind fields), these loads were estimated as three times the standard deviation of the response ($3\sigma$) similar to previous work on foundation damping [3]. The definition of the cyclic amplitude influences the calculations of stiffness and damping – higher cyclic amplitudes lead to higher damping but lower stiffness.

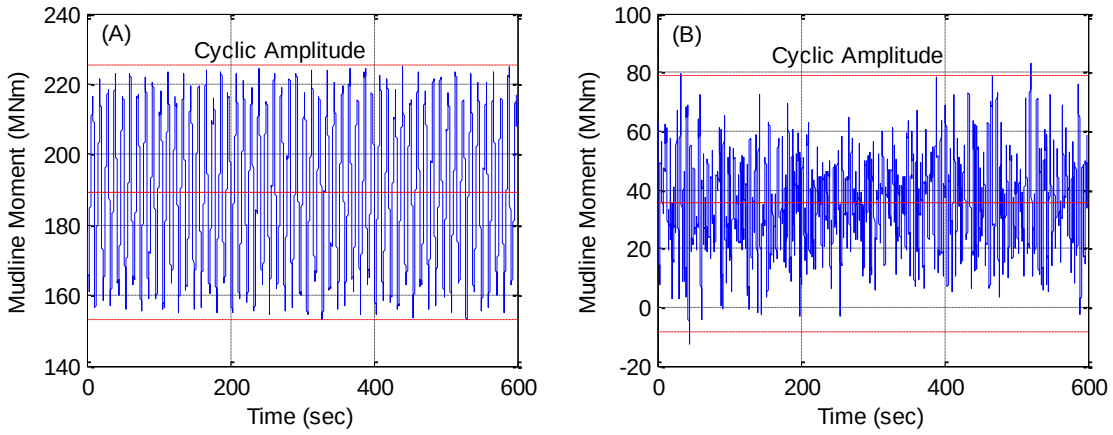


**Figure 3.2 Example (A) regular wave train/steady wind and (B) stochastic time histories of mudline moment**

The emergency shutdown design situation required a somewhat different approach due to the nonstationary nature of the response. In this case, the cyclic amplitude of concern was taken to be the difference between the mean pre-shutdown response and the absolute minimum response (Figure 3.3).

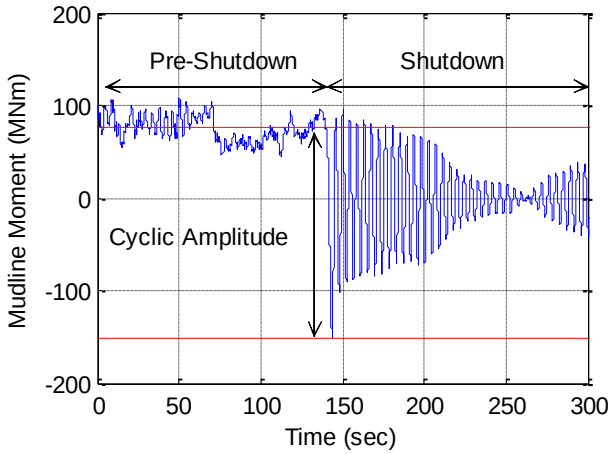


**Figure 3.3 Example emergency shutdown time history of mudline moment during rated wind speeds**

The mudline loads ($H$, $M$) were then used as input to INFIDEL to obtain $u$ and $\theta$. In order to compute the linear stiffness elements ($k_{xx}$, $k_{x\phi}$, $k_{\phi\phi}$) comprising $k_{mud}$, two runs of INFIDEL were required:

1) Using cyclic mudline load amplitudes $H$ and $M$ (denoted $H_{x,1}$ and $M_{\phi,1}$ in Eq. (1)) to obtain cyclic mudline displacement and rotation amplitudes $u$ and $\theta$ (denoted $u_1$ and $\theta_1$ in Eq. (1)), and
2) Using just the horizontal mudline shear amplitude $H$ ($H_{x,2}$ in Eq. (1)) but setting $M = 0$ to obtain a second set of displacement and rotation amplitudes ($u_2$ and $\theta_2$).

The displacement and rotation results were then used in conjunction with the input loads to determine $k_{mud}$, calculated per [17] using

$$\begin{pmatrix} k_{xx} \\ k_{x\phi} \\ k_{\phi\phi} \end{pmatrix} = \begin{pmatrix} u_1 & \theta_1 & 0 \\ 0 & u_1 & \theta_1 \\ u_2 & \theta_2 & 0 \end{pmatrix}^{-1} \begin{pmatrix} H_{x,1} \\ M_{\phi,1} \\ H_{x,2} \end{pmatrix} \quad \textbf{(1)}$$

where $k_{xx}$ is the horizontal translational stiffness, $k_{\phi\phi}$ is the rotational stiffness, $k_{x\phi}$ is the cross-term of $k_{mud}$, and assuming that $k_{mud}$ is symmetric.

Foundation damping was determined using the same method described in [3], which converts hysteretic energy loss $E_h$ (calculated by INFIDEL as a function of mudline loading) into a viscous rotation dashpot value $c_{\phi\phi}$ by

$$c_{\phi\phi} = \frac{E_h}{2\theta^2 \pi^2 f} \quad \textbf{(2)}$$

where $\theta$ is the mudline rotation amplitude in rad, $f$ is the loading frequency in Hz, taken here to be the first (fore-aft) natural frequency of the NREL 5MW.

## 3.3 Offshore Wind Turbine Models

The NREL 5MW Reference Turbine (NREL 5MW) was analyzed assuming the substructure, foundation, and soil (clay) properties shown in Figure 3.4 and Table 3.2. The process used in this paper is similar to prior studies of foundation damping [3] but considers different environmental site parameters. Because soil profile data (e.g. undrained shear strength $s_u$, Poisson's ratio $\nu$, and shear modulus at small strains $G_0$) were unavailable for the Delaware data buoy location, the soil profile from [3] was used in this analysis because it represents a specific North Sea offshore site and because it facilitated comparison with the damping studies performed in literature which are primarily in clayey soils [3,5–7,18,19].

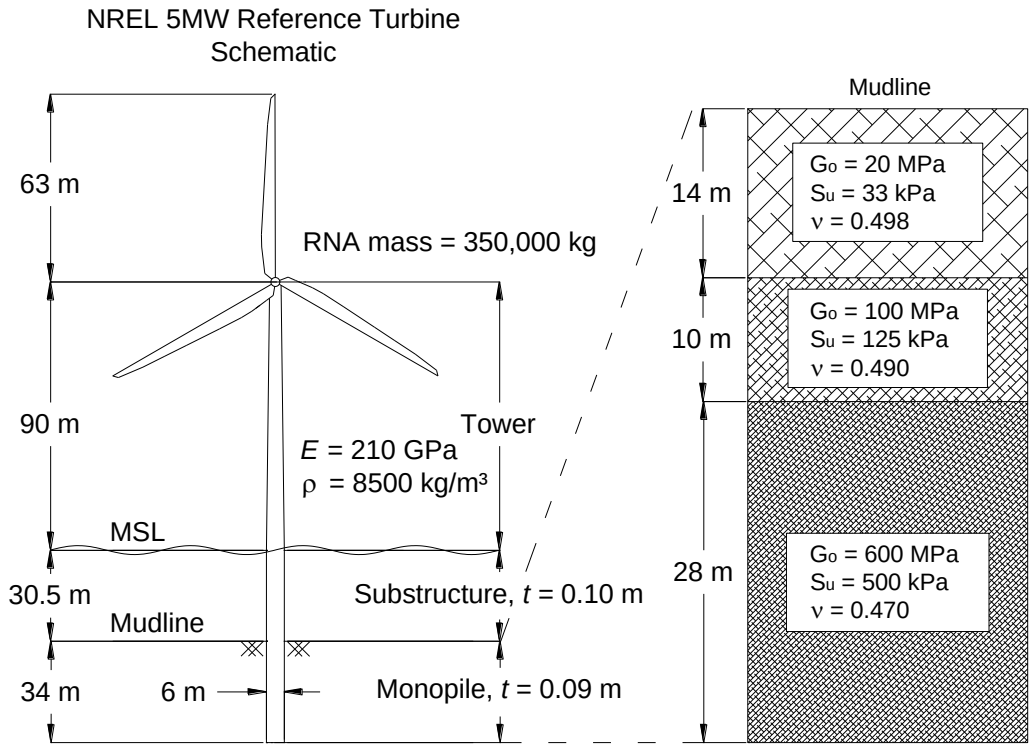


**Figure 3.4 NREL 5MW Reference Turbine Site**

**Table 3.2 Structural properties of the NREL 5MW Reference Turbine, substructure, and foundation assuming linearly tapering properties**

| Location on Support Structure | Diameter, Thickness |
|---|---|
| Tower top | 3.87 m, 0.019 m |
| Tower base (MSL) | 6 m, 0.027 m |
| Substructure | 6 m, 0.10 m |
| Monopile | 6 m, 0.09 m |

### 3.3.1 Environmental Load Models

This paper used the aero-hydro-elastic simulation code FAST [9] (version 7) to estimate OWT monopile foundation design loads. FAST uses Blade Element Momentum (BEM) theory to calculate wind loads on OWT blades and includes the effects of the spinning rotor on overall support structure dynamics. Time history simulation is carried out using modal superposition to determine dynamic behavior, and the support structure modes are informed by the first and

second fore-aft and side-to-side mode shapes. These mode shapes were determined using the NREL-distributed software BModes [13] and are defined by sixth-order polynomial coefficients in the FAST tower property file.

Depending on the requirements of the DLC, wind can be defined as either steady or turbulent and waves as regular or irregular. Turbulent wind conditions were modeled in FAST using the Kaimal spectrum. Linear wave theory was used to generate wave conditions using the JONSWAP spectrum and Wheeler stretching. The effects of breaking waves were neglected.

The environmental site conditions which inform this study are taken from the NOAA data buoy 44009 [20] sited off the coast of Delaware (DE). The DE buoy data used for this paper include the 1-hr average wind speed at 5 m above sea level and 1-hr average significant wave height $H_s$ from 1986-2014. Wind speed at hub height was calculated using the power law for vertical wind shear, with an exponent of 0.14 per [2]. Wind speeds and significant wave heights at particular return periods (Table 3.3) used for the DLCs in the parked design situation were calculated using a Generalized Extreme Value (GEV) distribution fit to the maximum annual wind speed and wave height from 1986-2014. This approach is conservative, as the maximum wind speed and maximum wave height are not necessarily simultaneous. The 5-year significant wave height $H_{s,5\text{-}yr}$ was also determined here, as the Reduced Wave Height model used in DLC 6.2b requires a reduction in the 50-year wave height $H_{s,50\text{-}yr}$ by the factor $\psi$, which is a ratio of $H_{s,5\text{-}yr}/H_{s,50\text{-}yr}$.

**Table 3.3 Wave height and wind speed at particular mean return periods for the Delaware data buoy site used for parked design situation**

| Site Condition | Value |
|---|---|
| 5-year Significant Wave Height, $H_{s,5\text{-}yr}$ | 7.08 m |
| 50-year Significant Wave Height, $H_{s,50\text{-}yr}$ | 8.12 m |
| 50-year Wind Speed at Hub Height (1-hr average), $U_{1hr,50\text{-}yr}$ | 36.9 m/s |

Peak spectral period $T_p$ was calculated similarly to [21], where

$$T_p = 1.05\left(11.1\sqrt{\frac{H_s}{g}}\right) \quad \textbf{(3)}$$

where $H_s$ is the significant wave height and $g$ is the acceleration due to gravity.

The DLCs in the power production design situation model sea states using significant wave height conditional on 10-min average hub height wind speed ($H_s|U_{10,hub}$). Wind speeds from the DE data buoy were separated into 2 m/s bins ranging from 3 m/s (cut-in wind speed) to 25 m/s (cut-out wind speed), and the expected and 50-yr ($98^{th}$ percentile) significant wave heights were calculated as a function of a Weibull probability density function [2] fit to the wave data associated with the wind data within each bin. The mean and 50-yr wave heights conditional on wind speed (Table 3.4) were used to model Normal Sea State (NSS) and Severe Sea State (SSS), respectively. The DE buoy data is taken from 1-hr averages; however, it was assumed for the purposes of this study that the relationship between 1-hr wind speed and wave height was similar to 10-minute hub height wind speed ($U_{10,hub}$) and wave height.

**Table 3.4 Significant wave height values conditional on wind speed**

| **Mean Wind Speed, $U_{10,hub}$ (m/s)** | **Expected Value Conditional on $U_{10,hub}$** | | **50-yr Value Conditional on $U_{10,hub}$** | |
|---|---|---|---|---|
| | **Significant Wave Height, $H_s$ (m)** | **Peak Spectral Period, $T_p$ (sec)** | **Significant Wave Height, $H_s$ (m)** | **Peak Spectral Period, $T_p$ (sec)** |
| 4 | 0.87 | 3.48 | 1.83 | 5.03 |
| 6 | 0.89 | 3.51 | 1.85 | 5.06 |
| 8 | 0.95 | 3.63 | 1.96 | 5.21 |
| 10 | 1.08 | 3.87 | 2.13 | 5.43 |
| 12 | 1.27 | 4.19 | 2.44 | 5.81 |
| 14 | 1.51 | 4.57 | 2.78 | 6.21 |
| 16 | 1.78 | 4.96 | 3.19 | 6.65 |
| 18 | 2.07 | 5.35 | 3.63 | 7.09 |
| 20 | 2.36 | 5.71 | 4.11 | 7.54 |
| 22 | 2.78 | 6.21 | 4.91 | 8.25 |
| 24 | 3.22 | 6.67 | 5.69 | 8.88 |

The rated wind speed for the NREL 5MW is 11.4 m/s and cut-out is 25 m/s; for power production DLCs, the mean (turbulent) wind speed cases 12 m/s and 24 m/s (ranging from 11-13 m/s and 23-25 m/s) were used for rated and cut-out conditions.

### 3.3.2 Soil-Pile Models

The NGI-developed INFIDEL software used to compute foundation stiffness and damping is primarily intended for analyzing offshore piles and caissons [3,11,12]. INFIDEL defines an axisymmetric three-dimensional soil-pile space with infinite extents. A nonlinear elastic constitutive model to capture cyclic clay behavior based on stress-strain curves and soil damping curves as a function of modulus defined by the user. Linear elastic pile behavior was assumed. The hysteretic energy loss $E_h$ calculated by INFIDEL corresponds to the area of one load-strain cycle (hysteresis loop) summed over all the soil elements. The input shear modulus at small strains $G_0$, undrained shear strength $s_u$, and Poisson's ratio $\nu$ used for the OWT site in this paper can be found in Figure 3.4. The Poisson's ratio for the pile was assumed to be 0.3. For further details on the soil-pile model and methodology of INFIDEL, please refer to [3].

The output cyclic mudline displacement and rotation amplitudes from INFIDEL were used to determine a mudline stiffness matrix $k_{mud}$ (a process which is described in more detail in Section 3.2.2). The elements of $k_{mud}$ are then used as input to the user defined subroutine *UserPtfmLd* in FAST, which calculates "platform" loads (in this case, loads at the mudline). For this paper, perfect fixity was assumed in the vertical *z*-direction as well as in torsion (rotation about the *z*-axis, Figure 3.5).

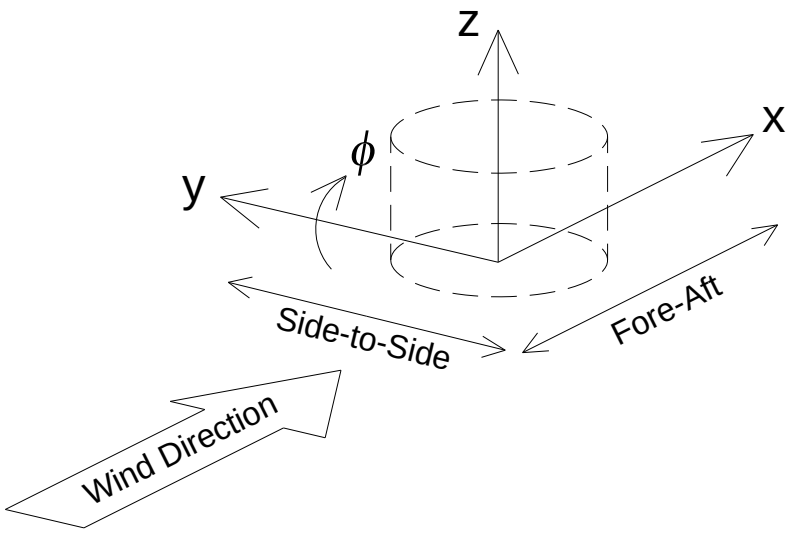


**Figure 3.5 Degrees of freedom in FAST user subroutine**

Soil behavior is assumed to be radially symmetric (i.e. $k_{xx} = k_{yy}$) and that the coupled stiffness terms were assumed to be equal ($k_{x\phi} = k_{\phi x}$). Due to the sign conventions inherent in FAST, the stiffness matrix defined in *UserPtfmLd* is defined as

$$k_{mud} = \begin{pmatrix} k_{xx} & 0 & 0 & 0 & -k_{x\phi} & 0 \\ 0 & k_{xx} & 0 & k_{x\phi} & 0 & 0 \\ 0 & 0 & 0 & 0 & 0 & 0 \\ 0 & k_{x\phi} & 0 & k_{\phi\phi} & 0 & 0 \\ -k_{x\phi} & 0 & 0 & 0 & k_{\phi\phi} & 0 \\ 0 & 0 & 0 & 0 & 0 & 0 \end{pmatrix} \quad \textbf{(4)}$$

and the mudline damping matrix as

$$c_{mud} = \begin{pmatrix} 0 & 0 & 0 & 0 & 0 & 0 \\ 0 & 0 & 0 & 0 & 0 & 0 \\ 0 & 0 & 0 & 0 & 0 & 0 \\ 0 & 0 & 0 & c_{\phi\phi} & 0 & 0 \\ 0 & 0 & 0 & 0 & c_{\phi\phi} & 0 \\ 0 & 0 & 0 & 0 & 0 & 0 \end{pmatrix}, \quad \textbf{(5)}$$

where $c_{\phi\phi}$ is a rotational dashpot calculated as a function of hysteretic energy loss, mudline rotation amplitude, and load frequency (see Section 3.2.2 for further details). It is unclear whether

the hysteretic energy loss from INFIDEL could be decomposed into damping contributions from different degrees of freedom (i.e., into translational and rotational contributions), and doing so would require an assumption for how to distribute damping between rotational and translational dashpots; consequently, all hysteretic energy loss was attributed to a rotational dashpot.

## 3.4 Results

The cyclic mudline load amplitudes ($H_x$, $M_\phi$, Table 3.5) were used as input to INFIDEL, which produced cyclic mudline displacements, rotations, and hysteretic energy loss ($u$, $\theta$, and $E_h$, respectively) which were then used to determine the mudline stiffness matrix $k_{mud}$ variables $k_{xx}$, $k_{x\phi}$, and $k_{\phi\phi}$.

The DLCs were grouped based on $k_{mud}$ and $E_h$, and representative $k_{mud}$ matrices were selected to represent each group (Table 3.6). It was not preferable to define different $k_{mud}$ for a different yaw angle or wind speed bin within a DLC, so a representative $k_{mud}$ was selected such that the DLC could be analyzed using one $k_{mud}$ and therefore also one corresponding compiled version of FAST. The rotational mudline dashpot value $c_{\phi\phi}$ was calculated using the first fore-aft natural frequency of the NREL 5MW, taking into account mudline flexibility defined by $k_{mud}$.

Only DLCs 6.1 and 6.2a (Table 3.5) required iteration during analysis – that is to say, a second compiled version of FAST was required using the $k_{mud}$ cyclic amplitude results – all other DLCs met the criteria of less than 20% difference between input and output cyclic mudline loads ($H_x$, $M_\phi$).

**Table 3.5 Cyclic mudline load amplitudes and displacements used to define mudline stiffness matrix and rotational dashpot coefficients. Mudline response for unshaded cells represent the values obtained from a fixed-base analysis in FAST; the values for shaded cells were obtained from a subsequent flexible-mudline analysis in FAST.**

| DLC | Condition | $H_x$ (MN) | $M_\phi$ (MNm) | $u$ (mm) | $\theta$ ($10^{-3}$ rads) | $E_h$ (kJ) | $k_{xx}$ $\left(\frac{GN}{m}\right)$ | $k_{x\phi}$ $\left(\frac{GN}{rad}\right)$ | $k_{\phi\phi}$ $\left(\frac{GNm}{rad}\right)$ |
|---|---|---|---|---|---|---|---|---|---|
| 1.1 | $v_{rated}$ | 0.556 | 39.1 | 3.44 | 0.407 | 1.74 | 2.58 | 20.4 | 269 |
| | $v_{out}$ | 1.18 | 38.2 | 4.15 | 0.453 | 2.73 | 2.56 | 20.8 | 276 |
| 1.3 | $v_{rated}$ | 0.607 | 44.0 | 3.92 | 0.462 | 2.36 | 2.60 | 20.8 | 272 |
| | $v_{out}$ | 1.18 | 47.9 | 5.05 | 0.556 | 4.24 | 2.61 | 21.5 | 282 |
| 1.5 | $v_{rated}$ | 0.463 | 13.7 | 1.33 | 0.152 | 0.17 | 2.45 | 18.5 | 253 |
| | $v_{out}$ | 1.15 | 27.4 | 3.18 | 0.339 | 1.47 | 2.50 | 20.1 | 269 |
| 1.6a | $v_{rated}$ | 0.914 | 41.9 | 4.14 | 0.468 | 2.70 | 2.58 | 20.9 | 275 |
| | $v_{out}$ | 1.98 | 48.9 | 6.29 | 0.645 | 7.03 | 2.59 | 22.2 | 292 |
| 1.6b | $v_{rated}$ | 1.32 | 46.1 | 5.07 | 0.549 | 4.29 | 2.59 | 21.5 | 282 |
| | $v_{out}$ | 2.83 | 59.2 | 8.72 | 0.853 | 14.2 | 2.61 | 23.4 | 309 |
| 5.1 | $v_{rated}$ | 1.75 | 205 | 25.9 | 2.60 | 104 | 3.32 | 32.4 | 400 |
| | $v_{out}$ | 1.72 | 137 | 16.2 | 1.69 | 45.1 | 3.02 | 28.0 | 350 |
| 6.1a | Yaw = 0˚ | 2.87 | 95.99 | 11.7 | 1.19 | 32.0 | 2.78 | 25.8 | 333 |
| | Yaw = 8˚ | 2.91 | 95.58 | 11.6 | 1.18 | 32.1 | 2.78 | 25.8 | 334 |
| 6.1c | Yaw = 0˚ | 1.79 | 35.0 | 4.67 | 0.475 | 3.66 | 2.52 | 21.1 | 281 |
| | Yaw = 15˚ | 1.80 | 36.7 | 4.84 | 0.493 | 3.95 | 2.53 | 21.2 | 282 |
| 6.2a | Yaw = 0˚ | 2.87 | 86.1 | 10.9 | 1.09 | 26.6 | 2.73 | 25.2 | 327 |
| | Yaw = 60˚ | 2.82 | 102 | 12.2 | 1.24 | 34.8 | 2.80 | 26.1 | 336 |
| | Yaw = 90˚ | 2.95 | 123 | 14.1 | 1.45 | 50.4 | 2.89 | 27.5 | 352 |
| 6.2b | Yaw = 0˚ | 3.25 | 57.3 | 9.23 | 0.879 | 16.2 | 2.59 | 23.5 | 312 |
| | Yaw = 90˚ | 3.26 | 67.1 | 10.4 | 0.999 | 20.5 | 2.63 | 24.1 | 318 |
| | Yaw = 180˚ | 3.27 | 60.6 | 9.67 | 0.922 | 17.8 | 2.61 | 23.8 | 315 |

**Table 3.6 Representative mudline stiffness matrices for design load case groups**

| $k_{xx}$ $\left(\frac{GN}{m}\right)$ | $k_{x\phi}$ $\left(\frac{GN}{rad}\right)$ | $k_{\phi\phi}$ $\left(\frac{GNm}{rad}\right)$ | Freq. (Hz) | $c_{\phi\phi}$ $\left(\frac{GNs}{rad}\right)$ | Design Load Cases |
|---|---|---|---|---|---|
| 2.58 | 20.4 | 269 | 0.234 | 2.28 | 1.1, 1.5, 6.1c |
| 2.59 | 22.2 | 292 | 0.233 | 3.67 | 1.6a, 1.6b |
| 3.32 | 32.4 | 400 | 0.228 | 3.41 | 5.1 ($v_{rated}$) |
| 3.02 | 28.0 | 350 | 0.230 | 3.49 | 5.1 ($v_{out}$) |
| 2.80 | 26.1 | 336 | 0.231 | 4.02 | 6.1a, 6.2a |
| 2.59 | 23.5 | 312 | 0.232 | 4.59 | 6.2b |

Using the representative mudline stiffness matrices from Table 3.6, aero-hydro-elastic analyses were performed in FAST including foundation damping ("damped", Table 3.7) and considering no foundation damping ("undamped"). Cyclic amplitudes for mudline loads, displacements, and rotations decreased for all DLCs when mudline foundation damping was included in the analysis.

**Table 3.7 Mudline cyclic load amplitude comparison between the damped and undamped analyses in FAST. Damped analyses included mudline foundation damping in the form of a viscous rotational dashpot.**

| *Load Case* | *Condition* | UNDAMPED | | | | DAMPED | | | |
|---|---|---|---|---|---|---|---|---|---|
| | | $H_x$ (MN) | $M_\phi$ (MNm) | $u_x$ (mm) | $\theta_\phi$ ($10^{-3}$ rads) | $H_x$ (MN) | $M_\phi$ (MNm) | $u_x$ (mm) | $\theta_\phi$ ($10^{-3}$ rads) |
| 1.1 | $v_{rated}$ | 0.590 | 41.5 | 3.49 | 0.419 | 0.566 | 41.1 | 3.44 | 0.413 |
| | $v_{out}$ | 1.27 | 43.5 | 4.27 | 0.484 | 1.24 | 42.7 | 4.18 | 0.474 |
| 1.3 | $v_{rated}$ | 0.664 | 46.4 | 4.49 | 0.499 | 0.609 | 45.7 | 4.38 | 0.489 |
| | $v_{out}$ | 1.35 | 52.9 | 5.71 | 0.614 | 1.25 | 51.2 | 5.45 | 0.588 |
| 1.5 | $v_{rated}$ | 0.469 | 17.1 | 1.62 | 0.185 | 0.460 | 16.6 | 1.57 | 0.180 |
| | $v_{out}$ | 1.21 | 34.2 | 3.63 | 0.402 | 1.21 | 34.0 | 3.60 | 0.399 |
| 1.6a | $v_{rated}$ | 0.980 | 45.9 | 4.76 | 0.518 | 0.959 | 45.4 | 4.69 | 0.511 |
| | $v_{out}$ | 2.08 | 55.9 | 6.81 | 0.707 | 2.05 | 54.9 | 6.68 | 0.694 |
| 1.6b | $v_{rated}$ | 1.41 | 51.7 | 5.75 | 0.613 | 1.40 | 51.4 | 5.70 | 0.608 |
| | $v_{out}$ | 2.92 | 65.0 | 8.56 | 0.872 | 2.90 | 64.4 | 8.48 | 0.864 |
| 5.1 | $v_{rated}$ | 2.09 | 223 | 28.8 | 2.89 | 1.98 | 220 | 28.4 | 2.85 |
| | $v_{out}$ | 1.86 | 145 | 17.0 | 1.77 | 1.67 | 140 | 16.0 | 1.68 |
| 6.1a | Yaw = 0˚ | 2.88 | 97.8 | 12.9 | 1.29 | 2.83 | 81.0 | 11.3 | 1.12 |
| | Yaw = 8˚ | 2.89 | 99.0 | 13.2 | 2.30 | 2.83 | 82.7 | 11.5 | 1.13 |
| 6.1c | Yaw = 0˚ | 1.83 | 38.0 | 5.70 | 0.551 | 1.80 | 36.9 | 5.56 | 0.537 |
| | Yaw = 15˚ | 1.83 | 36.8 | 5.57 | 0.537 | 1.80 | 36.2 | 5.49 | 0.529 |
| 6.2a | Yaw = 0˚ | 2.87 | 86.8 | 11.9 | 1.18 | 2.86 | 84.7 | 11.7 | 1.15 |
| | Yaw = 60˚ | 2.82 | 101 | 12.1 | 1.23 | 2.76 | 81.5 | 11.3 | 1.11 |
| | Yaw = 90˚ | 2.97 | 128 | 15.9 | 1.61 | 2.84 | 90.2 | 11.4 | 1.13 |
| 6.2b | Yaw = 0˚ | 3.29 | 61.2 | 9.59 | 0.918 | 3.29 | 60.5 | 9.54 | 0.912 |
| | Yaw = 90˚ | 3.31 | 69.5 | 10.2 | 0.988 | 3.30 | 63.1 | 9.72 | 0.934 |
| | Yaw = 180˚ | 3.35 | 64.1 | 9.88 | 0.949 | 3.32 | 63.0 | 9.75 | 0.935 |

Broadly speaking, mudline moment amplitudes ($M_\phi$) was reduced more than mudline horizontal force amplitudes ($H_x$) with the inclusion of foundation damping, which is similar to the results found by [3]. This result is somewhat interesting, given that foundation damping was

implemented in the form of a rotational dashpot rather than a traditional translational dashpot; however, given the large moment posed by wind thrust and wave loads on the OWT support structure, small reduction in horizontal force can be translated into larger reductions in moment.

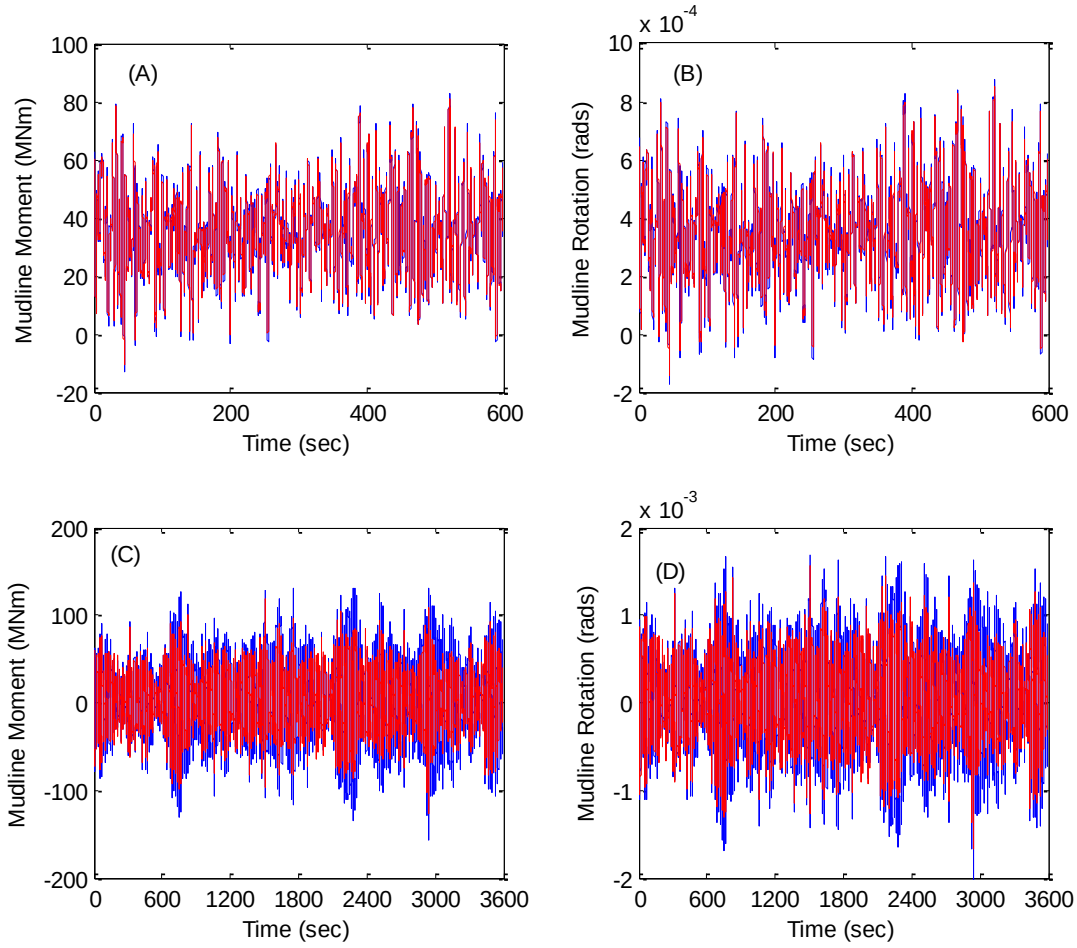


**Figure 3.6 Example time histories of undamped (blue) vs. damped (red) (A) DLC 1.1 mudline moment response at cut-out wind speed (B) DLC 1.1 mudline rotation response at cut-out wind speed (C) DLC 6.2a at Yaw = 90° mudline moment response and (D) DLC 6.2a at Yaw 90 mudline rotation response**

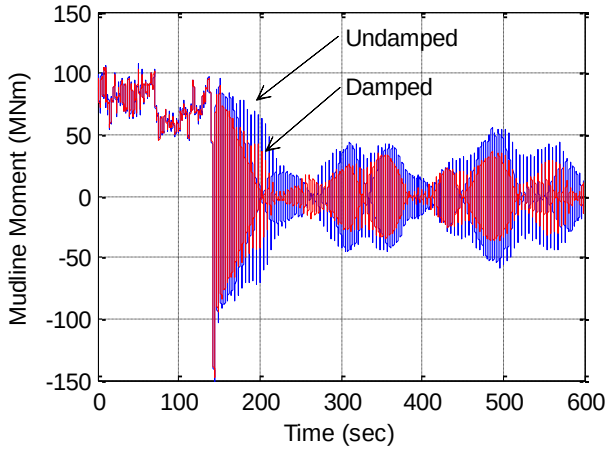


**Figure 3.7 Example time history of undamped vs. damped response for emergency shutdown DLC 5.1 at cut-out wind speed**

Power production cases were not as significantly affected by foundation damping as emergency shutdown and the parked cases were (Table 3.8, Figure 3.6). With the exception of approximately 8% reduction in $H_x$ and 2-5% reduction in $u_x$ and $q_\phi$ for DLC 1.3, the majority of the reductions in $H_x$ and $M_\phi$ for power production cases ranged from approximately 1-4% and for $u_x$ and $\theta_\phi$ the reductions were approximately 1-2%.

**Table 3.8 Percent reduction in mudline response with the inclusion of foundation damping**

| Design Situation | Load Case | Condition | $H_x$ | $M_\phi$ | $u_x$ | $\theta_\phi$ |
|---|---|---|---|---|---|---|
| 1) Power Production | 1.1 | $v_{rated}$ | 4.1% | 1.1% | 1.5% | 1.3% |
| | | $v_{out}$ | 2.7% | 1.8% | 2.2% | 2.0% |
| | 1.3 | $v_{rated}$ | 8.2% | 1.6% | 2.4% | 2.1% |
| | | $v_{out}$ | 7.3% | 3.3% | 4.5% | 4.2% |
| | 1.5 | $v_{rated}$ | 1.7% | 2.8% | 2.8% | 2.7% |
| | | $v_{out}$ | 0.4% | 0.8% | 0.7% | 0.8% |
| | 1.6a | $v_{rated}$ | 2.2% | 1.1% | 1.5% | 1.4% |
| | | $v_{out}$ | 1.4% | 1.8% | 1.8% | 1.8% |
| | 1.6b | $v_{rated}$ | 1.0% | 0.6% | 0.8% | 0.8% |
| | | $v_{out}$ | 0.6% | 0.9% | 0.9% | 0.9% |
| | Average | | 3.0% | 1.6% | 1.9% | 1.8% |
| 5) Emergency Shutdown | 5.1 | $v_{rated}$ | 5.3% | 1.1% | 1.5% | 1.4% |
| | | $v_{out}$ | 10.4% | 3.4% | 5.6% | 5.2% |
| | Average | | 7.8% | 2.2% | 3.5% | 3.3% |
| 6) Parked Conditions | 6.1a | Yaw = 0˚ | 1.9% | 17% | 12% | 13% |
| | | Yaw = 8˚ | 2.0% | 17% | 12% | 13% |
| | 6.1c | Yaw = 0˚ | 1.9% | 2.8% | 2.6% | 2.6% |
| | | Yaw = 15˚ | 2.0% | 1.5% | 1.4% | 1.4% |
| | 6.2a | Yaw = 0˚ | 0.8% | 2.3% | 1.9% | 2.0% |
| | | Yaw = 60˚ | 2.1% | 19% | 6.6% | 9.2% |
| | | Yaw = 90˚ | 4.4% | 30% | 28% | 30% |
| | 6.2b | Yaw = 0˚ | 0.1% | 1.1% | 0.5% | 0.6% |
| | | Yaw = 90˚ | 0.5% | 9.2% | 4.6% | 5.5% |
| | | Yaw = 180˚ | 0.8% | 1.6% | 1.3% | 1.4% |
| | Average | | 1.6% | 10% | 7.1% | 7.9% |

Interestingly, the emergency shutdown cases (DLC 5.1) had highest reduction $H_x$ (5-10%) and not $M_\phi$ (only 1-3%). Also of note, despite the significant reduction in mudline load amplitude, the reduction in $u_x$ and $\theta_\phi$ were modest (1-6%).

The parked DLCs showed the greatest reduction in mudline response with the inclusion of foundation damping. This is in line with the literature, which suggests that in comparison to aerodynamic damping during power production situations, foundation damping is much less significant [6,22]. It should also be noted that the reductions in response are much greater for the turbulent wind, irregular wave cases (DLCs 6.1a and 6.2a) than the steady wind, regular wave

cases (DLCs 6.1c and 6.2b). The largest reduction for the steady wind/regular wave cases was in $M_\phi$ for the 90˚ yaw case of DLC 6.2b; however, for the turbulent wind/irregular wave cases, the largest reduction in $M_\phi$ was nearly 30%.

DLC 6.1a was also considered in the foundation damping study performed in [3], but with lower reductions in $M_\phi$(approximately 9% compared to the 17% found here). The water depth, associated loads, and differences in structural design strongly influenced the results as the wind speeds and wave conditions were relatively similar (34 m/s wind with $H_s$ = 8.5 m and $T_p$ = 10.3 s in [3] vs. 36.9 m/s wind with $H_s$ = 8.12 m and $T_p$ = 10.6 s). The water depth analyzed in [3] was 20 m, whereas this paper analyzed the NREL 5MW in a water depth of 30.5 m; additionally, the dominant frequency considered in [3] was 0.302 Hz, and this paper considered a frequency of approximately 0.23 Hz.

The percent critical damping for each of the representative $k_{mud}$ rotational dashpots was computed using a free vibration analysis in FAST. Within the free vibration analysis, a static initial tower top displacement was imposed at hub height in the fore-aft direction and then the support structure was permitted to vibrate freely in conditions with no wind or waves, considering parked and feathered blades. The logarithmic decrement method [3] was then used on the resulting time history using a best-fit of a series of amplitudes (Figure 3.8). Two free vibration analyses were carried out for each representative case – first including structural damping in the tower property input file (1.0%) and then excluding it (structural damping = 0%).

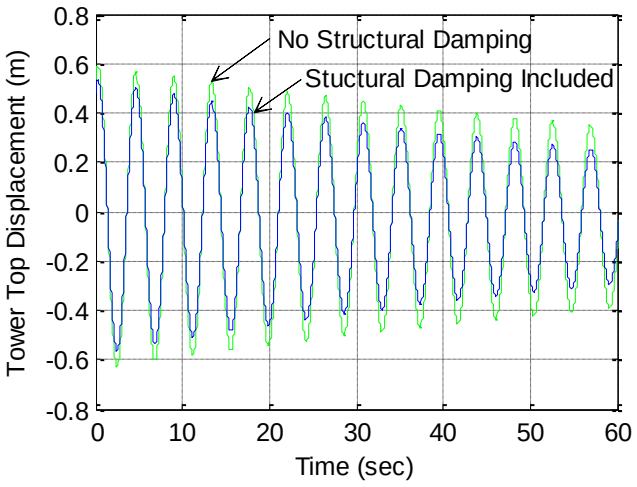


**Figure 3.8 Free vibration of tower top to determine percent critical damping associated with mudline rotational dashpot**

Foundation damping was calculated by taking the difference between these two cases (Table 3.9), assuming that damping for OWTs can be modeled independently and combined linearly, and that aerodynamic and hydrodynamic damping can be neglected in this case [3,5,6,19].

**Table 3.9 Percent critical damping for all representative mudline stiffness and damping cases**

| Representative Case | Percent Critical Foundation Damping | Percent Critical Structural Damping | Percent Critical Total Damping (Foundation + Structural) |
|---|---|---|---|
| DLC 1.1 $v_{rated}$ | 0.28% | 0.28% | 0.56% |
| DLC 1.6a $v_{out}$ | 0.49% | 0.30% | 0.79% |
| DLC 5.1 $v_{rated}$ | 0.65% | 0.31% | 0.96% |
| DLC 5.1 $v_{out}$ | 0.58% | 0.30% | 0.88% |
| DLC 6.2a Yaw = 60° | 0.64% | 0.31% | 0.95% |
| DLC 6.2b Yaw = 0° | 0.65% | 0.32% | 0.97% |

The foundation damping calculated here (ranging from 0.28% to 0.65%) is within the range found in the literature [3,5–7,19,18]. Most notably, the amount of foundation damping calculated for emergency shutdown cases is very similar to the foundation damping which was estimated by [19], considering a site with soil profile dominated by very stiff to very hard clay.

The variation in structural damping in Table 3.9 can likely be attributed to the manner in which structural damping is accounted for in FAST, which is effectively Rayleigh damping with the

mass-proportional coefficient set to zero [23]. Consequently, while 1.0% damping was defined in the tower property input file for the first and second fore-aft and side-to-side modes for all DLCs (defining the structural damping for the support structure between mudline and hub height), the net resulting damping attributed to the structure was approximately 0.3%.

## 3.5 Conclusions

This paper analyzed the influence of foundation damping on the behavior of a monopile-supported offshore wind turbine (OWT) considering the design situations of power production, emergency shutdown, and parked conditions. These design situations were modeled in FAST [9] according to the design standard IEC 61400-3 [10], considering the NREL 5MW Reference Turbine [8] and the environmental conditions in the U.S. Atlantic waters off the coast of Delaware. Because soil profile data was unavailable at the data buoy site, a clay soil profile from an offshore site in the North Sea [3] was used in order to better compare the results from this paper to those in literature [3,5–7,18,19].

Foundation damping was modeled using viscous rotational dashpots at the mudline. The dashpot coefficient was calculated as a function of hysteretic energy loss from the soil-pile system and mudline rotation amplitude using the NGI-developed program INFIDEL [11,12] and the first fore-aft natural frequency of the NREL 5MW. The rotational dashpots were used in conjunction with a mudline stiffness matrix to model soil-structure interaction for the OWT modeled in FAST.

Foundation damping played a more significant role in the emergency shutdown and parked design conditions than power production. For power production cases, the average reduction in cyclic demand (amplitude of mudline loads) due to the inclusion of foundation damping was approximately 3% for horizontal mudline force and 1.6% for mudline moment. Comparatively, the cyclic moment demand was reduced by 10% on average for the parked conditions and by as

much as 30% in some cases. The emergency shutdown cases experienced a larger reduction in horizontal force demand (5-10%) than mudline moment (1-3%).

The results of the free vibration study to calculate percent critical damping ranged from approximately 0.3-0.7% and were in good agreement with those found in literature [3,5–7,18,19], particularly with the experimental data from emergency shutdown of an OWT in clay soil from [19].

It may be concluded from this paper that the role of foundation damping in parked conditions is significant, and may also be important for emergency shutdown. While the reduction in cyclic demand calculated in this paper is inherently associated with the soil and structural properties specific to this site, past work [3] used an identical soil profile with different environmental and structural properties (deeper water depth and less stiffness in structure) but yielded similar values of percent critical damping and higher reductions in cyclic demand for DLC 6.1a. The influence of soil profile on foundation damping should be investigated in future work, particularly with regard to soil type – the majority of existing work on foundation damping has focused on clayey soils, with limited information regarding how much damping may be contributed by a monopile in sand and how it may be compared to the amount of damping from clays [3]. Additionally, sensitivity studies should be performed to determine how cyclic mudline loads used to calculate mudline stiffness and damping affect the results presented here. It should also be noted that the assumption that the first natural frequency is dominant may not be accurate for all power production cases, and that the dominant frequency for each case (e.g. peak wave frequency) may show greater impact of foundation damping under power production design situations.

## Acknowledgements

The research was supported by the grants CMMI-1234560, CMMI-1234656, the Massachusetts Clean Energy Center and the NSF-sponsored IGERT: Offshore Wind Energy Engineering,

Environmental Science, and Policy (Grant Number 1068864), and the Norwegian Geotechnical Institute.

## References

[1] Hamilton, B., Battenberg, L., Bielecki, M., Bloch, C., Decker, T., Frantzis, L., Paidipati, J., Wickless, A., and Zhao, F., 2013, Offshore Wind Market and Economic Analysis: Annual Market Assessment, Navigant Consulting, Inc., Burlington, MA.

[2] DNV, 2013, DNV-OS-J101 Design of Offshore Wind Turbine Structures, Det Norske Veritas AS.

[3] Carswell, W., Johansson, J., Løvholt, F., Arwade, S. R., Madshus, C., DeGroot, D. J., and Myers, A. T., 2015, "Foundation damping and the dynamics of offshore wind turbine monopiles," Renew. Energy, **80**, pp. 724–736.

[4] GL WindEnergie, 2005, Overall Damping for Piled Offshore Support Structures, Guideline for the Certification of Offshore Wind Turbines, Germanischer Lloyd WindEnergie.

[5] Tarp-Johansen, N. J., Andersen, L., Christensen, E., Mørch, C., Kallesøe, B., and Frandsen, S., 2009, "Comparing Sources of Damping of Cross-Wind Motion," European Offshore Wind 2009: Conference & Exhibition: 14-16 September, European Wind Energy Association, Stockholm, Sweden.

[6] Shirzadeh, R., Devriendt, C., Bidakhvidi, M. a., and Guillaume, P., 2013, "Experimental and computational damping estimation of an offshore wind turbine on a monopile foundation," J. Wind Eng. Ind. Aerodyn., **120**, pp. 96–106.

[7] Damgaard, M., Andersen, J., LB, I., and Andersen, L., 2013, "Time-Varying Dynamic Properties of Offshore Wind Turbines Evaluated by Modal Testing," Proceedings of the 18th International Conference on Soil Mechanics and Geotechnical Engineering, Paris, pp. 2343–2346.

[8] Jonkman, J., Butterfield, S., Musial, W., and Scott, G., 2009, Definition of a 5-MW Reference Wind Turbine for Offshore System Development.

[9] Jonkman, J., and Buhl, M. J., 2005, FAST User's Guide, National Renewable Energy Laboratory, Golden, CO.

[10] IEC 61400-3, 2009, Design Requirements for Offshore Wind Turbines, Brussels.

[11] NGI, 1991, Description of INFIDEL - a non-linear, 3-D finite element program.

[12] Hansteen, O. E., and Höeg, K., 1994, "Soil-Structure Interaction Analysis of Embedded Caisson Anchor Under Tension Load," BOSS '94, 7th International Conference on the Behavior of Offshore Structures, Cambridge, MA, pp. 49–62.

[13] Bir, G. S., 2007, User's Guide to BModes ( Software for Computing Rotating Beam Coupled Modes ), Golden, CO.

[14] ABS, 2010, "Offshore Wind Turbine Installations," US Pat. App. 13/318,316, (December).

[15] Pedersen, A. S., and Steiniche, C. S., 2012, "Safe Operation and Emergency Shutdown of Wind Turbines," Aalborg University.

[16] Andersen, K. H., 2009, "Bearing capacity under cyclic loading — offshore, along the coast, and on land. The 21st Bjerrum Lecture presented in Oslo, 23 November 2007," Can. Geotech. J., **46**(5), pp. 513–535.

[17] Zaaijer, M. B., 2006, "Foundation modelling to assess dynamic behaviour of offshore wind turbines," Appl. Ocean Res., **28**(1), pp. 45–57.

[18] Versteijlen, W., Metrikine, A., Hoving, J., Smid, E., and de Vries, W., 2011, "Estimation of the vibration decrement of an offshore wind turbine support structure caused by its interaction with soil," EWEA Offshore Conference, European Wind Energy Association, Amsterdam, the Netherlands.

[19] Damgaard, M., Andersen, J., Ibsen, L. B., and Andersen, L., 2012, "Natural Frequency and Damping Estimation of an Offshore Wind Turbine Structure," Proceedings of the Twenty-second International Offshore and Polar Engineering Conference, Rhodes, Greece, pp. 300–307.

[20] NOAA, 2015, "National Data Buoy Center" [Online]. Available: http://www.ndbc.noaa.gov/.

[21] Valamanesh, V., Myers, A. T., and Arwade, S. R., 2015, "Multivariate analysis of extreme metocean conditions for offshore wind turbines," Struct. Saf., **55**, pp. 60–69.

[22] Valamanesh, V., and Myers, A., 2014, "Aerodynamic Damping and Seismic Response of Horizontal Axis Wind Turbine Towers," J. Struct. Eng., **140**(11).

[23] Jonkman, B., 2013, "Natural frequency and damping ratio calculation" [Online]. Available: https://wind.nrel.gov/forum/wind/viewtopic.php?f=3&t=789. [Accessed: 14-Jul-2015].

# CHAPTER 4

# NATURAL FREQUENCY DEGRADATION AND PERMANENT ACCUMULATED ROTATION FOR OFFSHORE WIND TURBINE MONOPILES IN CLAY


## Authors

W Carswell, Arwade SR, DeGroot DJ, Myers AT



## Abstract

Offshore wind turbine (OWTs) monopile foundations are subjected to cyclic loading from wind, waves, and operational loads from rotating blades. Lateral monopile capacity can be significantly affected by cyclic loading, causing failure at cyclic load amplitudes lower than the failure load under monotonic loading. For monopiles in clay, undrained clay behavior under short-term cyclic soil-pile loading (e.g. extreme storm conditions) typically includes plastic soil deformation resulting from reductions in soil modulus and undrained shear strength which occur as a function of pore pressure build-up. These impacts affect the assessment of the ultimate and serviceability limit states of OWTs via natural frequency degradation and accumulated permanent rotation at the mudline, respectively. This paper introduced novel combinations of existing *p-y* curve design methods and compared the impact of short-term cyclic loading on monopiles in soft, medium, and stiff clay. The results of this paper indicate that short-term cyclic loading from extreme storm conditions are unlikely to significantly affect natural frequency and permanent accumulated rotation for OWT monopiles in stiff clays, but monopiles in soft clay may experience significant degradation. Further consideration is required for medium clays, as load magnitude played a strong role in both natural frequency and permanent rotation estimation.

## Keywords

offshore wind turbines; monopiles; p-y curves; cyclic loading

## Nomenclature

| | |
|---|---|
| DE | Delaware |
| MA | Massachusetts |
| NREL | National Renewable Energy Laboratory |
| OWT | Offshore wind turbine |
| SLS | Serviceability limit state |
| ULS | Ultimate limit state |
| $b$ | Pile diameter |
| $g$ | Acceleration due to gravity |
| $p$ | Soil resistance |
| $p_u$ | Ultimate soil resistance |
| $s_u$ | Undrained shear strength |
| $t$ | Wall thickness |
| $x$ | Depth below mudline |
| $y$ | Soil spring displacement |
| $y_c$ | Soil spring displacement at 50% of ultimate soil resistance |
| $E$ | Young's modulus |
| $H$ | Horizontal mudline force |
| $H_s$ | Significant wave height |
| $J$ | Empirical factor |
| $K_0$ | Initial spring stiffness |
| $K_1$ | Initial spring stiffness for piecewise linear *p-y* curve |
| $K_{sec}$ | Secant spring stiffness |
| $M$ | Mudline moment |
| $N$ | Number of cycles |
| $T_p$ | Peak spectral period |
| $U_{1\text{-}hr,hub}$ | One hour average wind speed at hub height |
| $\varepsilon_c$ | Strain at 50% of undrained compression tests of undisturbed soil samples |
| $\gamma'$ | Submerged unit weight |
| $\lambda_N$ | Degradation factor |
| $\rho$ | Density of steel |
| $\sigma$ | Standard deviation |
| $\xi$ | Empirical coefficient |

## 4.1 Introduction

Offshore wind turbines (OWTs) are subjected to cyclic environmental loading from wind and waves and cyclic operational loads from rotating blades. Most OWTs are supported by monopile foundations, which account for approximately 75% of currently installed OWT foundation systems [1]. Due to the lack of redundancy in the design of a monopile and the nature of OWT

loading, lateral soil capacity is one of the primary limit states for the foundation. Lateral monopile capacity can be significantly affected by cyclic loading, causing failure at a cyclic load amplitude lower than the failure load under monotonic loading [2].

In terms of soil behavior, cyclic loading can be categorized into long-term or short-term loading: during long-term cyclic loading, the pore pressure generated by cyclic loading dissipates and drained soil behavior may be assumed; conversely, short-term cyclic loading leads to undissipated pore pressures which decrease effective stress and consequently reduce soil stiffness and undrained shear strength [3–5]. This issue is particularly of importance for clays, as the time for pore pressure to dissipate is typically much longer than for sands. Undrained clay behavior under short-term cyclic soil-pile loading typically includes plastic deformation of the soil (and subsequent gap formation at the pile head [4–7]), which comes from the reduction in soil modulus and undrained shear strength as a function of pore pressure build-up. This paper is focused on short-term cyclic loading of clays, a situation which arises for OWTs during storm conditions.

The impacts of short-term cyclic loading for monopiles in clay affect the assessment of both the ultimate limit state (ULS) and serviceability limit state (SLS) of OWTs. In the context of geotechnical design, the ULS of an OWT monopile is dictated by lateral soil-pile resistance, which is affected by cyclic loading. Reduction in soil-pile stiffness decreases the natural frequency of the entire OWT structure, causing the OWT natural frequency to shift towards the wave frequency spectra and to the frequency of a single OWT blade rotation (or 1P frequency). Under these circumstances, loads can be dynamically amplified and the simultaneous reduction of foundation capacity from cyclic loading and the amplification of loading can exceed the ULS of the soil. In terms of SLS, OWT monopiles are often designed to not exceed 0.5° of tilt or rotation at the mudline (or other similar value as dictated by the turbine manufacturer). The 0.5° threshold considered here consists of 0.25° of construction tolerance and 0.25° of permanent accumulated rotation [8]. This permanent accumulated rotation arises from inelastic soil behavior which is

typically induced by cyclic wind and wave loads during the design life of the OWT [8]. In short, short-term cyclic loading of OWTs during storm conditions can induce two important and interactive effects: natural frequency degradation of the entire system and accumulated permanent rotation at the mudline. This paper considers both effects individually using novel combinations of existing design methods, since at present there is no consensus on a coherent design method for estimating either effect.

Laterally loaded OWT monopiles are usually designed and analyzed using the *p-y* curve method [8], which represents soil-pile interaction as a series of nonlinear springs along the length of the pile. Because the experimental work to derive these curves was originally performed on small-diameter piles, many researchers have examined the discrepancy between predicted pile response from the *p-y* method for large-diameter OWT monopiles and that which is predicted via finite element models or experimental modeling, e.g. [9–12]; however, the perceived complexity and computational expense of finite element models has prevented their widespread use, despite the increased accuracy of their constitutive models [5]. A detailed experimental investigation is required to assess the true behavior of large diameter monopiles in clay subjected to cyclic lateral loading; however, in the absence of such a study, existing cyclic *p-y* curve models are used in this paper as a best estimate.

This paper uses existing cyclic *p-y* methods to examine two effects: natural frequency degradation and permanent accumulated mudline rotation for monopile-supported OWTs in clay. Regarding natural frequency degradation, a novel, hybrid approach is proposed using the static Matlock [13] *p-y* curves determined by monotonic loading in conjunction with the ultimate soil resistance ($p_u$) cyclic degradation model proposed by Rajashree & Sundaravadivelu [14] as described in Section 2. Section 3 describes how rainflow counts of stochastic load time histories are used in conjunction with the established *p-y* methods to estimate the cumulative effect of cyclic degradation from a one-hour storm. An alternative, more generalized approach to cyclic

degradation is introduced in Section 4, wherein the stiffness of *p-y* springs within an embedment reduction zone is assumed to be negligible representing the effect of soil disturbance around the pile. The two hybrid methods for estimating natural frequency degradation (Section 5.2) and permanent mudline rotation (Section 5.3) are summarized schematically in Figure 4.1. The magnitude of permanent mudline rotations is predicted based on the unload-reload modulus proposed by [13] for cyclically loaded piles. In this paper, the soil-pile behavior is assumed to be elastic for *p-y* springs with loading less than $0.5p_u$ (half the ultimate resistance of the *p-y* spring).

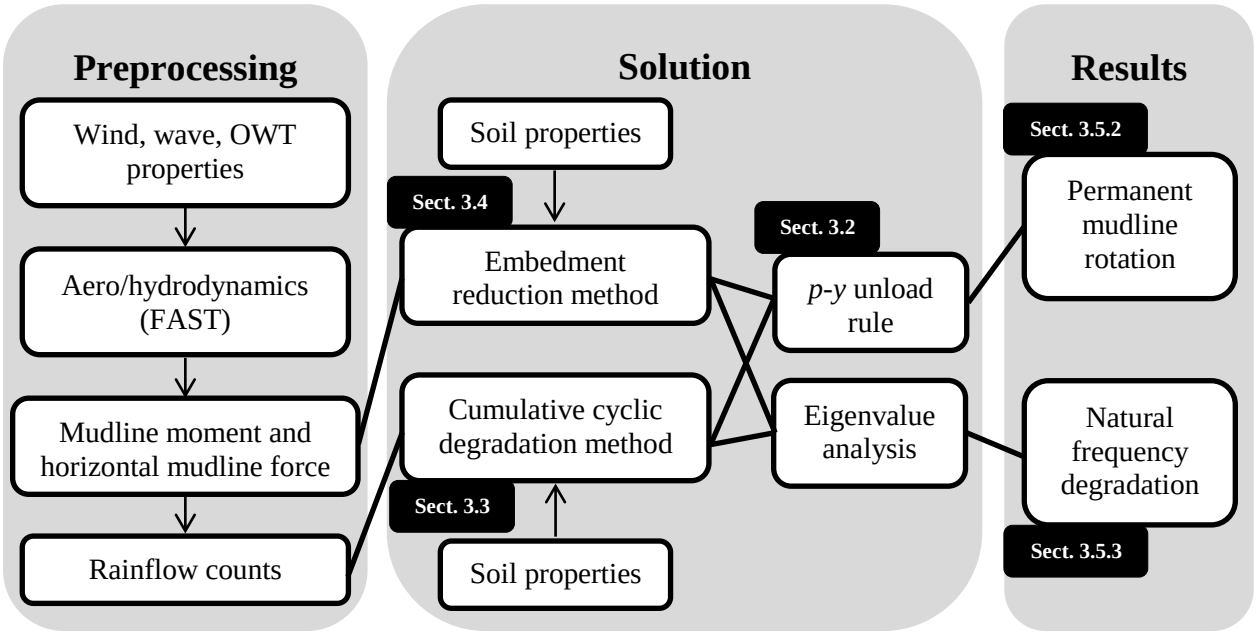


**Figure 4.1 Cyclic pile-soil analysis flowchart**

In Section 5, the effects of these two hybrid approaches are assessed for a range of conditions by examining the frequency degradation and permanent accumulated rotation of the National Renewable Energy Laboratory (NREL) 5MW Reference Turbine [15] supported by a monopile installed in homogeneous deposits of soft, medium, and stiff clay. The turbine and monopile are modeled in FAST [16] for extreme storm conditions representative of two different U.S. Atlantic offshore sites (off the coasts of Massachusetts and Delaware). For both sites, storm conditions are assessed for multiple return periods ranging from 50 to 500 years. While the extreme storm

loading presented here may not represent SLS loading in a traditional sense, the assessment of the SLS for monopiles should be performed for loads which may cause permanent deformation of the soil [8]. The embedment reduction method and the accumulated cyclic degradation method are compared for both natural frequency degradation and permanent accumulated rotation, and the results of this paper show that only the largest load cycles during extreme storms have significant impact on the natural frequency degradation or accumulated permanent rotation.

## 4.2 Existing Cyclic Models for Soil Stiffness and Strength

This section discusses existing models for analyzing monopile foundations in clay subjected to cyclic lateral loading. In most design situations, soil-pile interaction is considered through *p-y* curves which define the nonlinear relationship between lateral soil resistance *p* and displacement *y* along the length of the pile. Det Norske Veritas [8] recommends the *p-y* curves proposed by Matlock [13] for lateral soil-pile resistance, though several other *p-y* models for clay exist (e.g. [6,17]). The American Petroleum Institute (API) [18] recommends the *p-y* curves developed by Reese et al. [17] for stiff clays; however, research performed by [6] indicated that the clay imbibed water during testing and therefore manifested more degradation than other cases. For this reason, this paper uses the Matlock *p-y* curve formulation for monopiles in clay [8]. Further comparison of clay *p-y* curves and behavior under cyclic degradation can be found in [19].

The Matlock *p-y* curves are currently recommended by design guidelines (e.g. DNV [8]) for the analysis of laterally loaded OWT monopile foundations in clay, despite the fact that the curves were developed for slender piles and OWT monopiles exhibit stiff pile behavior [9]. The *p-y* curves are recommended primarily for assessing the lateral response of the pile using a quasi-static load associated with the ULS. Although Matlock has introduced a cyclic version of the *p-y* curve [13], it is neither cycle nor amplitude dependent [8], and provides only a lower bound on the soil-pile lateral stiffness. To overcome this shortcoming in this paper, a quasi-static *p-y* degradation model by Rajashree & Sundaravadivelu [14] is used in conjunction with

static/monotonic Matlock *p-y* curves to explicitly account for the effects of both load amplitude and number of cycles on soil-pile behavior. This hybrid cyclic *p-y* model is used for all calculations presented in this paper.

The estimation of permanent accumulated rotations at the mudline requires an additional model to define the elastic-plastic characteristics of the *p-y* curves. The *p-y* curves developed by Matlock [13] were based on monotonic lateral load tests of slender, small diameter (12.75 in = 0.32 m) piles in soft, saturated clay. In this paper, static *p-y* curve behavior is assumed to be perfectly plastic after the lateral resistance $p$ reaches the ultimate resistance $p_u$ with the full *p-y* curve defined by

$$p = \begin{cases} 0.5 p_u \left( \dfrac{y}{y_c} \right)^{1/3} & \text{for } y \le 8 y_c \\ p_u & \text{for } y > 8 y_c \end{cases} \quad \textbf{(1)}$$

where

$$p_u = (3 s_u + \gamma' x) b + J s_u x \le 9 s_u b \quad \textbf{(2)}$$

in which $s_u$ is the undrained shear strength, $\gamma'$ is the submerged unit weight, $b$ is the pile diameter, $J$ is an empirical factor ranging from 0.25 to 0.5 (for stiff to soft clays, respectively), and $x$ is the depth below mudline. The depth at which $9 s_u b$ controls $p_u$ is referred to as the transition point, $x_r$. Spring displacement is normalized by

$$y_c = 2.5 \varepsilon_c b \quad \textbf{(3)}$$

where $\varepsilon_c$ is the strain occurring at one-half the maximum stress in laboratory undrained compression tests of undisturbed soil samples.

Because clay *p-y* curves have infinite initial stiffness, a finite estimate of initial stiffness is needed here to estimate initial and degraded natural frequencies of the OWT system. Two finite initial stiffness estimates are given in [8]; the first (denoted as $K_0$ here) is defined as

$$K_0 = \xi \frac{p_u}{b\varepsilon_c^{0.25}} \tag{4}$$

where $\xi$ is an empirical coefficient equal to 10 for normally consolidated clay and 30 for overconsolidated clay. If piecewise linear segments are used to represent the nonlinear *p-y* curves however, the recommended endpoint of the first linearized segment is $p/p_u = 0.23$ and $0.1y_c$ [8], thereby making an alternative estimation of the initial stiffness defined as

$$K_1 = \frac{0.23p_u}{0.1y_c}. \tag{5}$$

Permanent accumulated rotation after loading is assessed by assuming that soil springs unload elastically following the nonlinear loading path of the *p-y* curve for soil resistance $p < 0.5p_u$ and spring displacements $y < y_c$ and linearly for $p > 0.5p_u$ and $y > y_c$; for inelastic soil springs in which $p > 0.5p_u$, the unload/reload modulus of the springs is assumed to behave as proposed in [13]. It should be noted that large mudline pile loads generally cause springs near the soil surface to load beyond the elastic range, with increases in mudline loading causing progressively more soil springs along the length of the pile to enter the inelastic range.

Both of initial stiffness estimates are shown in Figure 4.2, assuming $\xi = 30$, along with a schematic representation of the unload/reload modulus assumption from [13].

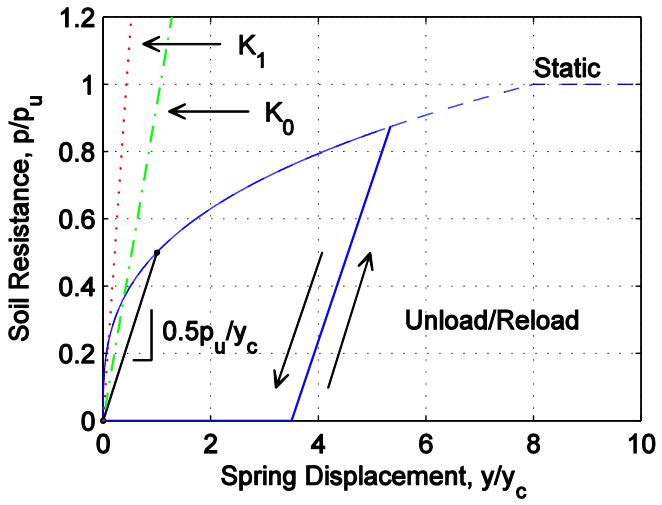


**Figure 4.2 Static Matlock** [13] ***p-y*** **Curve with Cyclic Unload/Reload Modulus Assumption and Estimations of Initial Stiffness from** [8]**.**

The Rajashree & Sundaravadivelu [14] *p-y* degradation model is used in conjunction with the static Matlock [13] *p-y* curves to define soil-pile resistance as a function of load amplitude (via soil spring displacement) and number of cycles. The *p-y* degradation model degrades the initial (first cycle) ultimate soil resistance $p_u$ to a degraded ultimate soil resistance $p_{uN}$ after a number of cycles $N$ by

$$p_{uN} = (1-\lambda_N)\,p_u \tag{6}$$

with degradation factor $\lambda_N$ defined as

$$\lambda_N = \frac{y_1}{0.2b}\log(N) \le 1. \tag{7}$$

in which $y_1$ is the displacement predicted by the static *p-y* curve and $b$ is the pile diameter. The degradation method is therefore a function of the number of cycles and spring displacement (and consequently also mudline load amplitude and corresponding pile-soil deformation shape), but is independent of load frequency. Figure 4.3 demonstrates the degradation of a *p-y* curve with 10 and 100 cycles of loading assuming an initial static displacement of $0.01b$ and $0.05b$. For a 6 m diameter pile, a spring displacement of $0.05b$ corresponds to 0.3 m, which is relatively significant

in the context of OWT monopile displacements given the mudline displacement design limitation of 0.2 m used by [20]. A spring displacement of 0.01*b* corresponds to 0.06 m of spring displacement and as shown in Figure 4.3, approximately 5% degradation of the ultimate soil resistance ($p/p_u \approx 0.95$).

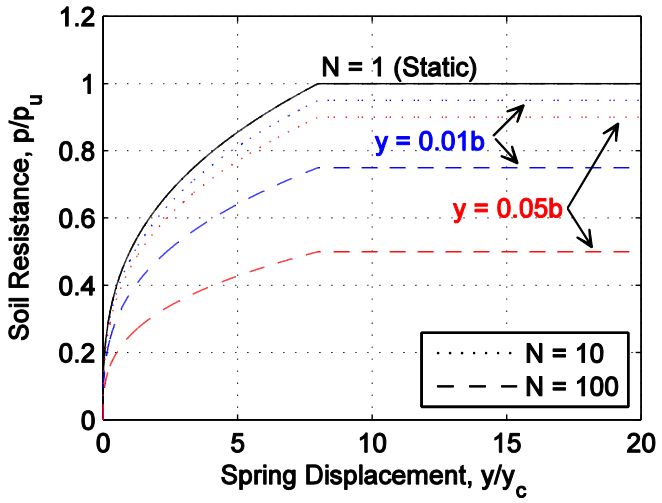


**Figure 4.3 *P-y* Curve Degradation by Rajashree & Sundaravadivelu** [14]

This form of *p-y* curve degradation compared favorably to one-way cyclic experimental testing of a small diameter pile (25.4 mm) in soft clay using the ultimate soil resistance relationship proposed by Matlock and for cyclic load magnitudes up to approximately 70% of the static lateral pile capacity [14]. It is assumed here that the same caveats associated with the *p-y* curves also apply to the hybrid Matlock-Rajashree & Sundaravadivelu degradation model proposed here.

## 4.3 Cumulative Cyclic Degradation Model

Because the *p-y* method is recommended for ULS conditions, cyclic loading effects are typically taken into account using a quasi-static cyclic load amplitude and applied to a soil-pile system supported by *p-y* curves modified to represent the lower bound resistance of a pile which has reached equilibrium under cycling [8,18]. Using this method assumes an infinite number of

cycles at constant load amplitude, which neglects the potential cumulative effects of varying load amplitudes from a storm time history.

In contrast, the cyclic accumulation method developed at the Norwegian Geotechnical Institute [2,21] considers cumulative cyclic degradation for application to piles supported by *p-y* curves, wherein cyclic load histories (e.g. from extreme storm loading) are idealized using load parcels consisting of numbers of load cycles at different load amplitudes. These load parcels are then applied in order of increasing load amplitude using a cyclic accumulation/degradation method between each step to account for the equivalent degradation from the number of load cycles *N* associated with that load amplitude.

In the case of the NGI method, the cyclic accumulation method is applied in a three-dimensional finite element model with the degradation of soil properties evaluated at each node using a custom constitutive model informed by cyclic strain contour diagrams. While this consideration of cyclic accumulation is likely a more accurate assessment of pore pressure accumulation and consequent cyclic degradation, the computational expense and complexity of the model are limiting factors.

A simplified cyclic degradation method is proposed in this paper based on a hybrid of static/monotonic *p-y* curves [13] and *p-y* curve degradation [14]. The process is as follows:

- Idealize storm load history into *i* load parcels consisting of horizontal mudline force, mudline moment, and associated number of cycles ($H_i$, $M_i$, $N_i$) using rainflow counting (Section 4.5.1).
- Find the static *p-y* spring displacement associated with first load parcel ($H_1$, $M_1$).
- Determine the ultimate soil resistance $p_{u,N1}$ for each spring according to the *p-y* degradation model (Eqs. 6-7) using $N_1$ and the displacement associated with ($H_1$, $M_1$).
- Load the degraded *p-y* pile-spring model with ($H_1$, $M_1$) and unload the degraded *p-y* pile-spring model using the unloading rules described in Figure 1.

- Find the *p-y* spring displacement for the next load parcel ($H_{i+1,}$ $M_{i+1}$) using the current pile-spring model.
- Further degrade the ultimate soil resistance by $p_{u,Ni+1} = (1-\lambda_{Ni+1})\ p_{u,N1}$ for each spring using $N_{i+1}$ and the displacement associated with ($H_{i+1}$, $M_{i+1}$).
- Load the degraded *p-y* pile-spring model with ($H_{i+1}$, $M_{i+1}$) and unload the degraded *p-y* pile-spring model.
- Repeat process for remainder of load parcels.

An example of this process is demonstrated in Figure 4.4 using a single *p-y* spring and three load parcels consisting of a lateral force only (no moment): (1) represents the static/monotonic initial *p-y* curve which informs the degradation of the first load parcel; (2) illustrates the load-unload cycle for the first load parcel, which in this instance remains elastic; the *p-y* curve associated with the first load parcel informs the degradation for the second load parcel; (3) denotes the peak of the second load parcel which exceeds the elastic limit and unloads linearly; (4) demonstrates the final permanent displacement after the third and final load parcel. It should also be noted that because degradation occurs between the second and third load parcels, the linear reloading of the third load parcel at (3) is at a different slope than the unloading branch of the second load parcel.

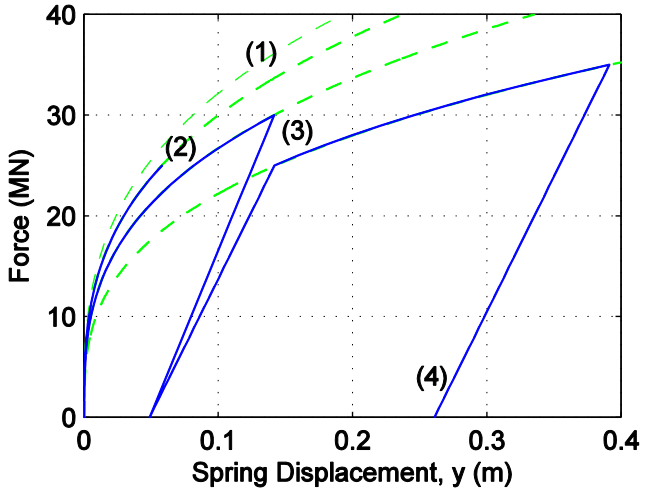


**Figure 4.4 Single spring depiction of cumulative load effect from rainflow count degradation. Dashed lines represent degrading *p-y* curves and solid lines represent the load-unload path of the single *p-y* spring.**

## 4.4 Degradation via Embedment Depth Reduction

The *p-y* degradation model presented by Rajashree & Sundaravadivelu [14] primarily degrades the strength of the soil rather than the stiffness. This section outlines an alternative method which explicitly reduces the embedment depth of the monopile to reflect the effects of the degradation of soil stiffness due to short-term cyclic loading. This method is motivated by observations of a zone of soil disturbance around the circumference of the pile in the natural frequency experimentation performed in [22], demonstrating inelastic soil behavior post-cycling with a significant amount of permanent monopile rotation. The disturbance of the soil around the perimeter of the pile may be indicative of gapping, which occurs when soil in the passive zone behind the pile is loaded beyond the linear range and residual soil displacements remain post-loading. Upon reloading, the pile travels freely through the gap before re-contacting soil. This gapping behavior has been approached in a *p-y* context using gap elements [23], but generally speaking it is a difficult behavior to characterize; moreover, in a linearized *p-y* model (required for determining the natural frequency of the OWT via eigenvalue analysis), it is not clear how these gap elements would contribute to soil-pile stiffness.

While the cumulative cyclic degradation model described in the previous section takes soil disturbance into account implicitly, cyclic degradation could also be modeled more simply and explicitly in terms of embedment reduction (Figure 4.5). This method assumes that there is no stiffness contribution from the *p-y* soil springs within a user-defined embedment reduction zone; in this paper, the results from embedment reduction of 0.5*b* and 1*b* are presented to demonstrate a range of possible behavior.

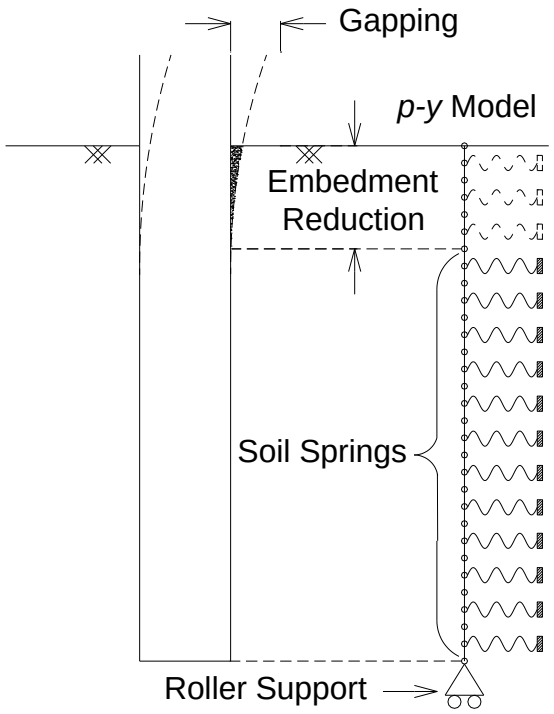


**Figure 4.5 Pile embedment reduction method**

OWT natural frequency was calculated as a function of load level using *p-y* secant stiffness (Figure 4.6) and including embedment reduction as follows:

- Mudline loads (*H*,*M*) were applied to the top of a *p-y* pile-spring model, assuming pile springs in the embedment reduction zone contribute zero lateral stiffness.
- From the resulting displacement *y* for each spring along the length of the pile, the soil resistance *p* for each spring was determined from Eq. 1.
- The secant stiffness $K_{sec}$ was then calculated as *p/y*.
- The natural frequency of the system was calculated via eigenvalue analysis.

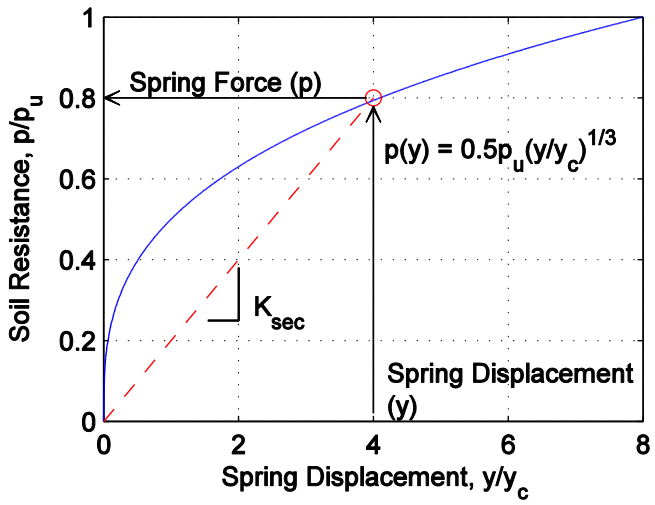


**Figure 4.6 Determination of Secant Stiffness for Natural Frequency Degradation**

## 4.5 Application to the NREL 5MW Reference Turbine

The effects of short-term cyclic loading are examined in this section for the NREL 5MW Reference Turbine supported by a 6 m diameter monopile embedded in clay (Figure 4.7). The NREL open-source wind turbine simulation program FAST [16] was used to calculate structural loads caused by one hour stochastic wind and wave time histories representative of the extreme storm for two locations off the U.S Atlantic coast. Two different approaches (Figure 4.1) are compared here for assessing OWT natural frequency and permanent accumulated pile rotation:

(1) The average maximum horizontal mudline force ($H$) and mudline moment ($M$) from the stochastic time histories is used with a *p-y* curve pile-spring system including embedment reduction.

(2) Rainflow counts of the time histories were used to idealize the stochastic time histories into load parcels of ($H$, $M$, $N$) and were used in conjunction with the cumulative cyclic degradation method proposed in Section 3.

The pile design in this paper consists of a 6 m diameter pile with wall thickness of 0.09 m embedded 34 m into homogeneous clay with submerged unit weight of 9.2 kN/m$^3$. Three different undrained shear strengths are considered (35 kPa, 50 kPa, and 100 kPa) to examine the degradation and inelastic behavior of soft, medium, and stiff clays, as shear strength is the most

influential property in *p-y* curve formulation. In a true design context, the embedment depth of the piles would likely vary from site to site in order to approach fixity at the base of the pile (i.e., zero pile kick) and adequate force-displacement behavior over the range of expected loads; however, the focus of this paper is to examine the behavior which could occur as a function of soil properties and not to focus strictly on the behavior of the pile itself.

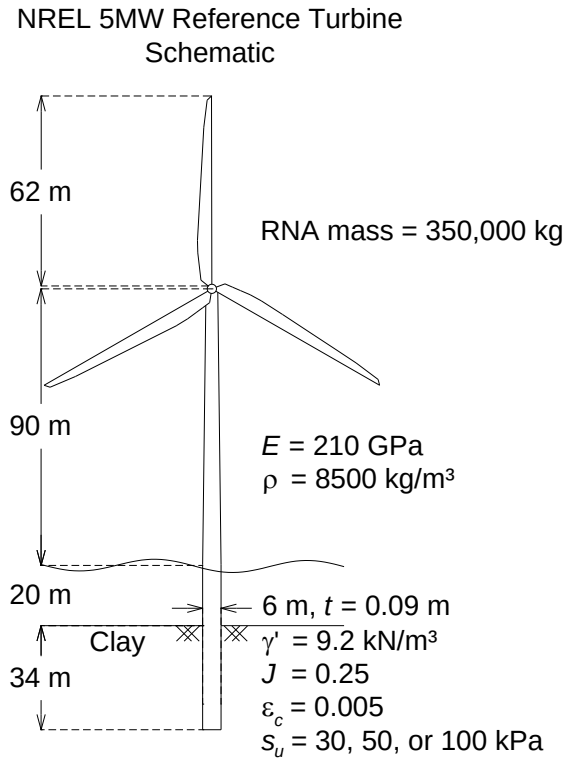


**Figure 4.7 NREL 5MW Reference Turbine**

### 4.5.1 Environmental Condition and Load Effect Models

The 1-hr average wind speed at hub height ($U_{1\text{-}hr,hub}$) and significant wave height ($H_s$) from two sites were considered in this study: a Massachusetts (MA) site between Martha's Vineyard and Block Island [24] and the National Data Buoy Center (NDBC) buoy 44009 off the coast of Delaware (DE) [25]. Because water depths for the MA and DE sites were 15 m and 30 m

respectively, $H_s$ values were scaled linearly for the NREL 5MW Reference Turbine model's 20 m water depth.

The site conditions (Table 2.5) represent storm conditions for mean return periods between 50 and 500 years. In the case of the MA site, the 50- and 500-year conditions are taken from [24], using two methods to estimate the 50-year conditions: 1) using data only from tropical storms and 2) from approximately 20 years of measured data. The site conditions for the DE site are calculated by the authors using independent extreme value distributions fit to 30 years of annual maxima of wind and wave measurements from the National Data Buoy Center [25].

The peak spectral period $T_p$ was calculated as a function of $H_s$ for extreme sea states [8] using

$$T_p = 11.1\sqrt{H_s / g} \quad \textbf{(8)}$$

where $g$ is the acceleration due to gravity, similar to the approach taken in [19,26]. The minimum estimate of $T_p$ is conservative, as smaller values of $T_p$ shift the wave frequency spectra closer to the natural frequency of the NREL 5MW Reference Turbine (thereby increasing dynamic loads) and also because smaller $T_p$ contributes to steeper waves and consequently greater particle velocity and acceleration.

Mudline loads for the NREL 5MW Reference Turbine were generated using NREL's aeroelastic code FAST [16] for the environmental site conditions in Table 4.1. Six 1-hr time histories per environmental site condition were simulated with a perfectly fixed mudline condition, 0° yaw, co-directional wind and waves, and parked and feathered blades, similar to design load case 6.1a [8,28]. The average of the maximum horizontal mudline force and mudline moment from the six 1-hr time histories is denoted as $H_{max,avg}$ and $M_{max,avg}$. Turbulent winds were generated according to the Kaimal spectrum assuming a turbulence intensity of 0.11. Wind loads on the OWT blades were calculated using Blade Element Momentum (BEM) theory assuming a power law for

vertical wind shear with an exponent of 0.14. Linear irregular wave kinematics were generated using the JONSWAP spectrum and converted into wave loads using Morison's equation with $C_m$ and $C_d$ equal to 1.75 and 1.26, respectively.

**Table 4.1 Environmental site conditions and load summary for NREL 5MW Reference Turbine in 20 m water depth**

| **Site** | | **MA** | | **DE** | |
|---|---|---|---|---|---|
| **Mean Return Period** | 50 years | 50 years | 500 years | 50 years | 500 years |
| **Wind-Wave Estimation Method** | Tropical Storm | Measured | Measured | Measured | Measured |
| $\boldsymbol{U_{1\text{-}hr,hub}}$ **(m/s)** | 47.6 | 38.1 | 42.2 | 32.8 | 37.4 |
| $\boldsymbol{H_s}$ **(m)** | 11.3 | 8.3 | 9.9 | 5.4 | 5.7 |
| $\boldsymbol{T_p}$ **(s)** | 11.9 | 10.2 | 11.1 | 8.2 | 8.5 |
| $\boldsymbol{H_{max,avg}}$ **(MN)** | 6.32 | 3.64 | 4.26 | 2.48 | 2.51 |
| $\boldsymbol{\sigma_{H,avg}}$ **(MN)** | 1.12 | 0.861 | 1.00 | 0.618 | 0.633 |
| $\boldsymbol{M_{max,avg}}$ **(MNm)** | 119 | 66.2 | 80.8 | 45.5 | 47.7 |
| $\boldsymbol{\sigma_{M,avg}}$ **(MNm)** | 16.6 | 13.4 | 14.4 | 10.6 | 10.5 |
| **Avg. Correlation Coefficient (*H*,*M*)** | 0.860 | 0.834 | 0.872 | 0.806 | 0.817 |

It should be noted that the wave heights and periods shown in Table 4.1 may lead to breaking waves, but the effects of these waves are neglected in this paper. Figure 4.8A shows an example of the time histories of *H* and *M* from one 1-hr realization of the 50-year (storm) condition at the MA site. In Figure 4.8B, the assumption of *H* and *M* concurrence is further justified by the similar trends in the rainflow counts for all six 1-hr realizations of the time histories from the storm-based 50-year conditions at the MA site.

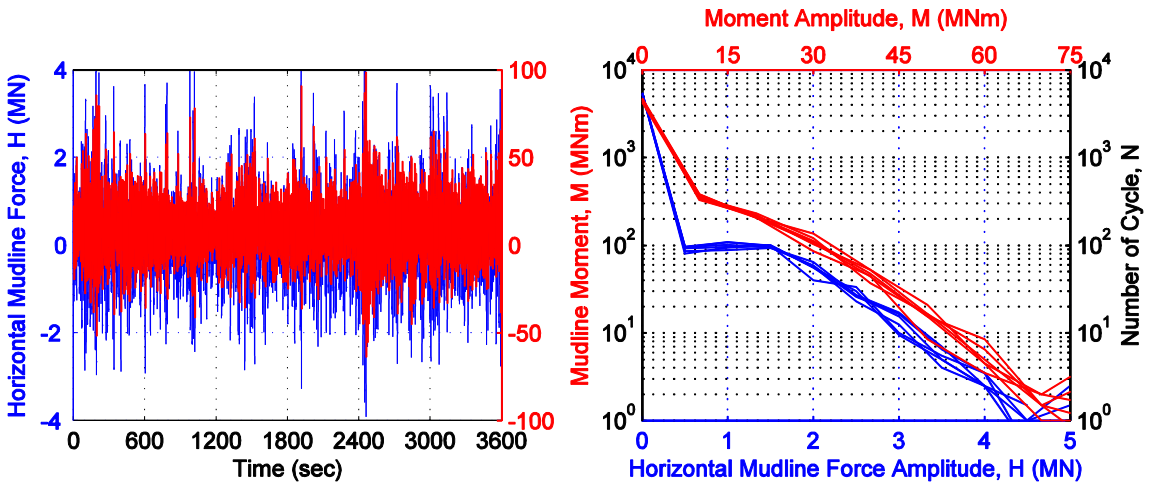


**Figure 4.8 Example (A) One realization of a 1-hr storm load time history and (B) rainflow cycle counts of horizontal mudline force and moment from six random 1-hr storm load histories for 50-year (storm) MA site**

For degradation analysis it was necessary to idealize the storm time histories into load parcels of ($H$, $M$, $N$). Because rainflow counts for $H$ and $M$ are calculated separately and $H$ and $M$ are not perfectly correlated, there is no precise way of linking $N$ to a simultaneous pair of ($H$, $M$); consequently, a synthetic rainflow count of $H$ was created deterministically as a function of $M$ using the relationship between $H$ and $M$ for the FAST time histories from each load scenario. For the storm-based 50-year MA time histories, the average slope relating $H$ to $M$ is 1/0.0582 with a correlation coefficent of 0.860; after determining the rainflow count for $M$, a synthetic rainflow count for $H$ was created by using the number of cycles $N$ from the moment count and by scaling $M$ by a factor of 0.0582 (Figure 4.9). While the synthetic rainflow count overpredicts the number of cycles at lower amplitudes, the higher amplitude cycles influence degradation results much more strongly than the lower amplitude cycles. Additionally, the magnitude of $M$ influences results more strongly than $H$.

The average rainflow counts of the six realizations for each load scenario (Table 4.2) indicate that the storm-based 50-year MA load scenario will lead to greater degradation of the ultimate soil resistance $p_u$ and therefore to greater degradation of the OWT natural frequency and larger permanent accumulated rotation.

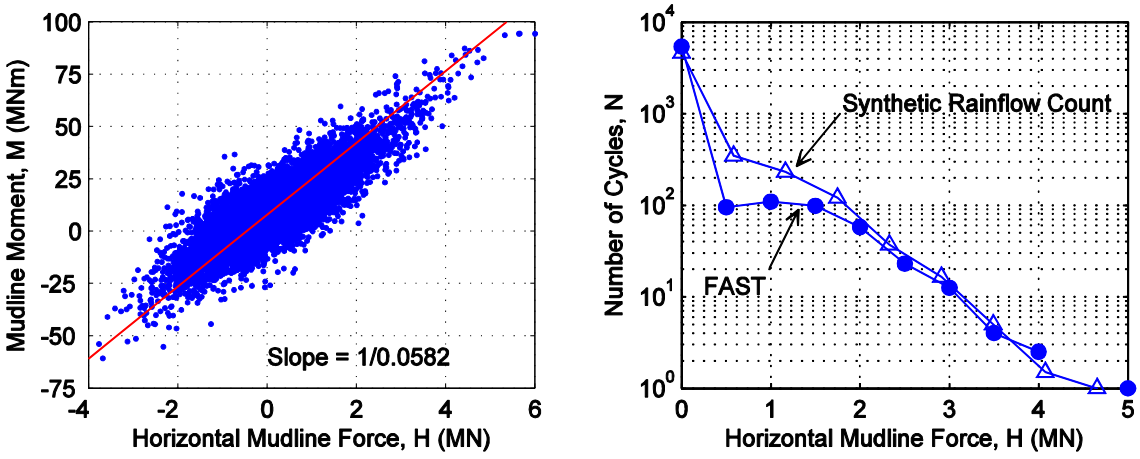


**Figure 4.9 Example (A) Relationship between horizontal mudline force and mudline moment and (B) comparison of synthetic rainflow cycle count from mudline moment and horizontal mudline force from one realization of a 1-hr storm load history for 50-year (storm) MA site**

**Table 4.2 Average Rainflow Counts and Slope for the MA and DE Load Scenarios**

| **Mudline Moment Amplitude (MNm)** | **MA** | | | **DE** | |
|---|---|---|---|---|---|
| | 50 years Tropical Storm | 50 years Measured | 500 years Measured | 50 years Measured | 500 years Measured |
| 0 | 4519 | 3761 | 4394 | 3454 | 4033 |
| 10 | 357 | 359 | 344 | 431 | 435 |
| 20 | 215 | 247 | 211 | 238 | 236 |
| 30 | 111 | 93 | 100 | 52 | 45 |
| 40 | 46 | 26 | 29 | 4.9 | 4.7 |
| 50 | 16 | 4.3 | 8.4 | 0.2 | 0.3 |
| 60 | 5.4 | 1.6 | 2.3 | 0 | 0 |
| 70 | 1.6 | 0 | 0.6 | 0 | 0 |
| 80 | 1.3 | 0 | 0.1 | 0 | 0 |
| 90 | 0.3 | 0 | 0 | 0 | 0 |
| 100 | 0.4 | 0 | 0 | 0 | 0 |
| ***M/H* slope (m)** | 1/0.0582 | 1/0.0536 | 1/0.0605 | 1/0.0470 | 1/0.0491 |

### 4.5.2 Natural Frequency Degradation

While calculating the natural frequency of the tower and RNA of an OWT is relatively straightforward, including soil-structure interaction in the calculation requires several modeling assumptions due to the nonlinearity of soil-structure behavior and the requirement of linear

springs in a natural frequency eigenvalue analysis. As mentioned in Section 2.1, two different estimates of initial stiffness can be used for clays (identified previously as $K_0$ and $K_1$); considering homogeneous deposits of clay with $s_u$ = 35 kPa, 50 kPa, and 100 kPa, Table 4.3 illustrates the slight (< 5%) variation in the estimation of the first natural frequency $f_1$ for the NREL 5MW as a function of initial stiffness, and approximately 7% difference in $f_1$ between the $s_u$ = 35 kPa and $s_u$ = 100 kPa clays.

**Table 4.3 Estimations of the Initial First Natural Frequency ($f_1$) for the NREL 5MW Reference Turbine**

| $s_u$ | $f_1(K_0)$ | $f_1(K_1)$ |
|---|---|---|
| 35 kPa | 0.234 Hz | 0.245 Hz |
| 50 kPa | 0.241 Hz | 0.250 Hz |
| 100 kPa | 0.251 Hz | 0.257 Hz |

The natural frequencies in Table 4.3 are only applicable for very small loads; for larger loads, the natural frequency of the OWT is determined by the secant stiffness of the *p-y* springs (using the method described in Section 4.2). Using the average maximum loads from the six load scenarios in Table 4.1 and limiting the maximum stiffness of the springs to $K_0$, Table 4.4 compares the difference in large strain natural frequency estimation to initial natural frequency for cases including no embedment depth reduction, one pile diameter *b* of embedment reduction, and cumulative cyclic degradation. For the cumulative cyclic degradation case, the secant *p-y* stiffness $K_{sec}$ was defined using the peak spring displacement from the final storm load parcel.

Table 4.4 shows that the dominant load scenario for all analyses is the 50-year MA storm case. The higher magnitude of the MA loads had a more significant effect on natural frequency than the lower magnitude DE loads. It is also interesting to note that the cumulative cyclic degradation method estimates higher natural frequencies (less reduction as compared to small strain estimates) when compared to the quasi-static *p-y* method using average maximum loads. This is likely due to the fact that the average maximum loads are significantly larger than the maximum load cycles

from rainflow counting, but in this case using a quasi-static *p-y* method with average maximum loads is more conservative than the cumulative effect of a storm time history.

**Table 4.4 Percent difference in first natural frequency from initial stiffness estimation ($K_0$) for the average maximum mudline loads and average percent difference for the cumulative load effect from rainflow counts. Negligible changes in natural frequency are denoted as "-".**

| Undrained Shear Strength ($s_u$) | | MA | | | DE | |
|---|---|---|---|---|---|---|
| | | 50 years Tropical Storm | 50 years Measured | 500 years Measured | 50 years Measured | 500 years Measured |
| No Embedment Reduction | 35 kPa | -28% | -7.1% | -13% | -1.5% | -1.7% |
| | 50 kPa | -14% | -2.5% | -4.4% | -0.2% | -0.3% |
| | 100 kPa | -2.6% | -0.2% | -0.7% | - | - |
| 0.5*b* Embedment Reduction | 35 kPa | -35% | -12% | -18% | -3.2% | -3.6% |
| | 50 kPa | -20% | -4.5% | -7.8% | -1.0% | -1.2% |
| | 100 kPa | -4.4% | -0.8% | -1.6% | - | - |
| 1*b* Embedment Reduction | 35 kPa | -45% | -19% | -26% | -6.7% | -7.4% |
| | 50 kPa | -28% | -8.6% | -14% | -2.7% | -3.0% |
| | 100 kPa | -8.0% | -2.0% | -3.1% | -0.4% | -0.5% |
| Cumulative Load Effect | 35 kPa | -24% | -6.0% | -12% | -0.8% | -1.1% |
| | 50 kPa | -9.3% | -2.0% | -4.0% | -0.2% | -0.3% |
| | 100 kPa | -1.5% | < 0.1% | -0.5% | < 0.1% | < 0.1% |

### 4.5.3 Estimation of Permanent Accumulated Mudline Rotation

As previously proposed, permanent inelastic soil deformation is assumed to occur when *p-y* springs are mobilized beyond $p/p_u = 0.5$; *p-y* springs for which $p/p_u < 0.5$ are assumed to behave elastically. In order to broadly measure the severity of the storm loading conditions above, the quasi-static average maximum mudline loads $H_{max,avg}$ and $M_{max,avg}$ from the most severe storm case (storm-based 50-year MA) were used to determine the degree of mobilization (i.e., the ratio of demand $p$ vs. ultimate resistance $p_u$) for *p-y* spring-supported monopiles embedded in homogeneous clay deposits of $s_u$ = 100 kPa, 50 kPa, and 35 kPa (Figure 4.10). The soil springs are assumed to be symmetric, thus Figure 4.10 demonstrates the degree of *p-y* mobilization in terms of the absolute value of $p$.

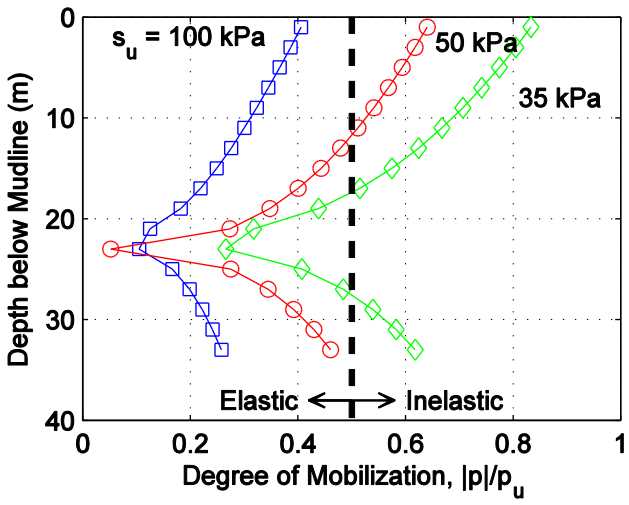


**Figure 4.10 Degree of *p-y* mobilization for undrained shear strengths of 100, 50, and 25 kPa considering average maximum loads from six random 1-hr storm load histories for 50-year (Tropical Storm) MA site**

For the monopile in stiff clay ($s_u$ = 100 kPa), even the most severe loading conditions from Table 2.5 do not push the soil beyond the elastic range. For the pile in medium (50 kPa) clay, the soil at approximately the top third of the pile exceeds the elastic range, and for the soft (35 kPa) clay the majority of the soil behaves inelastically. The influence of inelastic soil behavior is further demonstrated by the load-unload paths of the pile head for these three cases in Figure 4.11, where no permanent accumulated rotation can be seen for the 100 kPa case, a very small amount of permanent accumulated rotation for the 50 kPa case, and an exceedance of the 0.25° permanent mudline rotation SLS for the 35 kPa case.

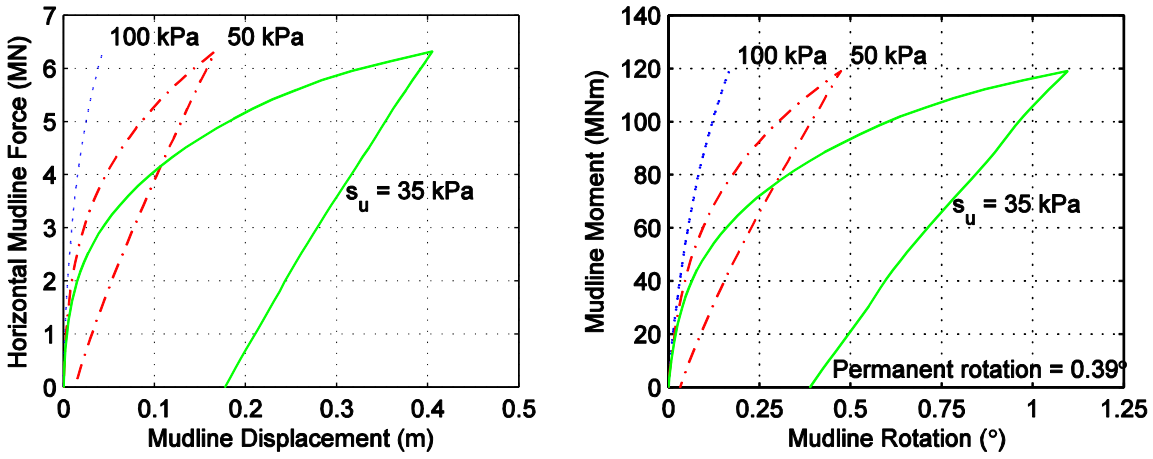


**(A)** **(B)**

**Figure 4.11 (A) Force-displacement and (B) Moment-rotation load-unload path for undrained shear strengths of 100, 50, and 25 kPa considering average maximum loads from six random 1-hr storm load histories for 50-year (Tropical Storm) MA site**

As in the prior section, the permanent accumulated rotation from the average maximum load cases was compared with the cumulative cyclic degradation method (Table 4.5). Permanent rotations less than 0.01˚ were considered to be negligible (denoted as "-" in Table 4.5). The results from the embedment reduction cases of 0.5*b* and 1*b* show significantly more permanent rotation than the cumulative cyclic degradation method for the 50-year MA (tropical storm) case; considering a monopile in $s_u$ = 35 kPa clay, the removal of *p-y* springs prior to applying the 50-year MA tropical storm loads exceeded the capacity of the pile for both 0.5*b* and 1*b* amounts of embedment reduction. It should also be noted however that the average maximum mudline loads used in the embedment reduction cases exceeds the magnitude of the highest cycles obtained from rainflow counting; as such, the results in Table 4.5 are also representative of the effect of load magnitude on the estimation of permanent accumulated rotation.

**Table 4.5 Permanent accumulated rotation for the average maximum mudline loads and average percent difference for the cumulative load effect from rainflow counts. Rotations denoted as "-" are negligible.**

| Undrained Shear Strength ($s_u$) | | MA | | | DE | |
|---|---|---|---|---|---|---|
| | | 50 years Tropical Storm | 50 years Measured | 500 years Measured | 50 years Measured | 500 years Measured |
| No Embedment Reduction | 35 kPa | 0.39˚ | - | - | - | - |
| | 50 kPa | 0.03˚ | - | - | - | - |
| | 100 kPa | - | - | - | - | - |
| 0.5*b* Embedment Reduction | 35 kPa | *failure* | - | 0.05˚ | - | - |
| | 50 kPa | 0.20˚ | - | - | - | - |
| | 100 kPa | - | - | - | - | - |
| 1*b* Embedment Reduction | 35 kPa | *failure* | 0.01˚ | 0.15˚ | - | - |
| | 50 kPa | 0.58˚ | - | - | - | - |
| | 100 kPa | - | - | - | - | - |
| Cumulative Load Effect | 35 kPa | 0.15˚ | - | 0.01˚ | - | - |
| | 50 kPa | 0.01˚ | - | - | - | - |
| | 100 kPa | - | - | - | - | - |

Figure 4.12 compares the cumulative cyclic degradation force-displacement paths considering monopiles in clays with $s_u$ = 35 kPa, 50 kPa, and 100 kPa. The monopile in 100 kPa clay does not sustain any significant cyclic degradation, which is expected given the results of the natural frequency study. For the monopile in 50 kPa clay, only the largest amplitude cycles induce inelastic soil behavior. Both cyclic degradation and highly inelastic behavior are present for the monopile in 35 kPa clay, with cyclic degradation clearly demonstrated between the ultimate and penultimate load parcels.

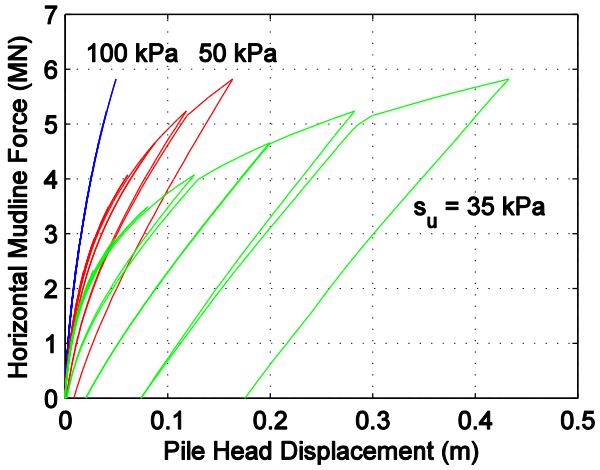


**Figure 4.12 Example force-displacement load-unload path of pile head for cumulative load effect from 1-hr storm load history for 50-year (storm) MA site**

## 4.6 Conclusions

Monopiles are the predominant foundation type for offshore wind turbines (OWTs) and are typically designed using the *p-y* method to model lateral soil behavior. The *p-y* method is relatively simple and easy to implement, making it a convenient alternative to finite element models; however, an important drawback when applied to OWT monopiles is that *p-y* models assume flexible pile behavior and have limited ability to model cyclic effects and permanent accumulated rotation after loading. This paper presents two options for how cyclic degradation may be taken into account (via cumulative cyclic *p-y* degradation and quasi-static *p-y* methods with embedment reduction) and how to estimate permanent accumulated mudline rotation for OWT monopiles in clay. The assumptions inherent in the *p-y* curve formulation necessitate experimental validation of the degradation and permanent accumulated rotation methods presented here for large diameter monopiles. It should be noted that this paper assumed the same embedment depth for the monopile supporting the NREL 5MW Reference Turbine (NREL 5MW) [15] in soft, medium, and stiff clays, and a full examination of appropriate embedment depth (such as the one performed by [20], e.g.) may change the results presented here.

One hour time histories of extreme storm loading (with turbulent winds and irregular waves) were assessed in FAST [16] for two sites off the coast of Massachusetts (MA) and Delaware (DE), considering mean return periods from 50 to 500 years. For each load scenario, six different random time histories were generated, and rainflow counts of the mudline moment *M* were assessed. For the cumulative cyclic degradation analysis, it was necessary to parcel mudline loading into a simultaneous pair of horizontal mudline force *H* and *M* associated with a certain number of cycles; consequently, a synthetic rainflow count of *H* was produced from the rainflow count of *M* using a site-specific coefficient determined from the relationship between *H* and *M* from the FAST time histories.

The natural frequency of the NREL 5MW was examined for monopiles in homogeneous clay deposits with undrained shear strength $s_u$ = 35 kPa, 50 kPa, and 100 kPa (representing soft, medium, and stiff clays respectively) to demonstrate a range of clay behavior subjected to extreme loading. Because the *p-y* curve formulation by [13] has infinite initial stiffness, the estimates of initial natural frequency from DNV [8] were compared. Using the average maximum load from each load scenario, the natural frequency calculated from the secant stiffness of the *p-y* springs was also examined. Using the quasi-static average maximum load to estimate natural frequency was more conservative than using the cumulative cyclic degradation method.

The serviceability limit state (SLS) imposed on OWT monopiles requires the designer to assess the accumulated permanent pile rotation after storm loading to ensure that the mudline rotation does not exceed a threshold magnitude (typically on the order of 0.25°). Design guidelines do not recommend a specific method for determining this permanent residual rotation [8], and consequently some designers conservatively choose to design piles which do not exceed the SLS at peak loading. This paper uses the cyclic unload-reload modulus proposed in [13], assuming that *p-y* springs behave elastically if loaded at or below half of the ultimate resistance $p_u$ at spring depth. Using the average maximum load from the storm-based 50-year MA loads, the monopile in 100 kPa clay remained fully elastic (all springs were loaded < $0.5p_u$), partially inelastic for the 50 kPa clay, and almost fully plastic for the 35 kPa clay (nearly all springs loaded > $0.5p_u$).

The conclusions of this paper indicate that extreme storm loading on OWT monopiles in stiff clays is unlikely to affect the natural frequency and permanent accumulated rotation; further consideration is required for OWT monopiles in medium clays, as storm load estimation and the number of storms experienced by the monopile during the design lifetime may affect future performance. Under the same design conditions, the monopile in soft clay is insufficient with respect to both natural frequency degradation and permanent rotation. The results of this paper also indicate that load magnitude plays a strong role in both natural frequency and permanent

rotation estimation, so using average maximum loads from storm time histories was more conservative than using a cumulative cyclic degradation model. It is recommended that further work on this topic be performed using calibrated *p-y* curves which more accurately represent lateral OWT monopile behavior, and to validate the cumulative cyclic degradation method experimentally or by using more robust modeling methods (e.g. the finite element methods developed by NGI [21]).

## Acknowledgements

The research was supported by the grants CMMI-1234560, CMMI-1234656, the Massachusetts Clean Energy Center and the NSF-sponsored IGERT: Offshore Wind Energy Engineering, Environmental Science, and Policy (Grant Number 1068864).

## References

[1] Hamilton, B., Battenberg, L., Bielecki, M., Bloch, C., Decker, T., Frantzis, L., Paidipati, J., Wickless, A., and Zhao, F., 2013, Offshore Wind Market and Economic Analysis: Annual Market Assessment, Navigant Consulting, Inc., Burlington, MA.

[2] Andersen, K. H., 2009, "Bearing capacity under cyclic loading — offshore, along the coast, and on land. The 21st Bjerrum Lecture presented in Oslo, 23 November 2007," Can. Geotech. J., **46**(5), pp. 513–535.

[3] Andersen, K., 1976, "Behaviour of clay subjected to undrained cyclic loading," Proc. International Conference on the Behavior of Offshore Structures, Trondheim, Norway, pp. 33–44.

[4] Gerolymos, N., and Gazetas, G., 2005, "Phenomenological model applied to inelastic response of soil-pile interaction systems," Soils Found., **45**(4), pp. 119–132.

[5] Heidari, M., Jahanandish, M., El Naggar, H., and Ghahramani, A., 2014, "Nonlinear cyclic behavior of laterally loaded pile in cohesive soil," Can. Geotech. J., **51**, pp. 129–143.

[6] Dunnavant, T. W., and O'Neill, M. W., 1989, "Experimental p-y Model for Submerged, Stiff Clay," J. Geotech. Eng., **115**, pp. 95–114.

[7] Pranjoto, S., and Pender, M., 2003, "Gapping effects on the lateral stiffness of piles in cohesive soil," Proc. Pacific Conf. Earthq. Eng.

[8] DNV, 2013, DNV-OS-J101 Design of Offshore Wind Turbine Structures, Det Norske Veritas AS.

[9] Klinkvort, R. T., Leth, C. T., and Hededal, O., 2010, "Centrifuge modelling of a laterally cyclic loaded pile," International Conference on Physical Modelling in Geotechnics, Taylor & Francis Group, Zurich, Switzerland, pp. 959–964.

[10] Hamre, L., Khankandi, S. F., Strøm, P. J., and Athanasiu, C., 2011, "Lateral behaviour of large diameter monopiles at Sheringham Shoal Wind Farm," Frontiers in Offshore Geotechnics II, pp. 575–580.

[11] Martínez-Chaluisant, V., 2011, "Static and Dynamic Response of Monopiles for Offshore Wind Turbines," University of Wisconsin-Madison.

[12] Hokmabadi, A. S., Fakher, A., and Fatahi, B., 2012, "Full scale lateral behaviour of monopiles in granular marine soils," Mar. Struct., **29**(1), pp. 198–210.

[13] Matlock, H., 1970, "Correlations for design of laterally loaded piles in soft clay," Offshore Technology Conference, Dallas, TX.

[14] Rajashree, S. S., and Sundaravadivelu, R., 1996, "Degradation model for one-way cyclic lateral load on piles in soft clay," Comput. Geotech., **19**(4), pp. 289–300.

[15] Jonkman, J., Butterfield, S., Musial, W., and Scott, G., 2009, Definition of a 5-MW Reference Wind Turbine for Offshore System Development.

[16] Jonkman, J., and Buhl, M. J., 2005, FAST User's Guide, National Renewable Energy Laboratory, Golden, CO.

[17] Reese, L., Cox, W., and Koop, F., 1975, "Field Testing and Analysis of Laterally Loaded Piles in Stiff Clay," Offshore Technol. Conf.

[18] American Petroleum Institute, 2005, "API RP-2A."

[19] Carswell, W., Fontana, C., Degroot, D. J., and Myers, A. T., 2015, "Comparison of Cyclic p-y Curves for Offshore Wind Turbine Monopiles Subjected to Extreme Storm Loading," Proceedings of the ASME 2015 34th International Conference on Ocean, Offshore, and Arctic Engineering (OMAE2015), St. Johns, Newfoundland, Canada.

[20] De Vries, W., and Krolis, V., 2007, "Effects of deep water on monopile support structures for offshore wind turbines," European Wind Energy Conference & Exhibition (EWEC), Milan, pp. 1–10.

[21] Shin, Y., Saue, M., Langford, T., Petter, H., Cho, K., and Park, J., 2014, "Pile-Soil Interaction under Cyclic Loadings for Offshore Wind Monopiles," Proceedings of the ASME 2014 33rd International Conference on Ocean, offshore, and Arctic Engineering (OMAE2014), pp. 1–8.

[22] Lombardi, D., Bhattacharya, S., and Muir Wood, D., 2013, "Dynamic soil–structure interaction of monopile supported wind turbines in cohesive soil," Soil Dyn. Earthq. Eng., **49**, pp. 165–180.

[23] Boulanger, B. R. W., Curras, C. J., Kutter, B. L., Wilson, D. W., and Abghari, A., 1999, "Seismic Soil-pile-strcture interaction experiments and analysis," J. Geotech. Geoenvironmental Eng., **125**(September), pp. 750–759.

[24] MMI Engineering, 2009, Comparative Study of OWTG Standards: Prepared for JIP Sponsorship.

[25] National Oceanic and Atmospheric Administration, 2014, "National Data Buoy Center."

[26] Valamanesh, V., Myers, A. T., and Arwade, S. R., 2015, "Multivariate analysis of extreme metocean conditions for offshore wind turbines," Struct. Saf., **55**, pp. 60–69.

[27] Carswell, W., Arwade, S. R., Degroot, D. J., and Lackner, M. A., 2014, "Soil – structure reliability of offshore wind turbine monopile foundations," Wind Energy.

[28] IEC 61400-3, 2009, Design Requirements for Offshore Wind Turbines, Brussels.

# CHAPTER 5

# MARINE GROWTH EFFECTS ON OFFSHORE WIND TURBINE SUPPORT STRUCTURES

## Authors

W Carswell, Arwade SR, DeGroot DJ

## Abstract

The support structure and foundation of offshore wind turbines (OWTs) can comprise nearly one quarter of the capital cost of an offshore wind project; consequently, any mechanism which requires increased structural material (thereby increasing the cost of the project) should be carefully considered by the designer. Marine growth (MG) increases mass and surface roughness for offshore structures, which can reduce natural frequency and increase hydrodynamic loads, and can also interfere with corrosion protection and fatigue inspections. Design standards and guidelines do not have a unified long-term approach for MG on OWTs, though taking into account added mass and increased drag is recommended. Some standards recommend inspection and cleaning of MG, but this would negate the artificial reef benefits which have been touted as a potential boon to the local marine habitat. This paper investigates the effects of MG on monopile-supported OWTs with respect to natural frequency and hydrodynamic loading. Specifically, the objective of this paper is to assess how significant the influence is of MG on support structure behavior in order to provide basis for designers and project planners to allow MG and therefore sponsor artificial reef effects in an OWT development.

## Nomenclature

ABS American Bureau of Shipping
DNV Det Norske Veritas

IEC International Electrotechnical Commission
MG Marine growth
NREL National Renewable Energy Laboratory
OWT Offshore wind turbine
$f_n$ Natural frequency associated with $n^{th}$ mode of structure
$g$ Acceleration due to gravity
$h$ Water depth
$k_r$ Surface roughness
$k_{wave}$ Wave number
$p_u$ Ultimate soil resistance
$s_u$ Undrained shear strength
$t$ Thickness
$u_{max}$ Maximum value of the orbital velocity at the bed
$z$ Depth below sea level
$\dot{x}, \ddot{x}$ Velocity and acceleration of water
$C_D$ Morison's equation drag coefficient
$C_{DS}$ Drag coefficient under steady state flow
$C_M$ Morison's equation inertia coefficient
$D$ Cylinder diameter
$E$ Modulus of elasticity
$F$ Wave force
$H$ Wave height
$H_{mud}$ Horizontal mudline force
$H_s$ Significant wave height
$\boldsymbol{K}$ Stiffness matrix
$KC$ Keulegan-Carpenter number
$\boldsymbol{M}$ Mass matrix
$M_{mud}$ Mudline moment
$T$ Wave period
$T_p$ Peak spectral wave period
$\varepsilon_c$ Strain at one-half the maximum stress in undrained compression test
$\xi$ Clay consolidation coefficient
$\rho$ Density
$\psi$ Wave amplification coefficient
$\omega$ Natural frequency

## 5.1 Introduction

The installment of offshore wind turbines (OWTs) greatly benefits global renewable energy generation goals, but there is concern about the potential impact of OWTs on local marine environments. The primary environmental concerns surrounding offshore wind development include noise from monopile installation and operation, physical habitat disruption from the presence of foundations, the electromagnetic fields created by transmission cables, and bird collisions [1–7]. Of these environmental considerations, this paper discusses the physical

presence of OWT foundations in the marine environment; more particularly, this paper focuses on monopile foundations, as monopiles are the most prevalent foundation type of currently installed OWTs [8].

Most OWT monopiles are installed in soils, and consequently the hard substrate of the steel foundation can provide habitat opportunities for benthic organisms and increase biodiversity (i.e., artificial reef effect [1,9–11]). Unfortunately, marine growth (otherwise known as fouling) can also adversely affect offshore infrastructure by increasing the mass of the substructure contributing to natural frequency, increasing the roughness and effective diameter of the structure and thereby increasing hydrodynamic loads [12–14], and can affect corrosion rate, interfere with corrosion control systems (coatings, linings, or cathodic protection), and impede structural fatigue inspection [14–16]. Because monopile-supported OWTs designed in the soft-stiff frequency regime are relatively close to the frequency spectra of wave loads [17], decreases in the natural frequency should be treated with caution and examined closely by the designer. Additionally, the cost of OWT foundations is proportionally large and can comprise approximately 20-25% of the capital cost of an offshore wind installation [8,18,19], therefore any mechanism which increases design loading of the support structure (thereby leading to increased structural material and increased cost) may be considered highly undesirable.

Some design guidelines acknowledge this potential increase in design loads and recommend that a strategy for inspection and possible removal of MG should be planned as a part of structural design [14], while other design guidelines recommend removal if the growth is found to be thicker than the original approved design [13]. In either case, removal of MG is costly [16] and would negate the possible environmental benefits associated with artificial reef effect.

This paper presents the results of an investigation of the effects of MG on monopile-supported OWT support structures with respect to natural frequency and hydrodynamic loading considering

ultimate limit state design load cases. While it has been acknowledged that MG plays a role in the fatigue limit state, it is assumed in this paper that the most critical fatigue location for monopiles is at the peak stress point near the mudline (i.e. scour zone), which is at a depth considered inaccessible to inspection and repair and as a consequence is designed conservatively [14].

The issue of MG has been well discussed in literature for offshore platforms (e.g. [21–24]) and for OWT jacket substructures (e.g. [16,25]), but the authors found few references in the literature which analyze the effects of MG on OWT monopiles from the engineering perspective. Research by Veldkamp briefly discusses the impact of MG on hydrodynamic loading, but does not trace MG directly to drag or inertia coefficients nor quantify any impact on natural frequencies [26,27]. This paper assesses the effects of MG on OWT monopile design: first, the impact of added mass on the natural frequency is analyzed by eigenvalue analysis; second, the increase in hydrodynamic loading as a function of increased effective diameter and drag. The NREL 5MW Reference Turbine ("NREL 5MW", [28]) is analyzed assuming a 6 m-diameter monopile sited off the U.S. Atlantic coast in Delaware in 30.5 m of water. The environmental conditions are informed by buoy data from the National Data Buoy Center which is managed by the National Oceanic and Atmospheric Administration [29]. Soil profiles are not available at that site, and consequently there is little emphasis on soil-structure effects in this paper. The eigenvalue analysis used to assess natural frequency considers a monopile supported laterally by so-called *p-y* springs for a variety of soil types, and the hydrodynamic analysis assumes a perfectly fixed (i.e. cantilevered) base at the mudline. Because the focus of this paper is on the effect of MG on OWT monopiles, the models used here are broadly representative and used as a basis for comparison.

The balance of engineering, environmental, and economics considerations with regard to artificial reef effect are discussed in Section 5.2, followed by explanations of the methods of natural frequency and hydrodynamic analysis in Sections 5.3 and 5.4. The results from these analyses are presented in Section 5.5, followed by conclusions and recommendations in Section 5.6.

## 5.2 Marine Growth

After installation, OWT substructures and monopiles can benefit the environment by providing an artificial reef and by creating a sanctuary from trawling and shelter from predation and provide enhanced feeding grounds [11,30,31]; in many situations, manmade structures have been placed in the marine environment to benefit fisheries and mitigate damage to the environment by rehabilitating habitats [1,10,11]. The hard substrate of offshore infrastructure provides an opportunity for the benthic organisms (e.g. mussels and barnacles) to colonize, and in some cases achieve biomass levels that exceed natural beds [9]. Conversely, the artificial reef effect can also impact fisheries by redistributing stock and facilitate the invasion of non-native species [1,9,11,30].

Putting aside the impacts of placing OWTs in the marine habitat, the impact of the marine environment on the engineering and design of the OWT is significant. OWTs must be designed to withstand stochastic loading from wind and waves for design lifetimes of 20 years [12,14], and must also consider the effects of sediment redistribution (i.e. scour). Sediment redistribution is also associated with artificial reef due to changes in local hydrodynamic patterns and increased biodiversity [9,10].

There are two types of MG: hard growth (e.g. mussels, barnacles, or tubeworms) and soft growth (e.g. hydroids, sea anemones, and soft corals). MG is most commonly seen in the upper submerged zone and the lower part of the splash zone, and generally decreases with depth as a function of access to space, food, and light [14,16,23–25,32]. In the North Sea, the greatest MG cover is to a depth of approximately 30 m and is typically dominated by mussels [16,23,24]. The colonization process is very dynamic, with MG growing not only on clean surfaces but also on top of existing MG [16,23–25], though typically tapers off after a few years [14].

For the purposes of this paper, the most important aspects of MG to be considered is the thickness of the growth on the monopile and added mass associated with the MG. Mass densities in literature typically range from 900-1300 kg/m$^3$ but may be as high as 2200 kg/m$^3$ [15,16,25,33] and thicknesses up to 200 mm have been suggested or reported [14,16]. No MG thicknesses have been suggested for the U.S. Atlantic coast, but 200 mm is common off the coast of California and 38 mm for the Gulf of Mexico [14]. Due to lack of site-specific data, this paper conservatively used a uniform MG thickness of 200 mm for the OWT substructure (from mudline to water line) and assumed a density of 2200 kg/m$^3$. It is assumed that the MG covers the substructure uniformly from mudline to waterline.

## 5.3 Eigenvalue Analysis

Natural frequencies of the NREL 5MW were determined using eigenvalue analysis, where the natural frequency $\omega$ (rad/s) is determined by the eigenvalue problem

$$\det\left(\boldsymbol{K} - \omega^2 \boldsymbol{M}\right) = 0 \quad \textbf{(1)}$$

where $\boldsymbol{K}$ is the linear stiffness matrix and $\boldsymbol{M}$ is a mass matrix representing the OWT. The OWT was modeled using Euler-Bernoulli beam elements to represent the steel structural elements of the OWT (tower, substructure, and monopile) using the properties and dimensions shown in Figure 5.1.

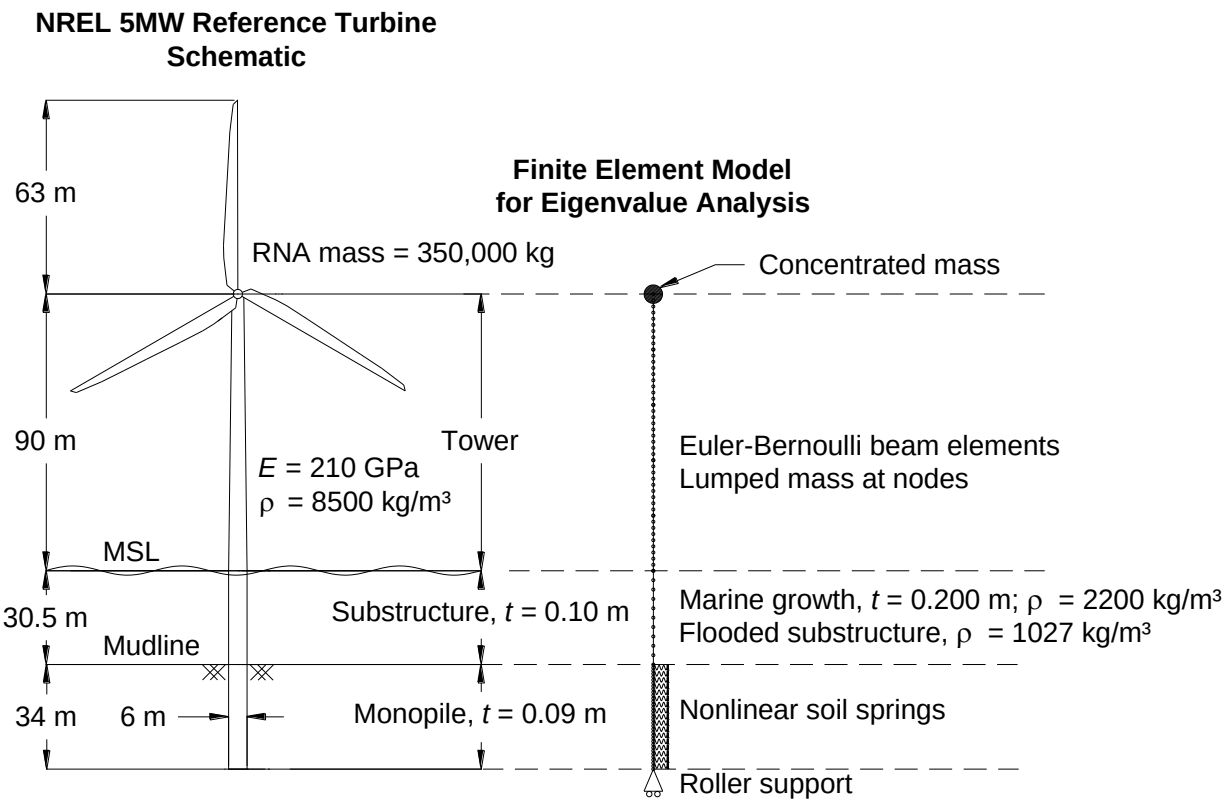


**Figure 5.1 NREL 5MW Reference Turbine finite element model for eigenvalue analysis**

Soil-structure interaction was modeled using nonlinear *p-y* springs for clay as defined by Matlock [34]. Initial stiffness $K_0$ of the *p-y* springs was defined as

$$K_0 = \xi \frac{p_u}{D\varepsilon_c^{0.25}} \tag{2}$$

where $p_u$ is the ultimate soil resistance at a given depth, $D$ is the diameter of the pile, $\varepsilon_c$ is the strain occurring at one-half the maximum stress in laboratory undrained compression tests of undisturbed soil samples, and $\xi$ is an empirical coefficient equal to 10 for normally consolidated clay and 30 for overconsolidated clay [14]. The secant stiffness of the *p-y* springs was also used by applying mudline loads from the NREL 5MW under extreme storm conditions (from the hydrodynamic load analysis, Section 5.4), determining the displacement experienced by each spring and corresponding spring force, and defining the secant stiffness as force divided by

displacement (*p/y*). The soil conditions considered in the eigenvalue analysis are representative of a medium stiff clay (with undrained shear strength $s_u$ = 50 kPa, submerged density of 9.2 kg/m$^3$, $\varepsilon_c$ = 0.005, and $\xi$ = 30), and are assumed to be constant for the depth of the monopile, with 2 m spacing between *p-y* curves. Further details on how *p-y* curves are implemented in this type of model can be found in [35,36].

For the eigenvalue analysis considering MG, additional mass was added to the lumped nodal masses between the mudline and mean sea level (MSL) from 200 mm of MG thickness fully covering the circumference of the substructure at a mass density of 2200 kg/m$^3$. MG in the splash zone was neglected. In addition to MG, it was assumed that the substructure was flooded during installation and therefore the added mass of the sea water (1027 kg/m$^3$) was included in the lumped nodal masses for the substructure.

## 5.4 Hydrodynamic Load Analysis

Hydrodynamic loading for monopiles is typically calculated using Morison's equation, where the wave force per unit length *dF* at a given depth below sea level *z* is defined as

$$dF = C_M \rho \pi \frac{D^2}{4} \ddot{x} dz + C_D \rho \frac{D}{2} |\dot{x}| \dot{x} dz \quad \textbf{(3)}$$

where $\rho$ is the density of the sea water (1027 kg/m$^3$), *D* is the diameter of the monopile, $\ddot{x}$ and $\dot{x}$ are the horizontal wave-induced acceleration and velocity of the water, $C_D$ and $C_M$ are drag and inertia coefficients. The drag and inertia coefficients are empirically determined, and a variety of recommendations have been presented in literature ([14,16,25–27,37,38], Table 5.1).

**Table 5.1 Morison's equation drag and inertia coefficients used in literature for offshore wind turbine foundation analysis. Values in bold were used in analysis; the values within parentheses are the acceptable or recommended range of values given.**

| Source | $C_D$ (Range) | $C_M$ (Range) |
|---|---|---|
| Jusoh & Wolfram (1996) | (0.6-1.8) | (1.7-2.0) |
| Veldkamp & van der Tempel (2005) | (0.65-1.05) | (1.8-2.0) |
| API (2005) | (0.65-1.05) | (1.2-1.6) |
| Veldkamp (2006) | **0.9** (0.6-1.2) | **2.0** (1.3-2.0) |
| Fischer (2006) | (0.6-1.0) | (1.6-2.5) |
| Fevåg (2012) | **1.0** (0.52-1.52) | **2.0** (1.2-1.6) |
| Shi et al. (2012) | **1.0** (0.6-1.2) | **2.0** (1.2-2.2) |
| DNV (2013) | (0.65-1.05) | (1.6-2.0) |

Design guidelines and standards take different approaches to the uncertainty in selecting $C_D$ and $C_M$ for offshore structures: IEC [12] does not recommend any particular range of values and directs the readers to reference documents (ISO 13819-2 for cylindrical members); API [37] recommends pairs of $C_D$ and $C_M$ depending on whether the substructure is smooth or rough ($C_D$ = 0.65, $C_M$ = 1.6 and $C_D$ = 1.05 and $C_M$ = 1.2, respectively); DNV [14] describes a process for selecting the appropriate values for $C_D$ and $C_M$ as a function of surface roughness ($k_r$) and Keulegan-Carpenter ($KC$) number. Generally speaking, $C_D$ increases with $k_r$ and $C_M$ decreases with $k_r$ [24].

The DNV drag coefficient is depending on the drag during steady-state flow $C_{DS}$, which is determined by

$$C_{DS} = \begin{cases} 0.65 & \text{for } k_r / D < 10^{-4} \text{ (smooth)} \\ \dfrac{29 + 4\log_{10}(k_r / D)}{20} & \text{for } 10^{-4} < k_r / D < 10^{-2} \\ 1.05 & \text{for } k_r / D > 10^{-2} \text{ (rough)} \end{cases} \quad \textbf{(4)}$$

and the wave amplification factor $\psi$ which is determined as a function of $KC$ and $C_{DS}$. The surface roughness $k_r$ is assumed to be 0.003 m for concrete and highly rusted steel and for MG can range between 0.005 and 0.05 m.

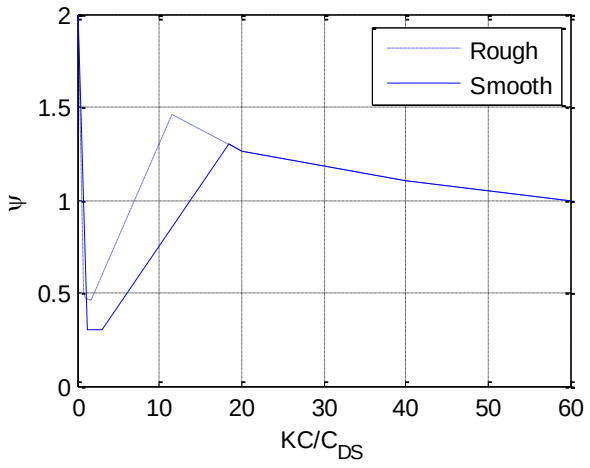


**Figure 5.2 Wave amplification factor as a function of drag coefficient for steady-state flow ($C_{DS}$) and Keulegan-Carpenter ($KC$) number**

The KC number can be calculated by

$$KC = \frac{u_{\max} \cdot T}{D} \tag{5}$$

where $T$ is the wave period and the maximum value of the orbital velocity at the bed $u_{max}$ is determined by

$$u_{\max} = \frac{\pi \cdot H}{T \sinh(k_{wave} h)} \tag{6}$$

which is a function of the wave height $H$, the water depth $h$, and the wave number $k_{wave}$. The wave number is determined for a given sea state by solving the equation

$$\left(\frac{2\pi}{T}\right)^2 = g \cdot k_{wave} \tanh(k_{wave} h) \tag{7}$$

where $g$ is the acceleration due to gravity. The drag coefficient $C_D$ is the product of the wave amplification factor $\psi$ and the drag coefficient under steady-state flow $C_{DS}$.

Morison's equation was used to calculate hydrodynamic loads on the NREL 5MW using the aero-hydro-elastic program FAST [38] assuming linear wave theory using the JONSWAP spectrum

with Wheeler stretching and constant $C_D$ and $C_M$ for the substructure. A sensitivity study of the full range of drag coefficients was conducted using the environmental conditions from IEC [12] design load case 6.1c followed by a comparison of the average rainflow count from the stochastic time history analysis of IEC design load case 6.2a. These design load cases were selected from the parked design conditions under the assumption that the sea states associated with these extreme storm loads (with mean return period of 50 years) are more likely to influence ultimate limit state OWT support structure design than more regularly occurring sea states (such as those during power production). Design load case 6.1c considers 10-min simulations of steady wind and regular waves using the Reduced Wind Model and Extreme Wave Height [12]. Design load case 6.2a consists of six 1-hr simulations of stochastic wind and irregular (stochastic) waves using the Extreme Wind Model and Extreme Sea State [12].

The environmental conditions used for each of these design load cases was determined using wind and wave data from the Delaware data buoy (Table 5.2). The power law was used to extrapolate wind speeds from the 5 m anemometer height to hub height using an exponent of 0.14. The 50-year wind speed was determined by fitting a Generalized Extreme Value distribution to the annual maxima of the 1-hr wind speed data from 1986-2014 and taking the 98$^{th}$ percentile value from the fitted distribution. Because design load case 6.1c is a 10 minute simulation, the 50-yr wind speed was increased by a factor of 1/0.95, then additionally by a factor of 1.1 according to the Reduced Wind Speed model [12,14].The peak spectral period $T_p$ was calculated as a function of the significant wave height $H_s$ in a manner similar to [39], where

$$T_p = 1.05\left(11.1\sqrt{\frac{H_s}{g}}\right) \quad \textbf{(8)}$$

for which $g$ is the acceleration due to gravity.

**Table 5.2 Environmental conditions for hydrodynamic study**

| Design Load Case: | 6.1c | 6.2a |
|---|---|---|
| Wave Type | Regular | Irregular |
| 50-yr Significant Wave Height | 8.12 m | 8.12 m |
| Peak Spectral Period | 10.6 s | 10.6 s |
| Wind Speed | 42.7 m/s | 36.9 m/s |
| Turbulence Intensity | 0% | 11% |
| Analysis Time History | 10 min | 1 hr |

## 5.5 Results

The effects of MG on monopile-supported OWTs with respect to natural frequency and hydrodynamic loads are discussed below. The focus of these analyses are on the engineering of the support structure and do not include environmental or policy considerations of MG.

### 5.5.1 Effect of Added Mass on Natural Frequency

Despite the conservative estimations of MG thickness and density (200 mm and 2200 kg/m$^3$, respectively), there was very little change in natural frequency when MG was included on the substructure (Table 5.3). In this scenario, the total mass of the MG (260,000 kg) is approximately 54% of the mass of the steel substructure (480,000 kg) and about 24% of the total structural mass (1,000,000 kg, including the substructure, tower, and rotor-nacelle assembly). Three mudline conditions were considered for the purposes of comparison: (1) perfect fixity between the substructure and the mudline, (2) the initial stiffness ($H_{mud}$ = $M_{mud}$ = 0) of a *p-y* spring supported monopile in medium stiff clay, and (3) the secant stiffness ($H_{mud}$ = 5.30 MN, $M_{mud}$ = 221 MNm) of a *p-y* spring supported monopile in medium stiff clay. In all cases considered, the addition of MG on the substructure did not change first natural frequency $f_1$, (considering a minimum threshold of natural frequency difference to be 0.01%) and at most the natural frequency changed by 0.50% (for $f_2$, considering perfect fixity at the mudline). For the fixed base condition, a change in natural frequency occurred for $f_3$ (0.24%), but the inclusion of *p-y* springs in the eigenvalue analysis caused the greatest difference to occur in $f_2$.

**Table 5.3 Natural frequencies as a function of marine growth thickness on the substructure**

| Mudline Condition | Natural Frequency, $f_n$ (Hz) | Marine Growth Thickness, 0 mm | Marine Growth Thickness, 200 mm | Reduction in Natural Frequency (%) |
|---|---|---|---|---|
| Fixed | $f_1$ | 0.256 | 0.256 | - |
| | $f_2$ | 2.02 | 2.01 | 0.50% |
| | $f_3$ | 4.22 | 4.21 | 0.24% |
| $s_u$ = 50 kPa<br>$H_{mud}$ = 0<br>$M_{mud}$ = 0 | $f_1$ | 0.215 | 0.215 | - |
| | $f_2$ | 1.00 | 0.999 | 0.10% |
| | $f_3$ | 2.72 | 2.72 | - |
| $s_u$ = 50 kPa<br>$H_{mud}$ = 5.30 MN<br>$M_{mud}$ = 221 MNm | $f_1$ | 0.163 | 0.163 | - |
| | $f_2$ | 0.677 | 0.675 | 0.30% |
| | $f_3$ | 2.45 | 2.45 | - |

In order to cause even 1% change in natural frequency (in $f_2$ for the *p-y* cases and $f_3$ for the fixed case), the required MG thickness for these cases would need to exceed 480 mm – over two times the thickness which was conservatively selected.

While nominally the changes in higher frequencies were more significant than for the first natural frequency, these results differ from those presented in literature for jacket foundations and platforms which indicate more significant changes in mode shape with the addition of marine growth [16,24]. Given that the change in $f_1$ changed by nearly 20% from the initial stiffness to the secant stiffness case, it can be concluded that soil conditions are much more significant in the assessment of monopile-supported OWTs than MG – changes of 0.5% attributed to MG can consequently be considered negligible in the face of other uncertainties in OWT modeling.

### 5.5.2 Marine Growth Effects on Hydrodynamic Loading

There are two considerations of MG when discussing hydrodynamic loading: first, small changes in natural frequency may affect the dynamic behavior of the OWT support structure when subjected to wave loading; second, MG increases surface roughness and the effective diameter of the substructure.

To isolate the impacts of added mass and natural frequency shift, aero-hydro-elastic time history simulations were performed in FAST considering the steady wind and regular wave conditions prescribed by IEC design load case 6.1c [12]. The added mass associated with MG thickness of 200 mm with density 2200 kg/m$^3$ was incorporated into the mass density of the NREL 5MW substructure, which required updating the distributed support structure properties in the FAST tower property input file and updating the polynomial coefficients which represent mode shape. Perfect fixity was assumed at the mudline, MG thickness was assumed to be constant in the submerged zone, and the Morison's drag and inertia coefficients were assumed to be $C_D$ = 1.0 and $C_M$ = 2.0, respectively.

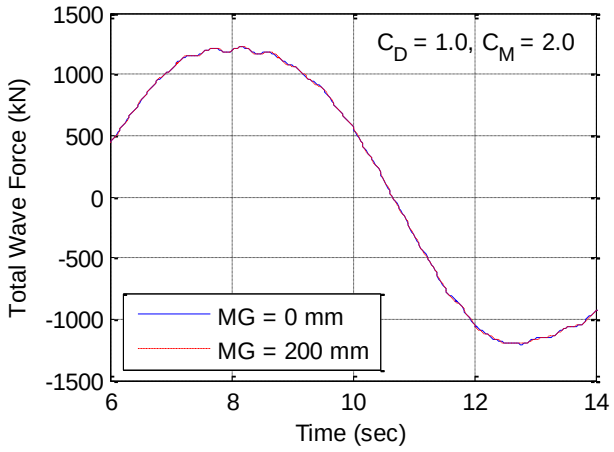


**Figure 5.3 Difference in total wave force as a function of marine growth (MG) mass**

Though small shifts in natural frequency can correspond to significant changes in hydrodynamic loading depending on the proximity of the natural frequency to the peak wave load frequency spectra, the very small changes in natural frequency attributed to MG found in the eigenvalue analysis are similarly reflected in the time history analysis (Figure 5.3). The total wave force was calculated by subtracting the thrust due to wind from the total mudline moment, and the difference between the case considering no added mass due to MG (MG = 0 mm) and that which included 200 mm of MG was negligible.

In more strict terms, the influence of MG on hydrodynamic loading is tied to the drag coefficient, $C_D$. The process suggested by DNV [14] to determine $C_D$ was used to estimate the difference in drag factor when considering a coarse, 200 mm thick layer of MG versus a smooth, newly installed OWT with painted steel subjected to the wave conditions of design load case 6.2a (Table 5.4).

**Table 5.4 Calculation of Morison's equation drag and inertia coefficients from DNV** [14] **for the NREL 5MW Reference Turbine**

| **Marine growth thickness** | **0 mm** | **200 mm** |
|---|---|---|
| Wave number, $k_{wave}$ | 0.0418 | |
| Keulegan-Carpenter Number, $KC$ | 2.58 | 2.42 |
| Surface Roughness, $k_r$ | 0.0001 | 0.05 |
| Steady-State Drag Coefficient, $C_{DS}$ | 0.65 | 1.03 |
| Wave Amplification Factor, $\psi$ | 0.38 | 0.53 |
| Drag Coefficient, $C_D = \psi C_{DS}$ | 0.25 | 0.55 |
| Inertia Coefficient, $C_M$ | 2.0 | 2.0 |

In this case, the drag coefficients are extremely low, and are likely a result of the ratio between the surface roughness and the diameter of the monopile when determining the steady-state drag coefficient. In fact, the drag coefficient for the smooth case is below the bottom of the range of $C_D$ recommended and seen in literature, and the MG = 200 mm case is just above the lowest $C_D$ reported ([16], Table 5.1). Consequently, the maximum range of $C_D$ reported (0.52 to 1.52, [16]) was used for comparative purposes to find the impact of increased drag on hydrodynamic loading, using the wave kinematics obtained from the regular-wave time history analysis design load case 6.1c (Figure 5.4).

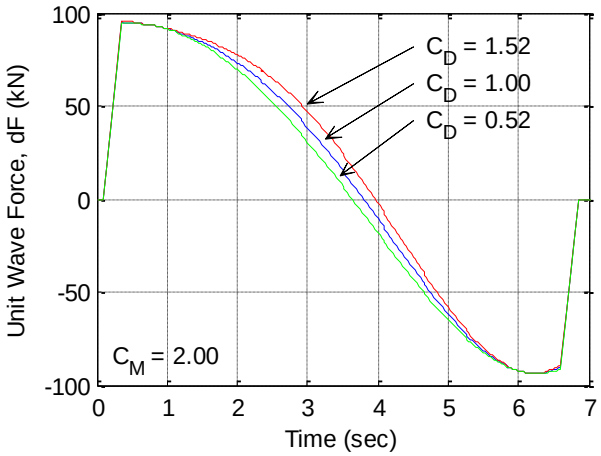


**Figure 5.4 Influence of drag coefficient on unit wave force at arbitrary depth *z* below sea level**

Because of large monopile diameters and the $D^2$ term in Morison's equation, hydrodynamic loading for monopile-supported OWTs is primarily inertia-dominated; while the drag coefficient $C_D$ does influence hydrodynamic loading (Figure 5.4), the influence of the inertia coefficient $C_M$ is much more significant. The unit wave force (wave force $dF$ per unit length $dz$) indicates a slight increase in wave force with increasing $C_D$, but the change is minimal. Even so, the change in $C_D$ does not affect the peak wave load and therefore is unlikely to impact a designer's assessment of ultimate limit state loading conditions – and consequently, the resulting OWT support structure design is not liable to change as a result of MG.

While a full fatigue analysis is outside the scope of this paper, a comparison of the average rainflow counts of mudline moment from the limiting drag cases ($C_D$ = 0.52 and 1.52, $C_M$ = 2.00) was made using the stochastic extreme storm time history associated with design load case 6.2a. The average rainflow count represents the average number of cycles at a given amplitude obtained from six realization of a 1-hr storm time history.

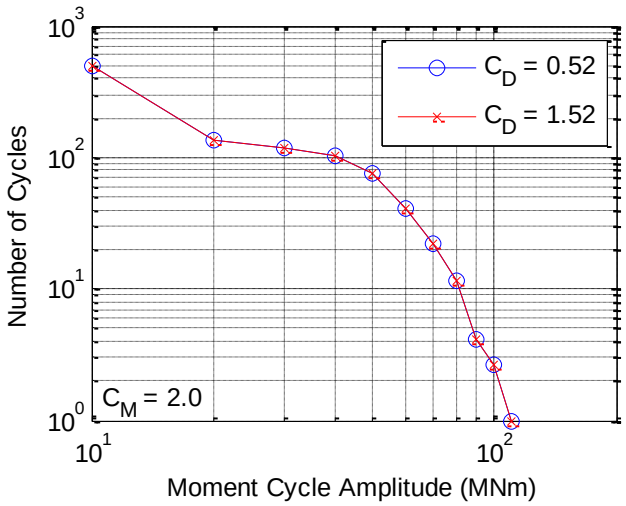


**Figure 5.5 Average rainflow counts of mudline moment considering drag coefficients $C_D$ of 0.52 and 1.52 from six realizations of the extreme storm time history associated with design load case 6.2a**

It is possible that the cumulative effect of increased drag may affect the fatigue life of the OWT, but the negligible change in cycle counts between the $C_D$ = 0.52 and $C_D$ = 1.52 cases imply that increased drag is not significant for OWT fatigue demand.

## 5.6 Conclusions

From an engineering perspective, there is minimal influence of marine growth (MG) on the design of monopile-supported offshore wind turbines (OWTs). Despite conservative estimates of 0.200 mm of MG thickness at a density of 2200 kg/m$^3$, the added mass due to MG had very little influence on natural frequency of the NREL 5MW; at most, the reduction was approximately 0.2% in the second natural frequency when considering the cases which included *p-y* springs. The very small changes in first, second, and third natural frequencies imply that MG does not play a significant role in the dynamic characteristics of the OWT support structure especially when compared to other uncertainties in OWT modeling (e.g. soil-structure interaction). Similarly, the small changes in natural frequency and increase in effective diameter attributed to MG had negligible effect on the time history of wave force when considering a regular wave train.

Because the substructure of monopile-supported OWTs typically has a large diameter, hydrodynamic loading calculated by Morison's equation is dominated by the $D^2$ in the inertial force term. While there is a small increase in wave force with increased drag, these increases do not occur at the peak of the wave force and are therefore unlikely to impact the ultimate limit state design of the OWT support structure. Fatigue analysis was outside the scope of this paper, but a comparison of the average rainflow count of mudline moment from six realizations of the stochastic 1-hr extreme storm history defined by IEC design load case 6.2a showed negligible change with increased drag.

The analyses and comparisons in this paper indicate that it is probably not necessary to clean MG off of a monopile-supported OWT for reasons related to the engineering of the structure. It is possible that MG may accelerate corrosion and in that way impact the fatigue life of the support structure; however, the location of highest stress on a monopile typically occurs at the mudline which is at a depth considered prohibitive for fatigue inspection [14] and will have little MG compared to the splash zone and upper portions of the submerged zone on the substructure. Further work is necessary to definitively conclude whether or not MG significantly influences the fatigue life of monopile-supported OWTs with respect to accelerated corrosion.

From an environmental perspective, installation of OWTs changes the marine habitat. If the goal is to mitigate change to the environment, then MG should be removed periodically from the substructure; however, if it is decided that artificial reef effects on OWTs is desirable, then sufficient evidence needs to be provided to conclude the positive effects of adding artificial substrate to the environment [1]. Further discussion of this topic is beyond the expertise of the authors; consequently, it is suggested that further work be performed to assess the positive and negative effects of artificial substrate and whether they outweigh the potential risk of species invasion. Moreover, because no offshore wind developments have been decommissioned, it is unclear what the best course of action is with regard to MG if it is anticipated that the OWTs will

be removed from the environment at the end of their design life. The role of offshore wind infrastructure in the marine environment needs to be assessed for all stages of the design life, from installation through decommissioning.

## References


[1] Petersen, J. K., and Malm, T., 2006, "Offshore windmill farms: threats to or possibilities for the marine environment.," AMBIO A J. Hum. Environ., **35**(2), pp. 75–80.

[2] Thomsen, F., Luedemann, K., Piper, W., Judd, A., and Kafemann, R., 2008, "Potential Effects of Offshore Wind Farm Noise on Fish," Bioacoustics, **17**(1-3), pp. 221–223.

[3] Bailey, H., Senior, B., Simmons, D., Rusin, J., Picken, G., and Thompson, P. M., 2010, "Assessing underwater noise levels during pile-driving at an offshore windfarm and its potential effects on marine mammals," Mar. Pollut. Bull., **60**(6), pp. 888–897.

[4] Brandt, M. J., Diederichs, A., Betke, K., and Nehls, G., 2011, "Responses of harbour porpoises to pile driving at the Horns Rev II offshore wind farm in the Danish North Sea," Mar. Ecol. Prog. Ser., **421**, pp. 205–216.

[5] Gill, A. B., and Kimber, J. a., 2005, "The potential for cooperative management of elasmobranchs and offshore renewable energy development in UK waters," J. Mar. Biol. Assoc. UK, **85**(05), p. 1075.

[6] Desholm, M., and Kahlert, J., 2005, "Avian collision risk at an offshore wind farm.," Biol. Lett., **1**(3), pp. 296–298.

[7] Hüppop, O., Dierschke, V., Exo, K.-M., Fredrich, E., and Hill, R., 2006, "Bird migration studies and potential collision risk with offshore wind turbines," Ibis (Lond. 1859)., **148**(s1), pp. 90–109.

[8] Hamilton, B., Battenberg, L., Bielecki, M., Bloch, C., Decker, T., Frantzis, L., Paidipati, J., Wickless, A., and Zhao, F., 2013, Offshore Wind Market and Economic Analysis: Annual Market Assessment, Navigant Consulting, Inc., Burlington, MA.

[9] Wilhelmsson, D., and Malm, T., 2008, "Fouling assemblages on offshore wind power plants and adjacent substrata," Estuar. Coast. Shelf Sci., **79**(3), pp. 459–466.

[10] Maar, M., Bolding, K., Petersen, J. K., Hansen, J. L. S., and Timmermann, K., 2009, "Local effects of blue mussels around turbine foundations in an ecosystem model of Nysted off-shore wind farm, Denmark," J. Sea Res., **62**(2-3), pp. 159–174.

[11] Langhamer, O., 2012, "Artificial reef effect in relation to offshore renewable energy conversion: state of the art.," ScientificWorldJournal., **2012**, p. 386713.

[12] IEC 61400-3, 2009, Design Requirements for Offshore Wind Turbines, Brussels.

[13] ABS, 2010, "Offshore Wind Turbine Installations," US Pat. App. 13/318,316, (December).

[14] DNV, 2013, DNV-OS-J101 Design of Offshore Wind Turbine Structures, Det Norske Veritas AS.

[15] Westgate, Z. J., and DeJong, J. T., 2005, "Geotechnical Considerations for Offshore Wind Turbines."

[16] Fevåg, L. S., 2012, "Influence of marine growth on support structure design for offshore wind turbines," Norwegian University of Science and Technology.

[17] Petersen, B., Pollack, M., Connell, B., Greeley, D., Davis, D., Slavik, C., and Goldman, B., 2010, Evaluate the effect of turbine period of vibrations requirements on structural design parameters, Groton, CT.

[18] Snyder, B., and Kaiser, M. J., 2009, "Ecological and economic cost-benefit analysis of offshore wind energy," Renew. Energy, **34**(6), pp. 1567–1578.

[19] Versteijlen, W., Metrikine, A., Hoving, J., Smid, E., and de Vries, W., 2011, "Estimation of the vibration decrement of an offshore wind turbine support structure caused by its interaction with soil," EWEA Offshore Conference, European Wind Energy Association, Amsterdam, the Netherlands.

[20] Gudmestad, O. T., and Moe, G., 1996, "Hydrodynamic coefficients for calculation of hydrodynamic loads on offshore truss structures," Mar. Struct., **9**(8), pp. 745–758.

[21] Gur, T., Choi, J. W., Soyoz, S., Engineering, M. M. I., Abadie, R. J., and Barrios, A. C., 2009, "OTC 20132 Assessment of Platform Cognac Using Instrumentation Data," (Figure 1), pp. 1–11.

[22] Forteath, G., Picken, G., Ralph, R., and Williams, J., 1982, "Marine Growth Studies on the North Sea Oil Platform Montrose Alpha," Mar. Ecol. Prog. Ser., **8**, pp. 61–68.

[23] Jusoh, I., and Wolfram, J., 1996, "Effects of marine growth and hydrodynamic loading on offshore structures," J. Mek.

[24] Shi, W., Park, H.-C., Baek, J.-H., Kim, C.-W., Kim, Y.-C., and Shin, H.-K., 2012, "Study on the marine growth effect on the dynamic response of offshore wind turbines," Int. J. Precis. Eng. Manuf., **13**(7), pp. 1167–1176.

[25] Veldkamp, H. F., and van der Tempel, J., 2005, "Influence of wave modelling on the prediction of fatigue for offshore wind turbines," Wind Energy, **8**(1), pp. 49–65.

[26] Veldkamp, H. F., 2006, "Chances in Wind Energy: A Probabilistic Approach to Wind Turbine Fatigue Design," Technical University of Delft.

[27] Jonkman, J., Butterfield, S., Musial, W., and Scott, G., 2009, Definition of a 5-MW Reference Wind Turbine for Offshore System Development.

[28] NOAA, 2015, "National Data Buoy Center" [Online]. Available: http://www.ndbc.noaa.gov/.

[29] Musial, W., and Ram, B., 2010, Large-Scale Offshore Wind Power in the United States: Assessment of Opportunitites and Barriers, Golden, CO.

[30] Langhamer, O., Wilhelmsson, D., and Engström, J., 2009, "Artificial reef effect and fouling impacts on offshore wave power foundations and buoys – a pilot study," Estuar. Coast. Shelf Sci., **82**(3), pp. 426–432.

[31] Malhotra, S., and Brinckerhoff, P., 2010, "Selection , Design and Construction of Offshore Wind Turbine Foundations."

[32] Zaaijer, M., 2002, Design methods for offshore wind turbines at exposed sites (OWTES): Sensitivity analysis for foundations of offshore wind turbines, Delft, The Netherlands.

[33] Matlock, H., 1970, "Correlations for design of laterally loaded piles in soft clay," Offshore Technology Conference, Dallas, TX.

[34] Carswell, W., Arwade, S. R., Degroot, D. J., and Lackner, M. A., 2012, "Probabilistic Analysis of Offshore Wind Turbine Soil-Structure Interaction," University of Massachusetts Amherst.

[35] Carswell, W., Arwade, S. R., DeGroot, D. J., and Myers, A. T., "Natural Frequency Degradation and Permanent Accumulated Rotation for Offshore Wind Turbine Monopiles in Clay," Renew. Energy.

[36] American Petroleum Institute, 2005, "API RP-2A."

[37] Fischer, T., 2006, "Load Mitigation of an Offshore Wind Turbine by Optimization of Aerodynamic Damping and Vibration Control."

[38] Jonkman, J., and Buhl, M. J., 2005, FAST User's Guide, National Renewable Energy Laboratory, Golden, CO.

[39] Valamanesh, V., Myers, A. T., and Arwade, S. R., 2015, "Multivariate analysis of extreme metocean conditions for offshore wind turbines," Struct. Saf., **55**, pp. 60–69.

# CHAPTER 6

# CONCLUSIONS AND RECOMMENDATIONS

The broad objective of this dissertation was to provide a body of research which can further inform designers and policy makers on several critical aspects of offshore wind turbine (OWT) design, analysis, and maintenance. In light of this broad objective, this research was more specifically targeted at issues relating to monopile support structures, as the majority of currently installed OWTs are supported by monopile foundations.

It is unclear how integrated the design of the support structure and the design of the foundation are in commercial OWT projects. In many cases, structural and geotechnical design are performed separately despite the dependence of OWT dynamics on the coupled behavior of the support structure and foundation. This dissertation combined the mechanics of complex programs suited for particular aspects of OWT design and analysis (e.g. FAST for aero-hydro-elastic modeling and INFIDEL for cyclic soil-pile modeling) via lumped parameter (i.e. reduced-order) modeling in order to more accurately capture the contributions of both the structural and geotechnical design to global OWT behavior.

The topics covered by this dissertation (foundation damping, cyclic degradation of soil properties, natural frequency degradation, and marine growth) were selected specifically with the goal of reducing the high costs associated with offshore wind energy. The results from these pursuits are summarized below, followed by recommendations for further work.

## 6.1 Summary of Results

Each of this dissertation's chapters (written as standalone papers) focused on an element of OWT monopile design which is not well understood by the current design community. While the NREL 5MW Reference Turbine ("NREL 5MW") [1] supported by a 6 m monopile was used in all of the following analyses, the wind, wave, and soil conditions vary from chapter to chapter. The

summary of results given here emphasizes the motivation for each chapter, the importance and novelty of the research performed, and focus on OWT behavior trends rather than site-specific results.

### 6.1.1 Foundation Damping

OWT are lightly damped structures, and thus the proximity of wind and wave load frequencies to OWT natural frequency requires careful consideration of different sources of damping – aerodynamic, hydrodynamic, structural, and soil damping – in order to reduce load demands and consequently required structural material costs. Of all the sources of damping, the contributions of soil damping (better termed "foundation damping" due to its reliance on soil-pile interaction) is least well defined, and currently there is no recommended methodology for calculating the contribution of the soil to the total damping of the OWT support structure. Chapter 2 proposed a method for converting hysteretic energy loss into a viscous, rotational mudline dashpot for a lumped parameter model (LPM), facilitating the inclusion of foundation stiffness and damping in OWT structural analysis without significantly increasing computational demand.

Using the logarithmic decrement method on tower top free vibration time histories of the NREL 5MW, mudline OWT foundation damping was estimated to contribute between 0.17-0.72% critical damping to total OWT damping. These results are broadly in agreement with previous estimates of foundation damping, taking into account differences in soil type, monopile foundation, wind turbine, and mudline load conditions. The majority of previous estimates of foundation damping were back-calculated from the logarithmic decrement of emergency shutdown or "rotor-stop" tests after subtracting out estimates for the other sources of damping, whereas this dissertation calculated foundation damping directly using soil mechanics.

In extreme storm conditions where the OWT rotor blades were parked and feathered, the inclusion of foundation damping reduced cyclic moment demand by 8-9%. Reductions in high

amplitude cycle counts were observed in the average rainflow count of mudline moment from extreme storm conditions, which indicate that foundation damping may contribute significantly to the fatigue life of monopile-supported OWTs.

### 6.1.2 Influence of Foundation Damping on Cyclic Demand

As aforementioned, there is currently no recommended methodology for taking into account foundation damping in OWT analysis. In order to quantify the reduction in cyclic demand which can be attributed to foundation damping (thereby also assessing the relative importance of foundation damping in the design process), the influence of foundation damping was analyzed considering the design situations of power production, emergency shutdown, and parked conditions in finite element models and using the NREL developed aero-hydro-elastic software FAST v7 [3]. These design situations were modeled according to the design standard IEC 61400-3 [10]. For stochastic time histories, three standard deviations ($3\sigma$) were used as a measure of cyclic amplitude for mudline response (i.e., shear, moment, displacement, and rotation); for emergency shutdown, the cyclic amplitude was defined as the difference between the mean response prior to shutdown and the absolute maximum response after shutdown; for cases with steady wind and regular waves, the cyclic amplitude was defined as half the difference between the maximum and minimum response. Foundation damping played a more significant role in the emergency shutdown and parked design conditions than power production. For power production cases, the average reduction in cyclic demand (mudline forces and moments) due to the inclusion of foundation damping was on the order of 2-3%. Comparatively, the cyclic moment demand was reduced by 2-10% on average for the parked conditions and by as much as 30% in some cases. The cyclic demand for emergency shutdown cases reduced by 1-10%.

It should be noted in particular here that the percent critical damping which was calculated for emergency shutdown design situations was in good agreement with the experimental emergency shutdown results from [2] considering similar soil profiles.

### 6.1.3 Cyclic Degradation of Soil Properties

Pile foundations are typically designed and analyzed using the *p-y* method to model lateral soil behavior due to simplicity and ease of implementation; however, *p-y* models are limited in their applications to OWT monopiles in that they assume flexible pile behavior, have limited ability to model cyclic effects, and contain no information for how to determine permanent accumulated rotation after cyclic loading. Two different *p-y* methods were presented for how cyclic degradation may be taken into account in a computational efficient manner: (1) cumulative cyclic *p-y* degradation and (2) quasi-static *p-y* methods with embedment reduction.

The cumulative cyclic degradation method used *p-y* degradation in conjunction with rainflow counts of cyclic loading to determine the degraded state of the soil-pile system after storm loading. Cyclic load histories are idealized using load parcels consisting of numbers of load cycles at different load amplitudes, applied in order of increasing load amplitude. A cyclic accumulation/degradation method between each step was used to account for the equivalent degradation from the number of load cycles associated with that load amplitude. This method was compared to a quasi-static *p-y* method which eliminated the contribution of soil spring stiffness within a pre-defined "embedment reduction" zone, representing disturbed soil around the perimeter of the monopile which can no longer contribute to pile resistance.

The natural frequency of the NREL 5MW was examined for monopiles in homogeneous clay deposits with undrained shear strength $s_u$ = 35 kPa, 50 kPa, and 100 kPa (representing soft, medium, and stiff clays respectively) to demonstrate a range of clay behavior subjected to extreme storm loading. Using the quasi-static average maximum load from six realizations of extreme storm loading resulted in greater reduction in natural frequency (with respect to natural frequency assessed with zero load) than using the cumulative cyclic degradation method.

The serviceability limit state (SLS) imposed on OWT monopiles requires the designer to assess the accumulated permanent pile rotation after storm loading to ensure that the mudline rotation does not exceed a threshold magnitude (typically on the order of 0.25°). Design guidelines do not recommend a specific method for determining this permanent residual rotation and consequently some designers conservatively choose to design piles which do not exceed the SLS at peak loading. Assuming the elastic limit of half the ultimate resistance ($0.5p_u$) and the cyclic unload-reload modulus proposed in [4], the monopile in 100 kPa clay remained fully elastic (all springs were loaded < $0.5p_u$), partially inelastic for the 50 kPa clay, and almost fully plastic for the 35 kPa clay (nearly all springs loaded > $0.5p_u$).

These results indicated that extreme storm loading on OWT monopiles in stiff clays is unlikely to affect the natural frequency and permanent accumulated rotation; further consideration is required for OWT monopiles in medium clays, as storm load estimation and the number of storms experienced by the monopile during the design lifetime may affect future performance. Under the same design conditions, the monopile in soft clay is insufficient with respect to both natural frequency degradation and permanent rotation. Load magnitude played a strong role in both natural frequency and permanent rotation estimation.

### 6.1.4 Marine Growth

Marine growth (MG) had very little impact on the engineering design of a monopile-supported OWT despite conservative estimates of MG thickness and density. Added mass due to MG caused minimal changes in natural frequency of the NREL 5MW (0.2% at most, given MG thickness of 200 mm with a density of 2200 kg/m$^3$), especially when compared to other uncertainties in OWT modeling (e.g. soil-structure interaction). Similarly, the small changes in natural frequency and increase in effective diameter attributed to MG had negligible effect on the time history of wave force when considering a regular wave train. While there was a small increase in wave force with increased drag, the increase did not occur at the peak of the wave

force and are therefore unlikely to impact the ultimate limit state design of the OWT support structure. A comparison of the average rainflow count of mudline moment from six realizations of the stochastic 1-hr extreme storm history for maximum and minimum drag coefficients were nearly identical.

In light of these results, it is probably not necessary to clean MG off of a monopile-supported OWT for reasons related to the engineering of the structure. Further discussion of the environmental benefits (e.g. artificial reef effects) and drawbacks (e.g. increased potential for invasive species) of OWT infrastructure may still be debated.

## 6.2 Recommendations for Further Work

One of the major limiting factors for offshore wind research, particularly in the U.S., is the lack of available site properties and OWT field performance data. Site specific information regarding soil properties, profiles, structural designs, and installation is typically proprietary, which means that unlike many fields of research, research chases the innovations of industry and rather than the other way around. Many aspects of this dissertation would have benefited tremendously from experimental validation – most notably with regard to the cumulative cyclic degradation and unload/reload modulus assumptions made in this body of work. The following recommendations are categorized generally by topic, with specific, idealized (i.e., unconstrained by budget, timeline, or proprietary boundary) research objectives identified by bullet points.

### 6.2.1 *P-y* Curves for Large Diameter Monopiles

Because of the prevalence of *p-y* curves in design, full-scale experimentation is imperative for developing a new set of *p-y* curves which take into account the rigid behavior of large-diameter OWT monopiles. The benefits of large-diameter calibrated *p-y* curves formulations for clays and sand under monotonic and cyclic conditions are required in order to make substantial progress on reducing conservatism in OWT substructure and monopile design. In the absence of full-scale

data and calibrated *p-y* curves, enormous amounts of time (on behalf of both engineers and computers) are spent developing and executing complicated three-dimensional finite element programs which remain, like the *p-y* curves, largely uncalibrated against full-scale results.

- **Experimental research.** Instrument large diameter (i.e., diameters exceeding 2 m) in a range of homogeneous soil profiles using *L/D* and *D/t* ratios which are similar to currently installed OWTs (where *L* is pile length, *D* is the diameter, and *t* is the thickness of the pile). These tests could be performed onshore in order to increase control over experimentation and results and to avoid the influence of wind and wave loading. Piles should be loaded monotonically and cyclically. Determine *p-y* curves as a function of soil type, soil properties, pile stiffness, load magnitude, and load frequency and number of load cycles (for cyclic testing).

- **Computational research.** Compare monotonic force-displacement curves from a pile supported by the original (small diameter) *p-y* curves, the experimentally-derived large diameter *p-y* curves, and three dimensional finite element model. Identify unloading modulus for *p-y* curves and define elastic/plastic behavior of the pile-soil system.

### 6.2.2 Foundation Damping

Foundation damping has some available data, in the form of emergency shutdown or "rotor-stop" tests; realistically, it is impossible to decompose the contributions of damping to OWT behavior, and consequently the only real necessity would be to aggregate a library of rotor-stop tests considering different soil conditions and turbines. Further work on foundation damping should include the influence of many aspects of soil behavior, e.g. dilative materials, such as dense sand, partially drained materials, scour and gapping that can cause loss of contact between foundation and soil, and combined static and cyclic loading. It is unknown at this time how much damping may be associated with sands versus clays, or the effects of soil layering (e.g., is the top layer of

soil the main contributor to foundation damping, or does the entire soil deposit within the embedment depth contribute to hysteretic behavior?). More tangible and finite aspects of foundation damping that should be explored including a sensitivity study of cyclic amplitude definition on the reduction in cyclic demand (e.g., $3\sigma$ was used for stochastic time histories, but perhaps $2\sigma$, root mean square, or some other metric is more appropriate).

The work here also assumed that the fore-after first natural frequency was the dominant frequency in all cases; while this is probably true for OWTs in parked conditions, it is possible that the wave load frequency may be more dominant than the OWT natural frequency. Full assessment of the dominant frequency in each design load cases should be taken into account in further work, or to determine a method which can take into account the frequency dependence of foundation damping.

All of the results presented in this paper were for mudline reactions in the fore-aft direction for co-aligned wind and waves. Further work should assess the impact of foundation damping on side-to-side loads, particularly for power production situations (when aerodynamic damping is much smaller in the side-to-side direction than the fore-aft direction) and for misaligned wind and wave load conditions.

- **Experimental research.** Collect emergency shutdown test data using methods similar to [2] during a range of wind speeds and for OWTs in a range of soil deposits. For OWTs of similar ratings and water depth, compare the contribution of foundation damping as a function of soil properties, as well as the relationship between wind speed (i.e., load level) and foundation damping.

- **Computational research.** Model the emergency shutdown tests using the foundation damping methodology proposed above. Additionally, conduct a sensitivity study of how the definition of cyclic load level from a stochastic time history informs the amount of

foundation damping and the consequent reduction in load demand. Additional sensitivity studies on the dominant frequency used to estimate foundation damping should be considered, particularly for power production design situations. Influence of foundation damping on side-to-side loads should be assessed, particularly due to misaligned wind and waves.

### 6.2.3 Fatigue Analysis

A large portion of the work presented in this dissertation included the use of rainflow counting and alluded to fatigue analysis, which was considered outside the scope of this research. Fatigue of monopile-supported OWTs should be investigated in detail, particular with regard the contributions of foundation damping and degradation of soil properties with cyclic loading – reductions in natural frequency over time may lead to amplification of fatigue load demands. Additionally, the impact of MG on fatigue needs to be assessed before any definitive statement can be made from the engineering perspective about whether MG needs to be cleaned from OWT substructures.

- **Experimental research.** The corrosion impact of MG on steel could be analyzed using different corrosion protection mechanisms (e.g. cathodic protection or protective coatings) as well as control cases which include MG removal. The added mass of MG over time could be measured and monitored. These experiments could be performed on scaled monopiles or newly installed metocean platforms.

- **Computational research.** Perform a full fatigue analysis of an OWT considering and neglecting foundation damping in order to ascertain the influence of foundation damping on OWT fatigue life. Additional work could include analyzing the impact of natural frequency degradation over the design life of the OWT to examine whether accelerated fatigue may occur.

### 6.2.4 Monopile Installation Effects

This work did also not include any driveability analyses or installation effects – the method of installation (hammering, vibration) can impact pile capacity and behavior (e.g. [5–7]), but here the pile was "wished in place" in all analyses. The following research objectives should be informed by a thorough literature review of the existing data and information regarding installation effects.

- **Experimental research.** This research could be included in the large diameter *p-y* pile campaign. Set-up time and force-displacement curves could be compared for piles which have been installed by hammering and by vibration.

- **Computational research.** Identify the limiting conditions of installation by vibration and hammering and compare the benefits and drawbacks of these methods. If significant difference is found in the force-displacement curves derived from piles installed by these methods, identify the impact of this difference in various OWT design situations.

## 6.3 Conclusion

The primary findings of this dissertation on monopile-supported OWTs may be summarized briefly as follows:

- For the North Sea offshore soil profile considered here, foundation damping contributed between 0.17-0.72% critical damping to the OWT support structure.

- The inclusion of foundation damping in analysis can significantly reduce cyclic foundation demand for parked and emergency shutdown design conditions (up to 30% and 10%, respectively).

- By the methodology proposed in this dissertation, monopiles in stiff clay are unlikely to experience significant permanent accumulated mudline rotation (i.e., unlikely to exceed

the mudline rotation serviceability limit state) nor cause significant degradation of the OWT natural frequency; the same monopile in soft clay will be inadequate with respect to serviceability limit state and natural frequency.

- Marine growth has negligible impact on the ultimate limit state design of monopile-supported OWTs considering added mass or increased drag on the substructure.

All of the recommendations for further work are made under the assumption that monopile-supported OWTs continue to be prevalent in offshore wind developments. Jacket structures and floating platforms are more suitable than monopiles for water depths which exceed approximately 30 m, and may be beneficial with respect to concerns of "visual pollution" from the shoreline since deeper water tends to be further from shore; however, the additional expense of these newer (or typically) technologies in the already strained economics of offshore wind energy leaves room for a future in which monopile-supported OWTs continue to be the most favorable support structure option. Larger diameter monopiles (beyond 6 m, perhaps 10-12 m) may be seen with the increase in wind turbine capacities, highlighting again the need for full-scale experimentation in order to better understand the interaction of OWTs with the offshore environment.

## References


[1] Jonkman, J., Butterfield, S., Musial, W., and Scott, G., 2009, Definition of a 5-MW Reference Wind Turbine for Offshore System Development.

[2] Damgaard, M., Andersen, J., Ibsen, L. B., and Andersen, L., 2012, "Natural Frequency and Damping Estimation of an Offshore Wind Turbine Structure," Proceedings of the Twenty-second International Offshore and Polar Engineering Conference, Rhodes, Greece, pp. 300–307.

[3] Jonkman, J., and Buhl, M. J., 2005, FAST User's Guide, National Renewable Energy Laboratory, Golden, CO.

[4] Matlock, H., 1970, "Correlations for design of laterally loaded piles in soft clay," Offshore Technology Conference, Dallas, TX.

[5] Jahr, A., and Tefera, T., 2015, “Effect of soil set-up during interruption of offshore pile driving,” Front. Offshore Geotech. III, pp. 978–1.

[6] Rausche, F., and Hussein, M., 2000, “Pile Driving in Calcareous Sediments,” Engineering for Calcareous Sediments, pp. 345–359.

[7] Jeanjean, P., Miller, D., Brooks, H., and Yogendrakumar, M., 2015, “Lessons learned from pile driving and monitoring in gravels on the Northstar Artificial Island,” Front. Offshore Geotech. III, pp. 978–1.

# REFERENCES


ABS. (2010). Offshore Wind Turbine Installations. US Patent App. 13/318,316. Houston, TX: American Bureau of Shipping. ADINA. (2014). Watertown, MA: ADINA R&D, Inc.

American Petroleum Institute. (2005). API RP-2A. American Petroluem Institute.

Andersen, K. (1976). Behaviour of clay subjected to undrained cyclic loading. In Proc. International Conference on the Behavior of Offshore Structures (pp. 33–44). Trondheim, Norway.

Andersen, K. H. (2009). Bearing capacity under cyclic loading — offshore, along the coast, and on land. The 21st Bjerrum Lecture presented in Oslo, 23 November 2007. Canadian Geotechnical Journal, 46(5), 513–535. doi:10.1139/T09-003

Andersen, L. V., Vahdatirad, M. J., Sichani, M. T., & Sørensen, J. D. (2012). Natural frequencies of wind turbines on monopile foundations in clayey soils—A probabilistic approach. Computers and Geotechnics, 43, 1–11. doi:10.1016/j.compgeo.2012.01.010

Bailey, H., Senior, B., Simmons, D., Rusin, J., Picken, G., & Thompson, P. M. (2010). Assessing underwater noise levels during pile-driving at an offshore windfarm and its potential effects on marine mammals. Marine Pollution Bulletin, 60(6), 888–897. doi:10.1016/j.marpolbul.2010.01.003

Beaudry-Losique, J., Boling, T., Brown-Saracino, J., Gilman, P., Hahn, M., Hart, C., … Wallace, W. (2011). A National Offshore Wind Strategy: Creating an Offshore Wind Energy Industry in the United States.

Bir, G. S. (2007). User's Guide to BModes ( Software for Computing Rotating Beam Coupled Modes ). Golden, CO.

Boulanger, B. R. W., Curras, C. J., Kutter, B. L., Wilson, D. W., & Abghari, A. (1999). Seismic Soil-pile-strcture interaction experiments and analysis. Journal of Geotechnical and Geoenvironmental Engineering, 125(September), 750–759.

Brandt, M. J., Diederichs, A., Betke, K., & Nehls, G. (2011). Responses of harbour porpoises to pile driving at the Horns Rev II offshore wind farm in the Danish North Sea. Marine Ecology Progress Series, 421, 205–216. doi:10.3354/meps08888

Bush, E., & Manuel, L. (2009). Foundation models for offshore wind turbines. In 47th AIAA Aerospace Sciences Meeting Including the New Horizons Forum and Aerospace Exposition. Orlando, FL.

Carswell, W., Arwade, S. R., Degroot, D. J., & Lackner, M. A. (2012). Probabilistic Analysis of Offshore Wind Turbine Soil-Structure Interaction. University of Massachusetts Amherst.

Carswell, W., Arwade, S. R., Degroot, D. J., & Lackner, M. A. (2014). Soil – structure reliability of offshore wind turbine monopile foundations. Wind Energy. doi:10.1002/we.1710

Carswell, W., Arwade, S. R., DeGroot, D. J., & Myers, A. T. (n.d.). Natural Frequency Degradation and Permanent Accumulated Rotation for Offshore Wind Turbine Monopiles in Clay. Renewable Energy.

Carswell, W., Fontana, C., Degroot, D. J., & Myers, A. T. (2015). Comparison of Cyclic p-y Curves for Offshore Wind Turbine Monopiles Subjected to Extreme Storm Loading. In Proceedings of the ASME 2015 34th International Conference on Ocean, Offshore, and Arctic Engineering (OMAE2015). St. Johns, Newfoundland, Canada.

Carswell, W., Johansson, J., Løvholt, F., Arwade, S. R., Madshus, C., DeGroot, D. J., & Myers, A. T. (2015). Foundation damping and the dynamics of offshore wind turbine monopiles. Renewable Energy, 80, 724–736. doi:10.1016/j.renene.2015.02.058

Chopra, A. K. (2007). Dynamics of Structures: Theory and Applications to Earthquake Engineering (3rd ed.). Upper Saddle River, NJ: Pearson Prentice Hall.

Conti, J. J., Holtberg, P. D., Beamon, J. A., Napolitano, S. A., Schaal, A. M., & Turnure, J. T. (2013). Annual Energy Outlook 2013 with Projections to 2040. Washington, D.C.

Damgaard, M., Andersen, J., Ibsen, L. B., & Andersen, L. (2012). Natural Frequency and Damping Estimation of an Offshore Wind Turbine Structure. In Proceedings of the Twenty-second International Offshore and Polar Engineering Conference (Vol. 4, pp. 300–307). Rhodes, Greece.

Damgaard, M., Andersen, J., LB, I., & Andersen, L. (2013). Time-Varying Dynamic Properties of Offshore Wind Turbines Evaluated by Modal Testing. In Proceedings of the 18th International Conference on Soil Mechanics and Geotechnical Engineering (pp. 2343–2346). Paris.

Damgaard, M., Ibsen, L. B., Andersen, L. V., & Andersen, J. K. F. (2013). Cross-wind modal properties of offshore wind turbines identified by full scale testing. Journal of Wind Engineering and Industrial Aerodynamics, 116, 94–108. doi:10.1016/j.jweia.2013.03.003

Darendeli, M. (2001). Development of a new family of normalized modulus reduction and material damping curves. Austin, TX: University of Texas at Austin.

De Vries, W., & Krolis, V. (2007). Effects of deep water on monopile support structures for offshore wind turbines. In European Wind Energy Conference & Exhibition (EWEC) (pp. 1–10). Milan.

Desholm, M., & Kahlert, J. (2005). Avian collision risk at an offshore wind farm. Biology Letters, 1(3), 296–298. doi:10.1098/rsbl.2005.0336

DNV. (2013). DNV-OS-J101 Design of Offshore Wind Turbine Structures. Det Norske Veritas AS.

Dunnavant, T. W., & O'Neill, M. W. (1989). Experimental p-y Model for Submerged, Stiff Clay. Journal of Geotechnical Engineering, 115, 95–114.

Fevåg, L. S. (2012). Influence of marine growth on support structure design for offshore wind turbines. Norwegian University of Science and Technology.

Fischer, T. (2006). Load Mitigation of an Offshore Wind Turbine by Optimization of Aerodynamic Damping and Vibration Control.

Forteath, G., Picken, G., Ralph, R., & Williams, J. (1982). Marine Growth Studies on the North Sea Oil Platform Montrose Alpha. Marine Ecology Progress Series, 8, 61–68. doi:10.3354/meps008061

Gerolymos, N., & Gazetas, G. (2005). Phenomenological model applied to inelastic response of soil-pile interaction systems. Soils and Foundations, 45(4), 119–132.

Gill, A. B., & Kimber, J. a. (2005). The potential for cooperative management of elasmobranchs and offshore renewable energy development in UK waters. Journal of the Marine Biological Association of the UK, 85(05), 1075. doi:10.1017/S0025315405012117

GL WindEnergie. (2005). Overall Damping for Piled Offshore Support Structures, Guideline for the Certification of Offshore Wind Turbines. Germanischer Lloyd WindEnergie.

Goyal, A., & Chopra, A. (1989). Simplified evaluation of added hydrodynamic mass for intake towers. Journal of Engineering Mechanics, 115(7), 1393–1412.

Gudmestad, O. T., & Moe, G. (1996). Hydrodynamic coefficients for calculation of hydrodynamic loads on offshore truss structures. Marine Structures, 9(8), 745–758. doi:10.1016/0951-8339(95)00023-2

Gur, T., Choi, J. W., Soyoz, S., Engineering, M. M. I., Abadie, R. J., & Barrios, A. C. (2009). OTC 20132 Assessment of Platform Cognac Using Instrumentation Data.

Hamilton, B., Battenberg, L., Bielecki, M., Bloch, C., Decker, T., Frantzis, L., … Zhao, F. (2013). Offshore Wind Market and Economic Analysis: Annual Market Assessment. Burlington, MA: Navigant Consulting, Inc.

Hamre, L., Khankandi, S. F., Strøm, P. J., & Athanasiu, C. (2011). Lateral behaviour of large diameter monopiles at Sheringham Shoal Wind Farm. In Frontiers in Offshore Geotechnics II (pp. 575–580).

Hansteen, O. E., & Höeg, K. (1994). Soil-Structure Interaction Analysis of Embedded Caisson Anchor Under Tension Load. In BOSS ’94, 7th International Conference on the Behavior of Offshore Structures (pp. 49–62). Cambridge, MA.

Heidari, M., Jahanandish, M., El Naggar, H., & Ghahramani, A. (2014). Nonlinear cyclic behavior of laterally loaded pile in cohesive soil. Canadian Geotechnical Journal, 51, 129–143. doi:dx.doi.org/10.1139/cgj-2013-0099

Hokmabadi, A. S., Fakher, A., & Fatahi, B. (2012). Full scale lateral behaviour of monopiles in granular marine soils. Marine Structures, 29(1), 198–210. doi:10.1016/j.marstruc.2012.06.001

Hüppop, O., Dierschke, V., Exo, K.-M., Fredrich, E., & Hill, R. (2006). Bird migration studies and potential collision risk with offshore wind turbines. Ibis, 148(s1), 90–109. doi:10.1111/j.1474-919X.2006.00536.x

IEC 61400-3. (2009). Design Requirements for Offshore Wind Turbines. Brussels.

Jahr, A., & Tefera, T. (2015). Effect of soil set-up during interruption of offshore pile driving. Frontiers in Offshore Geotechnics III, 978–1.

Jeanjean, P., Miller, D., Brooks, H., & Yogendrakumar, M. (2015). Lessons learned from pile driving and monitoring in gravels on the Northstar Artificial Island. Frontiers in Offshore Geotechnics III, 978–1.

Jonkman, B. (2013). Natural frequency and damping ratio calculation. Retrieved July 14, 2015, from https://wind.nrel.gov/forum/wind/viewtopic.php?f=3&t=789

Jonkman, J., & Buhl, M. J. (2005). FAST User's Guide. Golden, CO: National Renewable Energy …. Golden, CO: National Renewable Energy Laboratory.

Jonkman, J., Butterfield, S., Musial, W., & Scott, G. (2009). Definition of a 5-MW Reference Wind Turbine for Offshore System Development.

Jusoh, I., & Wolfram, J. (1996). Effects of marine growth and hydrodynamic loading on offshore structures. Jurnal Mekanikal.

Klinkvort, R. T., Leth, C. T., & Hededal, O. (2010). Centrifuge modelling of a laterally cyclic loaded pile. In International Conference on Physical Modelling in Geotechnics (pp. 959–964). Zurich, Switzerland: Taylor & Francis Group.

Langhamer, O. (2012). Artificial reef effect in relation to offshore renewable energy conversion: state of the art. TheScientificWorldJournal, 2012, 386713. doi:10.1100/2012/386713

Langhamer, O., Wilhelmsson, D., & Engström, J. (2009). Artificial reef effect and fouling impacts on offshore wave power foundations and buoys – a pilot study. Estuarine, Coastal and Shelf Science, 82(3), 426–432. doi:10.1016/j.ecss.2009.02.009

Lombardi, D., Bhattacharya, S., & Muir Wood, D. (2013). Dynamic soil–structure interaction of monopile supported wind turbines in cohesive soil. Soil Dynamics and Earthquake Engineering, 49, 165–180. doi:10.1016/j.soildyn.2013.01.015

Maar, M., Bolding, K., Petersen, J. K., Hansen, J. L. S., & Timmermann, K. (2009). Local effects of blue mussels around turbine foundations in an ecosystem model of Nysted off-shore wind farm, Denmark. Journal of Sea Research, 62(2-3), 159–174. doi:10.1016/j.seares.2009.01.008

Malhotra, S., & Brinckerhoff, P. (2010). Selection , Design and Construction of Offshore Wind Turbine Foundations.

Manwell, J. F., McGowan, J. G., & Rogers, A. L. (2009). Wind Energy Explained (2nd ed.). New York: John Wiley & Sons, Ltd.

Martínez-Chaluisant, V. (2011). Static and Dynamic Response of Monopiles for Offshore Wind Turbines. University of Wisconsin-Madison.

Matlock, H. (1970). Correlations for design of laterally loaded piles in soft clay. In Offshore Technology Conference. Dallas, TX.

MMI Engineering. (2009). Comparative Study of OWTG Standards: Prepared for JIP Sponsorship.

Musial, W., & Ram, B. (2010). Large-Scale Offshore Wind Power in the United States: Assessment of Opportunitites and Barriers. Golden, CO.

NGI. (1991). Description of INFIDEL - a non-linear, 3-D finite element program.

NOAA. (2015). National Data Buoy Center. Retrieved from http://www.ndbc.noaa.gov/

Pedersen, A. S., & Steiniche, C. S. (2012). Safe Operation and Emergency Shutdown of Wind Turbines. Aalborg University.

Petersen, B., Pollack, M., Connell, B., Greeley, D., Davis, D., Slavik, C., & Goldman, B. (2010). Evaluate the effect of turbine period of vibrations requirements on structural design parameters. Applied Physical Sciences. Groton, CT.

Petersen, J. K., & Malm, T. (2006). Offshore windmill farms: threats to or possibilities for the marine environment. AMBIO: A Journal of the Human Environment, 35(2), 75–80. doi:10.1579/0044-7447(2006)35[75:OWFTTO]2.0.CO;2

Pranjoto, S., & Pender, M. (2003). Gapping effects on the lateral stiffness of piles in cohesive soil. Proceedings of Pacific Conference on Earthquake Engineering.

Rajashree, S. S., & Sundaravadivelu, R. (1996). Degradation model for one-way cyclic lateral load on piles in soft clay. Computers and Geotechnics, 19(4), 289–300. doi:10.1016/S0266-352X(96)00008-0

Rausche, F., & Hussein, M. (2000). Pile Driving in Calcareous Sediments. In Engineering for Calcareous Sediments (pp. 345–359).

Reese, L., Cox, W., & Koop, F. (1975). Field Testing and Analysis of Laterally Loaded Piles in Stiff Clay. Offshore Technology Conference.

Salzmann, D. J., & van der Tempel, J. (2005). Aerodynamic Damping in the Design of Support Structures for Offshore Wind Turbines. In Paper of the Copenhagen Offshore Conference.

Seidel, M. (2010). Load characteristics of axially loaded jacket piles supporting offshore wind turbines, 1–12.

Shi, W., Park, H., Chung, C., Baek, J., Kim, Y., & Kim, C. (2013). Load analysis and comparison of different jacket foundations. Renewable Energy, 54, 201–210. doi:10.1016/j.renene.2012.08.008

Shin, Y., Saue, M., Langford, T., Petter, H., Cho, K., & Park, J. (2014). Pile-Soil Interaction under Cyclic Loadings for Offshore Wind Monopiles. In Proceedings of the ASME 2014 33rd International Conference on Ocean, offshore, and Arctic Engineering (OMAE2014) (pp. 1–8).

Shirzadeh, R., Devriendt, C., Bidakhvidi, M. a., & Guillaume, P. (2013). Experimental and computational damping estimation of an offshore wind turbine on a monopile foundation. Journal of Wind Engineering and Industrial Aerodynamics, 120, 96–106. doi:10.1016/j.jweia.2013.07.004

Snyder, B., & Kaiser, M. J. (2009). Ecological and economic cost-benefit analysis of offshore wind energy. Renewable Energy, 34(6), 1567–1578. doi:10.1016/j.renene.2008.11.015

Tarp-Johansen, N. J., Andersen, L., Christensen, E., Mørch, C., Kallesøe, B., & Frandsen, S. (2009). Comparing Sources of Damping of Cross-Wind Motion. In European Offshore Wind 2009: Conference & Exhibition: 14-16 September. Stockholm, Sweden: European Wind Energy Association.

Thomsen, F., Luedemann, K., Piper, W., Judd, A., & Kafemann, R. (2008). Potential Effects of Offshore Wind Farm Noise on Fish. Bioacoustics, 17(1-3), 221–223. doi:10.1080/09524622.2008.9753825

U.S. Department of Energy. (2008). 20% Wind Energy by 2030: Increasing Wind Energy's Contribution to U.S. Electricity Supply. DOE/GO-102008-2567. doi:DOE/GO-102008-2567 • July 2008

Valamanesh, V., & Myers, A. (2014). Aerodynamic Damping and Seismic Response of Horizontal Axis Wind Turbine Towers. Journal of Structural Engineering, 140(11). doi:10.1061/(ASCE)ST.1943-541X.0001018

Valamanesh, V., Myers, A. T., & Arwade, S. R. (2015). Multivariate analysis of extreme metocean conditions for offshore wind turbines. Structural Safety, 55, 60–69. doi:10.1016/j.strusafe.2015.03.002

Van der Horst, D. (2007). NIMBY or not? Exploring the relevance of location and the politics of voiced opinions in renewable energy siting controversies. Energy Policy, 35(5), 2705–2714. doi:10.1016/j.enpol.2006.12.012

Veldkamp, H. F. (2006). Chances in Wind Energy: A Probabilistic Approach to Wind Turbine Fatigue Design. Technical University of Delft.

Veldkamp, H. F., & van der Tempel, J. (2005). Influence of wave modelling on the prediction of fatigue for offshore wind turbines. Wind Energy, 8(1), 49–65. doi:10.1002/we.138

Versteijlen, W., Metrikine, A., Hoving, J., Smid, E., & de Vries, W. (2011). Estimation of the vibration decrement of an offshore wind turbine support structure caused by its interaction with soil. In EWEA Offshore Conference. Amsterdam, the Netherlands: European Wind Energy Association.

Westgate, Z. J., & DeJong, J. T. (2005). Geotechnical Considerations for Offshore Wind Turbines.

Wilhelmsson, D., & Malm, T. (2008). Fouling assemblages on offshore wind power plants and adjacent substrata. Estuarine, Coastal and Shelf Science, 79(3), 459–466. doi:10.1016/j.ecss.2008.04.020

Zaaijer, M. (2002). Design methods for offshore wind turbines at exposed sites (OWTES): Sensitivity analysis for foundations of offshore wind turbines. OWTES Task 4.1. Delft, The Netherlands.

Zaaijer, M. B. (2006). Foundation modelling to assess dynamic behaviour of offshore wind turbines. Applied Ocean Research, 28(1), 45–57. doi:10.1016/j.apor.2006.03.004